Desarrollo de hormigones conductores con adición de fibras de carbono recicladas

Tesis por artículos

TESIS DOCTORAL

Autor:
Gerard Faneca Llesera

Directores:
Antonio Aguado de Cea
Ignacio Segura Pérez

Barcelona, **Mayo 2020**

Universitat Politècnica de Catalunya

Departamento de Ingeniería Civil y Ambiental
Programa de Doctorado de Ingeniería de la Construcción

UNIVERSITAT POLITÈCNICA DE CATALUNYA BARCELONATECH

Agradecimientos

Esta tesis doctoral es resultado de un proceso de colaboración universidad-empresa y formación continua desarrollado durante prácticamente 20 años, durante los cuales se ha forjado no solo una relación académica y empresarial, sino también una relación de amistad y confianza mutua. Gracias a ello se ha establecido una cooperación fluida, no solo en el tema tratado en esta tesis, sino en multitud de otras, desde las más disruptivas a las más focalizadas en el día a día de una industria.

Es por ello qué, en el ámbito académico, no dispongo de suficientes palabras de agradecimiento a los directores de esta tesis Antonio Aguado e Ignacio Segura que me convencieron para embarcarme y guiarme en esta parte de la travesía. Seguiremos codo con codo en otras travesías, no me cabe la menor duda. También mi más sincero agradecimiento a Tai Ikumi y Josep maría Torrens, que tan directamente han participado en esta tesis. Quedo a vuestra disposición para lo que haga falta.

Por la parte industrial mi más sincera gratitud a Escofet 1886 S.A y el AGAUR., por su apoyo económico en el estudio y por creer en este tipo de colaboración Universidad-Empresa, que nos permite crecer y madurar técnicamente a todos los involucrados. También es de agradecer la paciencia y apoyo de Javier Medina y Juan Fernández, compañeros de amasadora, pruebas, ideas, inventos etc. Sin su apoyo todo hubiera sido más lento y tedioso.

Y finalmente disculparme con mi familia, por robarles tiempo y cuidados que desgraciadamente tanto necesitan, pero que entienden mis motivaciones y me han apoyado igualmente, animándome a realizar y acabar esta tesis.

Seguro que me olvido de alguien, pero si en su momento colaboraron y no lo agradecí lo suficiente, mis disculpas, saben perfectamente que tengo la puerta abierta generosamente a cualquier aventura.

Resumen

Dentro del ámbito de los materiales inteligentes y considerando el hormigón como uno de los principales materiales de la construcción, conseguir dotarle de nuevas funcionalidades le proporcionaría nuevos usos y aplicaciones a las meramente estructurales o de revestimiento habituales. Factor que permitiría evolucionar el material manteniendo su vigencia ante nuevos retos que se plantean en ámbitos de las infraestructuras, como la ciudad inteligente, movilidad, sensorización de estructuras y otras aplicaciones posibles todavía por desarrollar.

Con este objetivo marcado e introduciendo factores como la sostenibilidad y una industrialización a medio plazo, esta tesis se centra en la utilización de fibras de carbono recicladas de productos o procesos, adicionadas al hormigón, con el fin de modificar sus propiedades eléctricas y transformarlo de un material aislante a otro con propiedades conductivas.

Por ello y basándose en estudios previos, se caracterizan dos matrices de hormigón con marcadas diferencias en lo que refiere al tamaño de sus agregados, que reciben la adición de diferentes tipos de fibra de carbono recicladas en distintos porcentajes.

En una primera fase, el estudio se centra en la caracterización de las diferentes propiedades básicas del hormigón, como la capacidad estructural o trabajabilidad en estado fresco, a la que se añade la determinación de las propiedades eléctricas a la vez que se establecen tipologías de ensayo específicos con los que poder evaluar, comparar y analizar el efecto de las diferentes fases presentes en el material en la conductividad eléctrica de todas las combinaciones de dosificaciones propuestas.

Posteriormente, focalizándose en las combinaciones de matriz, tipo y cantidad de fibra con mejores propiedades conductivas, se profundiza en la caracterización eléctrica, contrastándola con funcionalidades asociadas como el efecto piezoeléctrico y el efecto Joule, funcionalidades que gobiernan la sensorización del hormigón y autocalentamiento en aplicaciones como el control de deformaciones de estructuras o pavimentos con efecto deshielo respectivamente.

Finalmente se aplica el material desarrollado en una prueba piloto a escala real, en la que se testean la funcionalidad de autocalentamiento en un elemento de mobiliario urbano de la empresa ESCOFET 1886 S.A., que ha participado en la realización de esta tesis doctoral en el marco del Programa de Doctorado Industrial de la Generalitat de Catalunya.

Summary

Inside the studies of intelligent materials and considering concrete as one of the most building material used, getting new functionalities to him, would provide new uses and applications to the usual structural or facing purposes. Factor that would allow the material to evolve while maintaining its validity in new challenges that arise in infrastructure areas, such as the smart city, mobility, self-sensing of structures and other possible applications still to be developed.

With this objective marked and introducing factors such as sustainability and medium-term industrialization, this thesis focuses on the use of recycled carbon fibers from products or processes, added to concrete, in order to modify its electrical properties and transform it, from one insulating material, to another with conductive properties.

Therefore, based on previous studies, two concrete matrix are characterized with particular differences in the size of their aggregates. Both two matrix receive the addition of different types of carbon fiber recycled in different percentages.

In a first phase, the study focuses on the characterization of the different basic properties of concrete, such as structural capacity and workability in fresh condition. The determination of electrical properties is added and established specific test typologies to evaluate, compare and analyze the effect of the different phases present in the material, on the electrical conductivity of all combinations of proposed mixes.

Subsequently, focusing on the combinations of matrix, type and quantity of fiber with better conductive properties, deeper electrical characterization is done, contrasting it with associated functionalities such as the piezoelectric effect and the Joule effect. Functionalities that govern the self-sensing and self-heating of concrete applications such as the control of deformations of structures or pavements with de-icing effect.

Finally, the material developed in a full-scale pilot test is applied, in which the functionality of self-heating is tested in an element of urban furniture by the company ESCOFET 1886 S.A., which has participated in the realization of this doctoral thesis inside the framework of the Industrial Doctoral Program of the Generalitat de Catalunya.

ÍNDICE

Capítulo 1: INTRODUCCIÓN

1.1.- JUSTIFICACIÓN Y MOTIVACIÓN

En los últimos años, ha tomado gran auge el concepto de ciudad inteligente, proveniente del término inglés “Smart City”. El mismo quiere reflejar a las ciudades que se aprovechan del potencial de la tecnología y la innovación para que, de forma conjunta con el resto de recursos, mejorar la calidad de vida de sus ciudadanos. Para conseguir este objetivo persiguen un uso más eficaz de los recursos y promover un desarrollo sostenible en las mismas

En la práctica, se concibe una ciudad inteligente, como una ciudad comprometida con su entorno, con elementos arquitectónicos de vanguardia y donde las infraestructuras están dotadas de las soluciones tecnológicas más avanzadas. Todo ello con el fin de facilitar la interacción de la población con el medio, en este caso la ciudad, para constituirse en elementos muy participativos en la definición de los parámetros de creación de ciudad.

Este planteamiento, requiere disponer de un número muy elevado de datos, disponibles en tiempo real, para dar respuesta satisfactoria a cada ciudadano, cuando lo necesita. Ello requiere una gestión de la información muy completa, no sólo desde el punto de vista de centralización, sino del proceso de retorno hacia el ciudadano, ya sea de forma activa o pasiva. Se entiende como activa, cuando el ciudadano se implica y accede, por ejemplo, a una aplicación (apps) y pasiva, cuando no se conecta directamente, sino que se beneficia de una gestión centralizada. En la figura 1.1. se intenta visualizar, la complejidad que este planteamiento de Big Data y la diversidad de elementos implicados, dentro de la propia ciudad.

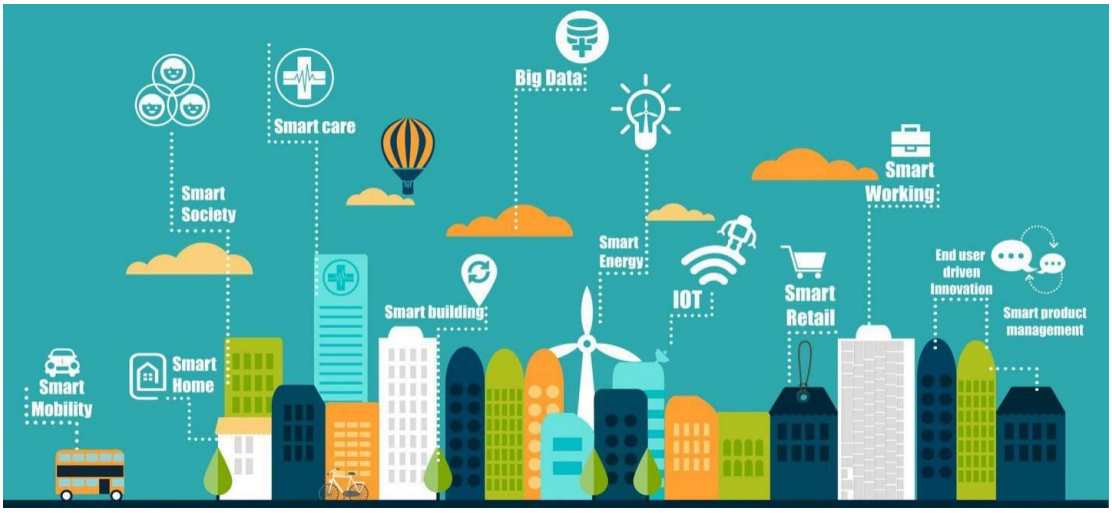

Figura 1.1. Ciudades inteligentes y Big Data (Fuente: Sergio Álvarez en: https://www.diariomotor.com/2015/10/24/big-data-ciudades-inteligentes/)

Es en este ámbito, en el cual, ciudades como Barcelona, intenta hacerse un hueco, independientemente de las políticas partidistas. Así en el periodo 2011-2015, el tema de Smart City se convirtió en un eje estratégico de la ciudad y, con posterioridad se intenta mantener la línea de actuación. Por ello, recientemente, Barcelona lideró el consorcio MOBILus y, consiguió un gran proyecto europeo, instalando en la ciudad la sede de Knowledge Innovation Community (KIC) on Urban Mobility encargada de desarrollar las innovaciones en movilidad urbana de la Unión Europea, al menos, hasta 2026.

Si bien el proyecto citado es el proyecto estrella de los próximos años, Barcelona, también desarrolla otros proyectos transversales orientados a conseguir desde otros campos una ciudad inteligente. Estos proyectos incluyen campos tales como: la autosuficiencia de recursos, niveles de emisiones, consumo de energía, iluminación adaptada, eficiencia administrativa, etc.

En este contexto y dado que el hormigón es uno de los principales materiales de la construcción de una ciudad, resulta lógico plantear que, al añadir propiedades funcionales adicionales a materiales estructurales o de revestimiento de calzadas y fachadas, estaríamos avanzando en la dirección de un material multifuncional que puede cumplir varios requisitos, añadidos a la componente meramente estructural que ostentan los materiales de construcción en general.

El beneficio conseguido, si además cumple con requerimientos medioambientales, promoviendo sostenibilidad y aprovechamiento de recursos, multiplica su valor de forma ostensible. Es de esta forma cómo nace la posibilidad de convertir un hormigón con adición de subproductos o residuos de la industria, en un material adecuado al concepto de las ciudades inteligentes.

La funcionalidad principal del hormigón viene dada, en su utilización en los procesos de construcción civil y arquitectura, por su capacidad portante o estructural asociada la vez a unos costes económicos competitivos enfrente de otros materiales. Por ello el hormigón es actualmente el material de construcción más utilizado y probablemente lo siga siendo en un futuro inmediato.

Durante el siglo pasado, los desarrollos implementados en el hormigón han estado ligados principalmente a la mejora de sus capacidades resistentes, como por ejemplo con el empleo de adiciones y fibras de diferentes tipos, que mejoraran su resistencia en general o resistencia a tracción respectivamente.

El hormigón es un material aislante de la electricidad y últimamente esto ha despertado curiosidad entre los investigadores, ya que sería muy interesante su uso como un material multifuncional si se consiguiera bajar la resistividad del hormigón.

En las últimas décadas se han presentado a la comunidad científica, un número significativo de estudios sobre matrices base cemento con adición de diferentes materiales (fibras de acero, fibras de carbono, polvo de grafito, escoria siderúrgica etc.) como elementos conductores, con el fin de dotar al hormigón final de propiedades conductoras y conseguir la multifuncionalidad del material final.

Por ello se ha planteado en esta investigación, la adición de material carbonoso conductor, como lo es la fibra de carbono, que además de variar las propiedades mecánicas, establece la posibilidad de mejorar la capacidad conductiva eléctrica del material. Las envidiables propiedades mecánicas y eléctricas de la fibra de carbono, la hacen ser la adición ideal para implantar esta novedosa tecnología, razón por la cual se ha decidido estudiar las fibras de carbono en esta tesina, con el reto de profundizar sobre el tema con las pocas investigaciones disponibles realizadas hasta el momento.

Pero el problema de la fibra de carbono es su disponibilidad y su coste económico, así que paralelamente se ha pretendido verificar la viabilidad de fibras de carbono recicladas para poder conseguir hormigones conductores a menor coste.

1.2.- OBJETIVOS

La finalidad del estudio experimental, radica en obtener y desarrollar un hormigón conductor cuyas funcionalidades, puedan permitir su aplicación en nuevos productos y usos en la construcción.

Inicialmente, se realiza una prospección de artículos, bibliografía y experiencias previas existentes, que hayan planteado anteriormente, vías de desarrollo de este tipo de materiales compuestos y que nos proporcionen soluciones previas a las problemáticas que

se puedan anticipar, tanto a efectos de fabricación o procesamiento, como a la metodología de ensayos de caracterización de las propiedades.

Se plantea conseguir la conductividad del hormigón, mediante la adición de fibras de carbono y otros subproductos derivados del reciclaje de materiales compuestos reforzados con fibra de carbono, verificando a la vez el tipo de matriz más conveniente.

Con el fin de desarrollar y procesar un material multifuncional, como puede ser un hormigón con adición de fibras de carbono, conviene analizar el material con el objetivo de conocer de antemano su comportamiento ante las diferentes funciones que deberá desempeñar.

Los diferentes aspectos analizados, se engloban dentro de los siguientes campos

- Condiciones de procesamiento; con el objetivo de avanzar en una dirección reproducible industrialmente y de costes razonables, considerando la disponibilidad y costes de las fibras, así como su idoneidad en los procesos de mezcla y fabricación del hormigón.

- Selección de materiales, esqueleto granular base del hormigón y adición en porcentaje y tipo de las adiciones de fibras de carbono recicladas

- Caracterización estructural; necesaria para definir espesores de uso y compatibilidad con los formatos y productos existentes, o como base para redimensionar los elementos finales de aplicación.

- Caracterización eléctrica; utilizada para conocer la conductividad y resistividad del material en función de la matriz y adición de fibra empleada, dato que marcará la funcionalidad del material y la variación de las propiedades conductivas.

- Estudio de la capacidad de sensorización del hormigón, gracias a la conductividad eléctrica del material y su variación asociada a modificaciones geométricas, estableciendo el factor de galga correspondiente.

- Análisis del comportamiento térmico a partir de las características eléctricas obtenidas, se comprobará la función calefacción por efecto Joule, enfocada a la posibilidad de fabricar elementos calefactables para exterior o poder dimensionar estos productos de forma previa en función de sus características conductoras y propiedades calefactables.

1.3.- METODOLOGIA

Esta tesis es fruto de la colaboración, entre el Departamento de Ingeniería Civil y Ambiental de la Universitat Politècnica de Catalunya (ETSECCPB) y la empresa Escofet 1886

S.A., establecida mediante la concesión de una ayuda en el programa de Doctorados Industriales (DI-2015-013) de la Generalitat de Catalunya.

Toda la preparación de moldes, fabricación de probetas y pruebas de fabricación, se realizaron en la planta industrial de la compañía situada en Martorell; mientras que la caracterización experimental se ha llevado a cabo, tanto en la propia empresa, como en diversos laboratorios de la UPC. Así, los ensayos de caracterización mecánicos han sido realizados en el laboratorio de Tecnología de Estructuras "Luís Agulló" de la ETSECCPB, los ensayos de caracterización eléctrica en el Laboratorio de Instrumentación y Bioingeniería de la UPC y la prueba piloto a escala real en las instalaciones de ESCOFET 1886 S.A.

A la hora de estructurar la formalización de la tesis y a pesar de que el doctorando no sigue una trayectoria académica, sino que sigue una trayectoria profesional, se optó por una tesis mediante artículos. La razón final de la elección de la misma era el interés, por las dos partes, de utilizar una estrategia centrada en la máxima transmisión de los resultados hacia la comunidad científica y la industrial, con el fin de demostrar la viabilidad del planteamiento y el aprovechamiento positivo, por parte de la empresa, de las experiencias obtenidas durante la investigación. Ello da lugar a una Tesis Doctoral compuesta por una compilación de artículos estructurada en capítulos, tal como se muestra en la Figura 1.2.

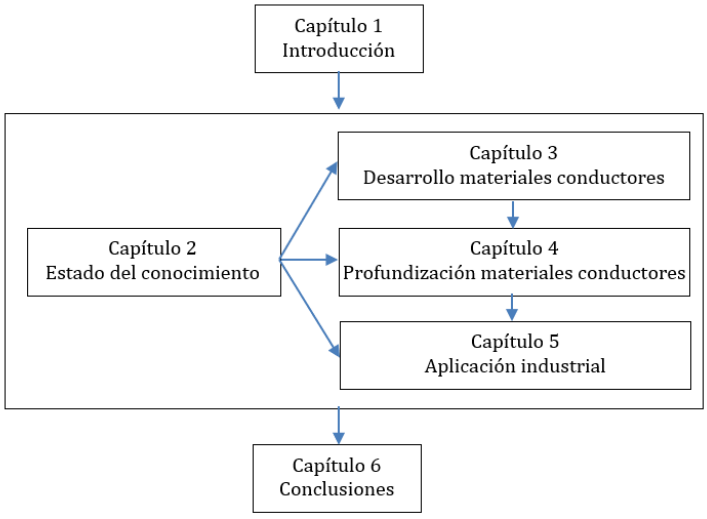

Figura 1.2. Organización documental de la Tesis Doctoral

En ella puede verse que el presente **capítulo 1** sirve a modo de Introducción y contextualización del proyecto, indicando la motivación de la tesis, los objetivos y el método utilizado.

El **capítulo** 2 se presenta un estado del conocimiento, para situar al lector en los caminos precursores a la presente tesis, en la misma dirección o en direcciones equivalentes. Ello no quita para que, en los capítulos posteriores, constituidos por los

artículos publicados, no exista una cierta referencia a trabajos previos en cada una de las líneas.

El **capítulo 3** presenta el artículo titulado *Development of conductive cementitious materials using recycled carbon fibres,* cuyos autores son: Faneca, G., Segura, I., Torrents, J.M. and Aguado. A., publicado en Cement and Concrete Composites. Vol. 92. September 2018 pp.: 135-144. https://doi.org/10.1616/ j.cemconcomp.2018.06.009.

El objetivo es evaluar el efecto de diferentes hormigones reforzados con fibras de carbono (HRFC) sobre las propiedades mecánicas y eléctricas de los materiales cementosos; para lo cual se incorporan diferentes tipos de fibras de carbono, con distintos contenidos (0.1–1.4% en volumen) a un hormigón convencional de partida convencional (HC) y un hormigón de ultra alta resistencia (UHPC).

En el **capítulo 4** se presenta el artículo titulado *Self-sensing concrete made from recycled carbon fibres* cuyos autores son: Segura, I., Faneca, G., Torrents, J.M. and Aguado. A., publicado en Smart Materials and Structures. Vol.28. Issue 10. October 2019. https://doi.org/10.1088/1361-665X/ab3d59

El objetivo es profundizar en lo mostrado en el capítulo anterior, haciendo énfasis, principalmente, en dos tipos de fibras (tipo fibrilado y de lámina), en diferentes contenidos (0.1 a 1.4% en volumen) para los hormigones de ultra alta resistencia. En este trabajo, las pruebas piezo-resistivas se realizaron tanto en condiciones de flexión como de compresión y teniendo en cuenta el efecto del contenido de humedad de las muestras

El **capítulo 5** presenta el artículo titulado *Conductive concrete made from recycled carbon fibres for self-heating and de-icing applications in urban furniture*, cuyos autores son Faneca, G., Ikumi, T., Segura, I., Torrents, J.M. and Aguado. A., aceptado para su publicación, en fecha del 10 de marzo de 2020 en la revista Materiales de Construcción. https://doi.org/10.3989/mc.2020.17019

Este artículo presenta un amplio estudio experimental que explora la capacidad conductora de transmisión de calor del hormigón con fibras de carbono recicladas para aplicaciones de descongelación y autocalentamiento a escala industrial y de laboratorio. A escala industrial, se fabricaron 3 bancos (700 × 2000 × 150 mm) con diferentes disposiciones de electrodos en las instalaciones industriales de Escofet 1886 y se probaron para evaluar la capacidad de calentamiento actual del material en aplicaciones de mobiliario urbano a escala real.

En el **capítulo 6** se presentan un análisis global del trabajo para intentar cohesionar los distintos artículos presentados, incluyendo las conclusiones tanto generales como específicas; así como las perspectivas de futuro de continuidad en esta línea de investigación, derivada de los trabajos realizados.

Como puede verse, los diferentes artículos incorporados, buscan un equilibrio de ámbitos entre el científico y el profesional, así como entre: materiales-estructuras-procesos. Esta estrategia responde a la creencia de que, para conseguir el éxito en la introducción de innovación en los procesos productivos, es necesario debe tener una visión global e integradora de los diferentes aspectos que conforman cada temática tratada.

Por último, hay que reflejar que se incorpora un capítulo específico de referencias, **capítulo 7**. El mismo integra, en un sólo capítulo, las referencias que hay en cada uno de los capítulos y artículos. Este planteamiento responde, por un lado, a evitar la repetición de referencias y, por otro lado, a intentar dar una mayor facilidad al lector y visibilidad a las propias referencias, al integrarlas en un capítulo único. Ello implica que las referencias que en los artículos viene por número, se transformen en este capítulo por orden alfabético.

La redacción de la presente tesis se ha realizado en lengua castellana, mientras que los capítulos correspondientes a los artículos publicados mantienen el idioma original en el que se han publicado en las correspondientes revistas científicas.

Capítulo 2: ESTADO DEL CONOCIMIENTO

2.1.- INTRODUCCIÓN

En cualquier proyecto de investigación, por una razón metodológica, antes de establecer cualquier nueva propuesta se requiere conocer hasta donde ha llegado el conocimiento en sus fases previas y cuáles son las lagunas existentes, en las que se pueda contribuir.

El objetivo del presente capítulo es realizar el estado del conocimiento que permitan identificar los puntos clave en los que se trabaja en este estudio de forma general. Para dar respuesta a este objetivo, en este capítulo se analiza trabajos previos existentes en la literatura técnica.

La búsqueda se ha centrado en las fibras y sus beneficios una vez adicionadas en el hormigón, la posibilidad que estas fibras sean conductoras, y económicamente sostenibles y finalmente analizar que funcionalidades pueden extraerse de su utilización.

Este análisis previo se destinaría también a recopilar datos útiles para el desarrollo de un hormigón conductor, a través de experiencias previas realizadas, analizando como otros autores han conseguido la conductividad de matrices cementicias y de qué forma han realizado su caracterización.

2.2.- DEFINICIÓN Y TIPOS DE HORMIGONES CONDUCTORES

2.2.1.- Definición

El hormigón, formulado como una mezcla de cemento portland, agregados finos y áridos gruesos minerales, con agua y aditivos químicos, es un material con escasa o despreciable conductividad eléctrica. Por ello no aporta característica funcional alguna distinta a las habitualmente requeridas de carácter estructural y de aislamiento.

Los materiales de construcción moderna de edificios, requieren cada vez más de propiedades funcionales que aporten posibilidades de calefacción, mejora de aislamiento térmico, aislamiento electromagnético, descarga electrostática etc., propiedades todas ellas que no están al alcance de un hormigón convencional, pero que sí podrían estarlo para un hormigón conductor.

Habitualmente, para la obtención de un hormigón conductor, se introducen en la matriz cementicia, fases conductivas como podrían ser partículas o fibras, que pueden afectar de forma positiva otras propiedades. Así, en el caso de la adición de fibras, además se mejoran las propiedades de ductilidad y absorción de energía del hormigón.

De las diferentes fibras que se pueden incorporar, las fibras de carbono, permiten obtener hormigón reforzado como el posteriormente investigado en este estudio, resultando un material con múltiples fases, en el que diferentes factores influyen en la conductividad resultante. La microestructura y naturaleza de la matriz, la fracción en volumen de la fibra adicionada y la humedad relativa del compuesto gobiernan la conductividad resultante.

La relación agua/cemento de la mezcla o las proporciones de fracciones de tamaño de áridos y la tipología de fibra empleada, también son parámetros que modificaran el comportamiento, ya que modificaran la conductividad y su naturaleza iónica o electrónica.

2.2.2.- Tipos de hormigones conductores

Existen diferentes experimentaciones con el objetivo de conseguir hormigones conductores, con distintas adiciones o fases de naturalezas diversas. Entre estas líneas de actuación está la incorporación de: *escorias de hornos*, *adición de finos o polvos conductores como el grafito*, *fibras de acero, nanofibras y nanotubos de carbono y fibras de carbono.*

Utilizando como fase conductora, *escorias de hornos de la producción de acero* compuestas químicamente por Ca, SiO_2 y Fe_2O_3 principalmente, se han estudiado pavimentos asfálticos y hormigones conductores (Xie *et al.*, 1995; Lu *et al.*, 2008). Gracias a la presencia de compuestos de hierro presentes en los áridos utilizados, la fase granular del hormigón pasa de ser aislante a conductora. Este tipo de adición tiene la ventaja de ser un

material de bajo coste económico, además de ser un material ambientalmente sostenible, en cuanto se está procesando un residuo.

Como contrapartida, hay que controlar cuidadosamente ciertos compuestos inestables que pueden afectar a las reacciones de hidratación del cemento. Las escorias de alto horno deben pasar por un periodo de estabilización a la intemperie de no menos de seis meses con el fin de eliminar residuos de óxido de calcio y magnesio libres, periodo tras el que se puede secar la escoria y triturar al tamaño deseado.

Otras experimentaciones en pavimentos de hormigón o asfalticos conductores, se ha desarrollado con la *adición de finos o polvos conductores como el grafito* (Liu and Wu, 2011), con el objetivo de conseguir un material que auto-monitorice sus tensiones con la variación de la conductividad asociada a la deformación geométrica del material y de su microestructura, factor que permitiría aplicar propiedades auto-sensitivas en las calzadas, para control del tráfico rodado, como serían por ejemplo frecuencias de paso o peso de vehículos.

Con la adición de *fibras de acero*, se han realizado ensayos a escala real (Yehia and Tua, 2000; Heymsfield *et al.*, 2013) con el objetivo de conseguir, gracias a la conductividad eléctrica del hormigón, pavimentos con capacidad propia de deshielo, gracias a la función de calefacción que puede adquirir el pavimento de hormigón, por efecto Joule. El empleo de fibras de acero suele acompañarse de grafito o humo de sílice (Bai *et al.*, 2017) como filler para mejorar la conductividad de pavimentos de hormigón, en los cuales las fibras de acero ya se emplean con asiduidad. Por contra, el flujo de cargas eléctricas a través de las fibras de acero genera corrosión de ellas mismas y degradación de propiedades resistentes y funcionales del material.

Las *Nanofibras y nanotubos de carbono*, son un tipo de adición investigadas más recientemente (Galao, 2012; Xun *et al.*, 2012; Nam and Lee, 2015; Jang, Kawashima and Yin, 2016; Yoo, You and Lee, 2017), pero con unos costes económicos elevados todavía para su aplicación en hormigones. Sus elevadas propiedades conductoras propiciarían elevada respuesta en el hormigón y su pequeño tamaño debería permitir mejores distribuciones en la matriz que otras fibras de mayor tamaño.

La utilización de *fibra de carbono* esta referenciada en diferentes estudios relacionados con la caracterización y con el desarrollo de diferentes funcionalidades de un hormigón conductor, bien en forma de fibra corta (D. D L Chung, 2000; Chen, Wu and Yao, 2004; Wen and Chung, 2007; Chung, 2012), analizando propiedades de sensorización (D. D L Chung, 2000; Chiarello and Zinno, 2005; Azhari and Banthia, 2012; Chung, 2012; Galao, 2012; Han, Ding and Yu, 2015), propiedades térmicas en aplicaciones para deshielo y curado a bajas temperaturas (Lai, Liu and Ma, 2014; Galao *et al.*, 2016), estudiando la conductividad en función de las dimensiones y relación de aspecto de la fibra (Wang, Wang and Jin, 2002), o en forma de malla de fibra de carbono (Lai, Liu and Ma, 2014).

En el caso de utilización de fibra de carbono, los factores precio y disponibilidad, también son determinantes en la transición de las investigaciones en laboratorio a aplicaciones a escala real, ya que la mayor parte de la producción de la fibra de carbono y otras fibras de elevadas prestaciones está directamente comprometida en aplicaciones aeroespaciales, de seguridad y deportivas, industrias con un alto valor añadido.

La utilización de fibra de carbono reciclada se antoja como una posible vía alternativa, si las propiedades de la fibra de carbono reciclada son similares a las de la fibra de carbono virgen utilizadas en los mencionados estudios.

2.2.3.- Funcionalidades de un hormigón conductor

Un hormigón conductor de la corriente eléctrica, como material funcional, puede cubrir nuevos requerimientos de aplicaciones novedosas o futuras. Estas aplicaciones pueden ser: *la sensorización del hormigón, apantallamiento electromagnético y funcionalidad térmica*, descritas posteriormente en esta apartado, pero además, entre otras, existen otras funcionalidades como; protección catódica de estructuras de hormigón armado (Carmona, Garcés and Climent, 2015), la captación de energía (Lee *et al.*, 2014; Wei *et al.*, 2014) o como toma de tierra de derivaciones eléctricas en edificios o torres de alta tensión (Zhang, Xu and Zhao, 2017). En base a estas aplicaciones, se pueden generar otros tipos de usos derivados, en diferentes campos de especialidades técnicas muy diferentes.

Sensorización del hormigón

Una forma de sensorizar o controlar las tensiones y deformaciones de una estructura, sin necesidad de sensores internos añadidos al material, pasa por la utilización de hormigones conductores (Chiarello and Zinno, 2005; Xun *et al.*, 2012; Han, Ding and Yu, 2015). Gracias a la conductividad del material y su variación al aplicar una carga, se puede percibir la deformación de la estructura y en régimen elástico la tensión correspondiente, tal como se muestra en la figura 2.1, donde se aprecia la variación de la resistividad longitudinal (línea continua) con la variación de la deformación longitudinal, en un ensayo dinámico de tensión axial (Chung, 2012).

La propia percepción de la deformación de un material se consigue gracias a que la variación unitaria de la resistividad eléctrica en volumen es proporcional y reversible (en régimen elástico) al esfuerzo al que es sometido y por tanto a su deformación unitaria. Si el esfuerzo es de compresión, la resistencia eléctrica en la dirección longitudinal del esfuerzo disminuye. En cambio, la resistencia aumenta al invertir la carga y aplicar una tensión de tracción (Galao, 2012; Yoo, You and Lee, 2017).

Para poder cuantificar la percepción de deformación, se emplea el factor de galga (FG), parámetro adimensional que representa la variación unitaria de la resistividad eléctrica frente a la deformación unitaria, según la siguiente ecuación 2.1:

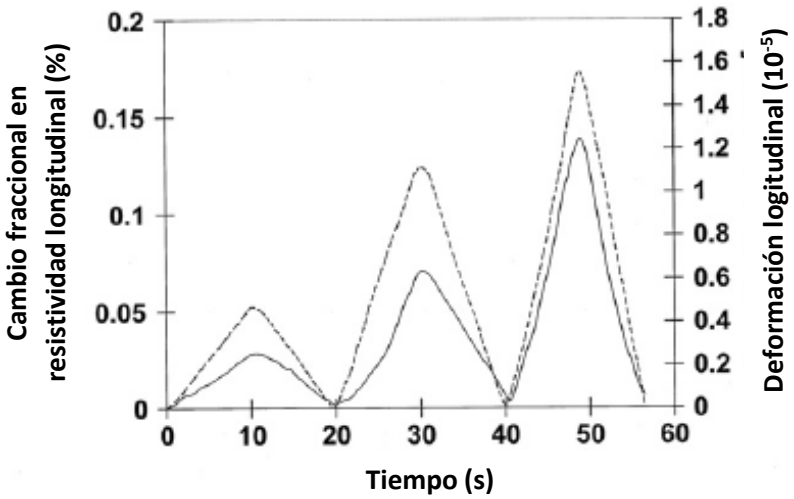

Figura 2.1.- Variación de la resistividad longitudinal (línea continua) con la variación de la deformación longitudinal, en un ensayo dinámico de tensión axial (Chung, 2012).

$$FG = \frac{\Delta\rho/\Delta\rho_0}{\Delta l/l_0} = \frac{\Delta\rho/\Delta\rho_0}{\varepsilon} \qquad \text{Ec [2.1]}$$

dónde: $\Delta\rho$ = variación de la resistividad eléctrica.
ρ_0 = resistividad eléctrica inicial.
Δl = variación de la longitud.
l_0 = longitud inicial.
ε = deformación unitaria.

La sensibilidad de la percepción de la deformación en hormigones conductores de la corriente eléctrica es muy elevada, con un (FG) de valor superior a 700 (en contraste con un (FG) de valor 2 para las galgas extensométricas de uso común (Chung, 2012). Esto es debido a que la variación de la resistencia eléctrica de un elemento, no se debe exclusivamente a los cambios dimensionales producidos por la aplicación de las cargas, sino también a la modificación de la resistividad eléctrica intrínseca del material. Modificaciones debidas a la variación del tipo de microestructura y la interacción de las fases que componen el material (matriz-fibra).

La funcionalidad de la percepción de la deformación es aplicable en el control de deformaciones en estructuras en servicio, o control de cargas y monitorización del tráfico en infraestructuras viales (Xun *et al.*, 2012). La percepción del daño estructural reportaría variaciones no reversibles de la resistividad eléctrica, de igual modo que se registrarían deformaciones permanentes, una vez superado el rango elástico del material.

El uso del hormigón conductor en la monitorización de infraestructuras, se ofrece como alternativa al empleo de otros sistemas de vigilancia y recogida de datos implantados con menor vida útil y costes de mantenimiento o sustitución asociados (Ceylan, 2014).

Apantallamiento electromagnético

El apantallamiento electromagnético de un material refiere a su capacidad de este para la protección electromagnética, evitando que esta lo traspase o si lo hace, sea atenuando su potencia.

El auge de las telecomunicaciones mediante sistemas de radiofrecuencia ha estimulado la aparición y estudio de materiales con función de apantallamiento electromagnético, capaces de proteger sistemas, principalmente electrónicos, sensibles a este tipo de radiación ambiental.

De la misma forma, pero en otro nivel, puede ser necesario este tipo de protección, en construcciones destinadas a albergar sistemas electrónicos estratégicos en instalaciones nucleares, aeroespaciales o militares. En estos casos la protección sería contra pulsos electromagnéticos producidos por detonaciones nucleares en altitud o sistemas armamentísticos similares en cuanto a efecto (Chung, 2012).

Si el apantallamiento se consigue por reflexión de las ondas electromagnéticas, este efecto puede utilizarse en sistemas de guiado de automóviles. Utilizando pavimentos conductores de corriente eléctrica con esta función mejorada y equipando a los vehículos con emisores y receptores de ondas electromagnéticas, sería posible desarrollar ayudas a la conducción autónoma y mejoras de sistemas de seguridad activos de los automóviles.

El apantallamiento de radiación electromagnética es una barrera en ambas direcciones. Una matriz base cemento no conductora se comporta como un dieléctrico, sin efecto de apantallamiento, por lo que necesita de una adición conductora de la electricidad. El efecto de apantallamiento se consigue mediante la reflexión y absorción de la radiación electromagnética, efecto gobernado por los dipolos eléctricos y magnéticos de la microestructura del material y fases que lo componen.

Existen diferentes tipos de materiales compuestos, con diferentes componentes, con funciones de apantallamiento útiles a diferentes frecuencias de radiación electromagnética (Chung, 2012). La utilización de un material para esta funcionalidad requeriría de una caracterización electromagnética además de la caracterización de la conductividad eléctrica.

Funcionalidad térmica

Como se ha mencionado en la introducción, la función calefacción de un hormigón conductor se consigue gracias al efecto Joule. Para poder utilizar un hormigón como resistencia, en la calefacción por efecto Joule, la resistencia eléctrica no puede ser muy elevada, ya que de lo contrario la intensidad de corriente circulante sería muy baja, haciendo ineficiente el sistema. Pero tampoco puede ser muy baja, pues se necesitaría de una intensidad de corriente eléctrica muy elevada para alcanzar la potencia suficiente.

Los materiales base carbono, como las fibras de carbono adicionadas en el hormigón, poseen una elevada conductividad térmica, además de eléctrica, un bajo coeficiente de expansión térmico y elevada resistencia a la corrosión. Estas características convierten a las fibras de carbono en candidatas para su adición en materiales compuestos cementicios destinados a aplicaciones térmicas como serían pavimentos con efecto deshielo (Galao *et al.*, 2016) o suelos radiantes par a interiores (Hambach *et al.*, 2016; Zhao *et al.*, 2019).

Un hormigón capaz de aumentar su temperatura de forma controlada, puede desarrollar muchas aplicaciones como la evaporación del agua de lluvia de una pista deportiva, calentar una habitación a través de paredes y/o suelo, derretir el hielo de una carretera o una pista de un aeropuerto sin el uso de sales descongelantes o calentar mobiliario urbano, habilitando su uso durante todo el año y evitando daños debidos a la nieve y el hielo.

Se han realizado pruebas piloto (Yehia and Tua, 2000) y ensayos a escala real (Heymsfield *et al.*, 2013) en zonas estratégicas como aeropuertos y puentes, donde los efectos adversos del hielo y la nieve en invierno, y las operaciones para su eliminación acarrean tanto problemas de seguridad como económicos. En las operaciones aeroportuarias, el tráfico aéreo y de servicios puede verse ralentizado o bloqueado en épocas invernales o ante tormentas de nieve, mientras que, en el caso rodado de carreteras, la seguridad puede verse afectada, así como la posibilidad de bloqueos kilométricos de vías de circulación. Adicionalmente, los sistemas empleados habitualmente para evitar estas situaciones, habitualmente mediante el uso de sales descongelantes, se debe realizar de forma externa y con métodos por los cuales estas sales ocasionan deterioro de las infraestructuras colindantes por oxidación o degradación e incluso la contaminación por escorrentía de suelos agrarios o ríos.

En estudios de pavimentos con efecto deshielo por calentamiento (Yehia and Tua, 2000; Galao *et al.*, 2016), sitúan la resistividad eléctrica en un orden de magnitud cercano a 10Ωm, como valor necesario de resistividad del hormigón para un efecto deshielo en un suelo con esta funcionalidad, valor necesario para poder incrementar como mínimo la temperatura del hielo adherido a la superficie de pavimento por encima de 3 °C y así poderlo fundir.

Si se consigue optimizar la dosificación económicamente (coste de la infraestructura) y restringir el consumo energético (coste de explotación), los materiales cementicios conductores, pueden ser una alternativa gracias a su durabilidad y prestaciones estructurales. Se han realizado estudios de costes asociados a diferentes sistemas de deshielo de pavimentos, reportando la utilización como pavimento de hormigones conductores, como alternativa viable a otros sistemas (Yehia and Tua, 2000).

Figura 2.2: Prueba piloto de pavimento conductor con efecto deshielo (Yehia and Tua, 2000)

En la tabla 2.1 se muestra una comparativa de costes entre diferentes alternativas, en la que se contabiliza tanto la inversión inicial, como los costes de explotación y mantenimiento, así como el consumo energético.

Sistema de calefacción	Coste aproximado $/m²	Coste anual de explotación $/m²	Consumo energético W/m²
Lámpara de infrarrojos	96	-	75
Calefacción por cable eléctrico	54	4.8	323 a 430
Agua caliente	161	250/nevada	473
Calefacción gas	378	2.1	-
Recubrimiento de hormigón conductor	48	5.4	516

Tabla 2.1.- Ejemplos de sistemas de calefacción comparados económicamente (Yehia and Tua, 2000).

Es interesante resaltar que la inversión necesaria comparando costes con un pavimento de hormigón convencional es prácticamente el doble (Heymsfield *et al.*, 2013), pero no superior a la inversión necesaria en instalaciones para calefactar pavimentos. Por el contrario, los costes de mantenimiento son reducidos, y similar el consumo energético, además tener la posibilidad de ser suministrado por energías renovables.

En el caso de interiores, ya existen aplicaciones de suelos radiantes por agua caliente o hilo conductor eléctrico, con costes de instalación y explotación superiores a sistemas de calefacción por caldera de agua caliente o bomba de calor tradicionales. El uso de un hormigón conductor en la ejecución de las soleras, simplificaría las instalaciones y su mantenimiento. No así el consumo, que habría que controlar mediante diseños de sectorización de las zonas calefactables y el empleo de energías renovables para el abastecimiento eléctrico.

La aplicación de esta funcionalidad del hormigón conductor en el ámbito urbano, permitiría dotar de mayor confort a equipamientos expuestos a bajas temperaturas, con limitación de su uso a estaciones cálidas, promoviendo lugares de encuentro ciudadano en el exterior. El uso del hormigón convencional en estas situaciones, genera superficies pétreas y frías no agradables para tal uso, sustituyéndose habitualmente por otros materiales como la madera, más susceptibles a la degradación, mayores costes de mantenimiento y menor vida útil.

2.3.- UTILIZACIÓN DE FIBRAS EN UN HORMIGÓN CONDUCTOR

2.3.1.- Uso general de las fibras en el hormigón

Las fibras son una forma efectiva de mejorar la resistencia a tracción del hormigón, añadiéndolas en un porcentaje relativamente pequeño. Adicionando fracciones en volumen de fibra entre un 0.5% y un 2.0%, mezcladas en el proceso de amasado del hormigón, estas actúan como puentes de unión de las fisuras y grietas que se producen en el proceso de fractura del hormigón. A efectos del Anejo 14 de la EHE, los hormigones reforzados con fibras (HRF), se definen como aquellos hormigones que incluyen en su composición fibras cortas, discretas, distribuidas aleatoriamente en su masa.

El objetivo del hormigón reforzado con fibras (HRF) es “coser” las fisuras que pueden producirse y que dejarían a la estructura fuera de servicio, como en el caso del hormigón armado. La diferencia está en que, en lugar de unas pocas barras, de diámetro relativamente grande y orientadas según una dirección determinada, en el HRF el refuerzo está constituido por infinidad de fibras de pequeño diámetro y aleatoriamente orientadas, a las cuales se transfieren los esfuerzos cuando la matriz empieza a fisurarse.

Gracias a la contribución de las fibras se puede controlar y mejorar la resistencia a tracción, la fisuración por retracción de los procesos de fraguado, la resistencia a impacto etc., estas mejoras de las propiedades han comportado en estos últimos tiempos a la reducción de espesores de diseño de las estructuras y aumentar la durabilidad (reducir la fisuración, disminuye la permeabilidad, reduciendo la posibilidad de ataques externos al hormigón).

Para posibilitar estos beneficios, es necesaria además de la resistencia mecánica propia de la fibra, una adecuada adhesión y/o anclaje de la fibra a la matriz cementicia, que pueda transmitir los esfuerzos de un componente a otro del hormigón. A demás es necesario que las fibras sean compatibles con el ambiente altamente alcalino de la matriz cementicia y no se degrade con el tiempo.

En la actualidad existen una gran variedad de tipos de fibras disponibles para uso comercial o en proceso de experimentación (ACI Committee 544, 2002). Estas tipologías

pueden clasificarse básicamente en función del tipo de refuerzo aportado (estructurales, no estructurales), o tipo de materia prima (acero, poliméricas, minerales…).

2.3.2.- Tipos de fibra.

Se pueden definir las fibras, empleadas en el hormigón, como elementos de reducida sección respecto de su longitud total. Los principales parámetros geométricos que las definen, son su forma, longitud (l_f), diámetro equivalente (d_f) y esbeltez (l_f/d_f).

La clasificación como estructural o no estructural de la finalidad de una fibra, depende de si se considera su contribución en el cálculo resistente de la estructura, sustituyendo parte o la totalidad del refuerzo de acero, o por el contrario solo se consideran efectos asociados a la resistencia al fuego, control de fisuración u otras funciones como por ejemplo la conductividad eléctrica, objeto de este estudio. Por supuesto cabe la posibilidad que se consideren combinadas todas las contribuciones que aporten.

Por su origen material las fibras más comúnmente utilizadas, serían las fibras metálicas, las fibras plásticas (polipropileno y polietileno) y las fibras de vidrio alcalino-resistentes. En un segundo escalón y con un uso más reducido o prácticamente residual, encontramos otros tipos como la fibra de aramida, basalto, alcohol de polivinilo y la fibra de carbono (objeto de análisis en este estudio).

Fibras metálicas

Principalmente de acero, con diámetros, longitudes y formas en función de la matriz de hormigón empleada, y sistema de producción. Fabricadas en acero al carbono, acero inoxidable y acero galvanizado. Densidad característica del acero (7800 kg/m^3) y una resistencia mínima de 345 MPa (según norma ASTM A820). Ampliamente utilizadas en pavimentos de hormigón, revestimientos de túneles, elementos prefabricados y estructuras de ingeniería civil. Tienen un módulo de elasticidad y resistencia a la tracción relativamente elevados, quedando protegidas contra la corrosión gracias el ambiente alcalino de la matriz cementicia. La unión a la matriz se produce por anclaje mecánico y adhesión, proporcionados por el conformado y rugosidad de la fibra respectivamente.

Fibras de polipropileno y polietileno

Se fabrican en varios formatos, medidas y formas, según al uso específico al que se destinan. Las microfibras de menor longitud y diámetro, se destinan principalmente a reducir la fisuración del hormigón por retracción en los procesos de fraguado, mejorando también la resistencia a impacto y al fuego. Fibras de mayor tamaño, denominadas macrofibras plásticas, si se utilizan como refuerzo del hormigón y permiten reducir la cuantía de armado de acero en situaciones específicas.

La mejora de la resistencia al fuego del hormigón reforzado con estas fibras, es consecuencia del bajo punto de fusión de estos polímeros, que permiten liberar espacio en la matriz de hormigón, posibilitando la expansión de gases del agua ocluida al aumentar la temperatura del material. Pueden ser fabricadas con superficies diseñadas para aumentar la capacidad de anclaje con la matriz o impregnadas con resinas que proporcionen mejor anclaje químico.

Fibras de vidrio

Fabricadas por extrusión de vidrio fundido a través de sistema de tamices, necesitan de un contenido mínimo del 16% de zirconio para mantener sus propiedades en el medio alcalino de las matrices de cemento. La utilización de estos tipos de fibras da lugar a los compuestos denominados AR-GFRC (*álcali-resitent-glass-fiber-reinforced-concret*). La matriz habitualmente empleada en los productos fabricados con refuerzo de fibra de vidrio, está formada por una mezcla de cemento y arena de hasta 1mm de diámetro en igualdad de proporción.

La fibra se añade en el proceso de amasado, o cortada en la boquilla de pistola en el caso de fabricar por proyección. Los productos finales son habitualmente prefabricados destinados a revestimientos de fachadas, cubiertas, elementos arquitectónicos, decorativos etc., normalmente excluidos de usos con prestaciones estructurales.

Fibras de aramida

Fabricadas a partir de copolímeros, cuentan con una elevada resistencia a la tracción y tenacidad. Altamente utilizada en materiales textiles y compuestos termoestables de uso militar, necesitan de un tratamiento superficial de recubrimiento epoxi, para mejorar la dispersión y adherencia en las matrices de hormigón. Al igual que las fibras de carbono, su empleo en hormigones es excepcional debido a su elevado coste material.

Fibra de basalto

Manufacturadas a partir de basalto fundido y centrifugado en un horno de gas, estas fibras de origen inorgánico, presentan propiedades intermedias entre la fibra de vidrio y la fibra de carbono. En particular cuentan con una elevada resistencia a elevadas temperaturas, que la habilitan para la mejora de la resistencia al fuego del hormigón.

Fibras de alcohol de polivinilo (PVA)

Son fibras de origen polimérico fabricadas a partir del alcohol de polivinilo $(C_2H_4O)_n$. Desarrolladas para el refuerzo de hormigones de ultra alta resistencia, gracias a su elevada resistencia (superior a las de la fibra de vidrio) y una unión molecular a la matriz de hormigón superior a la de cualquier otra fibra. Al ser poliméricas cuentan con las ventajas intrínsecas anteriormente mencionadas, para la mejora de la resistencia al fuego.

2.3.3.- Fibra de carbono.

La fibra de carbono es un material polimérico generado por síntesis a partir de otros compuestos, que se presenta en forma de multifilamentos compuesta principalmente por carbono (mínimo del 92% en peso). Cada filamento de carbono es la unión de muchos miles de fibras de carbono. Tiene propiedades mecánicas similares al acero y es tan ligera como la madera o el plástico. Por su dureza tiene mayor resistencia al impacto que el acero.

Por su estructura fibrosa o filamentosa posee propiedades ortotrópicas (diferentes propiedades mecánicas en sus ejes principales ortogonales) lo cual genera la necesidad de utilizarla junto con otros materiales, para generar otros materiales compuestos con mejores propiedades mecánicas o más equilibradas en sus ejes. De ahí que en sus aplicaciones se encuentre principalmente como una fase ordenada (en forma de tejidos) dentro de una matriz (generalmente termoestable de naturaleza epoxídica) de un material compuesto.

Sintesis de la fibra de Carbono

La fibra de carbono se sintetiza a partir de la oxidación de un polímero precursor, el más habitualmente utilizado es el poliacrilonitrilo (PAN), que normalmente se combina con otros polímeros: metil-acrilato, metil-metacrilato, vinil-acetato y cloruro de vinilo, todos derivados del petróleo, que es carbono concentrado, proveniente de restos de materia orgánica (fósiles).

En particular, el PAN es una fibra polimérica formada por largas cadenas de moléculas de carbono, oxigeno, nitrógeno e hidrógeno en forma de escalera, tal como se muestra en la figura 2.3. Cuando se calienta el PAN en correctas condiciones de temperatura, las cadenas de moléculas de carbono se juntan mientras los demás elementos se separan, los átomos de carbono del polímero cambian de distribución y forman una estructura estable de anillos fuertemente unidos que soportan los unos a los otros.

Cuando se calienta en las condiciones adecuadas, estas cadenas se unen una al lado de la otra, formando estrechas láminas de grafeno que con el tiempo se unen para formar un solo filamento cilíndrico. El resultado es generalmente 93-95% de carbono., tal como se muestra en la figura 2.4. Este proceso químico, más otros procesos mecánicos de hilatura combinados, dan como resultado la fibra de carbono.

Cada hilo de filamento de carbono es un conjunto de muchos miles de filamentos de carbono. Uno de estos filamentos es un tubo delgado con un diámetro de 5,8 micrómetros y se compone casi exclusivamente de carbono. La primera generación de fibras de carbono tenía un diámetro de 7,8 micras. Más tarde, se alcanzaron fibras con diámetros de aproximadamente de 5 micras.

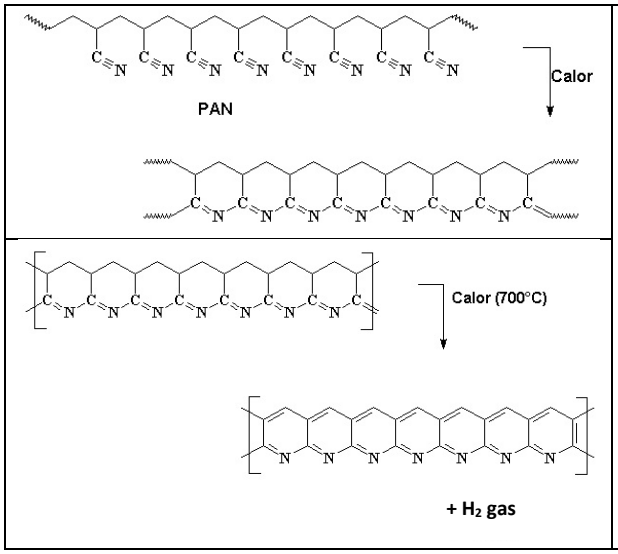

Figura 2.3: Formación de anillos por calentamiento del PAN (https://tecnologiadelosplasticos.blogspot.com)

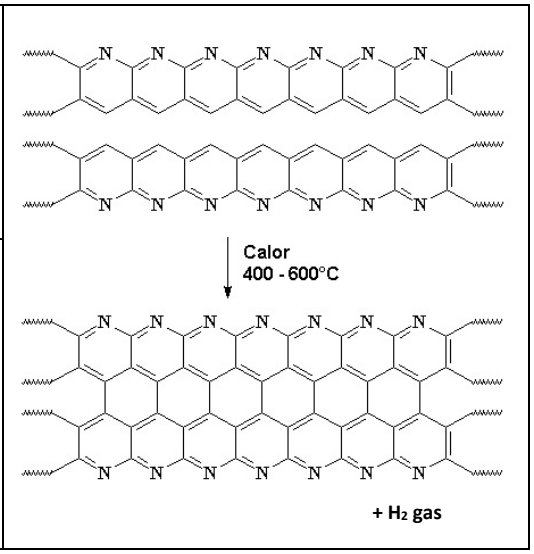

Figura 2.4: Proceso de síntesis por calor del polímero precursor (PAN) (https://tecnologiadelosplasticos.blogspot.com)

Otros fabricantes también utilizan precursores de rayón, proveniente de la celulosa y precursores de alquitrán, relativamente más baratos que el PAN pero menos efectivos. Cada tipo de precursor tiene su técnica de procesado, pero en general, todos siguen una secuencia similar.

Al material obtenido se le pueden variar algunas de sus propiedades, confiriéndoles alto módulo, o alta resistencia, mediante procesos de tratamiento térmico. El material que ha sido calentado de 1500 a 2000 °C (carbonización) exhibe la mayor resistencia a la tracción (5650 MPa), mientras que la fibra de carbono calentada de 2500 hasta 3000 °C (grafitización) muestra un alto módulo de elasticidad (531 GPa).

Propiedades de la fibra de carbono.

Las elevadas propiedades mecánicas de las fibras de carbono, combinadas con una baja densidad, dan como resultado unos valores de resistencia y rigidez específicos por encima de la gran mayoría de materiales. Los valores específicos de las propiedades mecánicas varían en función del tipo de fibra y de su proceso de manufactura, como se especifica en el capítulo anterior. Estas variaciones, determinan los diferentes tipos de fibra de carbono clasificadas por propiedades mecánicas:

- Ultra- alto módulo, tipo UHM (módulo > 450 GPa).
- De alto módulo, tipo HM (módulo de entre 350 – 450 GPa)
- Intermedio – módulo, tipo IM (módulo de entre 200 – 350 GPa)
- Módulo bajo y de alta resistencia a la tracción, tipo HT (módulo < 100 GPa, resistencia a la tracción > 3.0 GPa)
- Súper alta resistencia, tipo SHT (resistencia a la tracción > 4.5 GPa)

Fabricación de elementos con fibra de carbono

Los elementos manufacturados que cuentan con fibra de carbono son habitualmente materiales compuestos reforzados con fibras. Se entiende por material compuesto, aquel que está formado por dos o más materiales unidos, por diferentes procesos de fabricación, cuyo resultado es un material formado por dos o más fases diferentes que actúan de forma sinérgica, consiguiendo propiedades mecánicas y físicas superiores a las alcanzables por los mismos materiales por separado.

Especialmente valorados son los beneficios alcanzados en cuanto a propiedades específicas (características mecánicas en relación al peso). Esta particularidad ha generado el desarrollo de este tipo de materiales, primero en la industria aeroespacial, para después pasar otros sectores de mayor volumen, cuando sus costes de materia prima y fabricación se han reducido.

La concepción más habitual de los materiales compuestos con fibra de carbono es presentarse en forma de una matriz polimérica de tipo termoestable (epoxi, poliéster, viniléster, etc.), que recubren a una fibra habitualmente tejida (aramida, vidrio, carbono… etc.) que actúa como refuerzo. En estos casos la matriz polimérica, actúa como protectora de las fibras y permite la transmisión de esfuerzos entre las diferentes fibras no alineadas con las tensiones.

Existen multitud de procesos de fabricación, en función de los tipos de resina, fibra empleada y geometría final de la pieza, así como multitud de sectores que utilizan estos tipos de materiales reforzados con fibra de carbono.

La utilización de fibra de carbono en un material ya de por si compuesto como es el hormigón (material compuesto de matriz cerámica), no es una práctica habitual, ni extendida. Existen otras soluciones encaminadas a mejorar la resistencia a tracción del hormigón, empleando fibras más económicas y de diferentes procedencias como se describe en el apartado 2.3.2. Gracias la capacidad conductora de la fibra y su posible reutilización como residuo o subproducto abre vías de estudio y utilización de esta combinación.

2.4.- RECICLAJE DE MATERIALES REFORZADOS CON FIBRA DE CARBONO

2.4.1.- Origen de los residuos de fibra de carbono

Los materiales compuestos con fibra de carbono cuentan con numerosas aplicaciones y un aumento constante de su uso en diversos campos. Sectores tan variados como el aeronaval, transporte y generación eólica, utilizan este tipo de compuestos, gracias a su durabilidad, ligereza y posibilidad de realizar formas complejas respectivamente. En datos del año 2007 en el Reino Unido, un total de más de 2000 Tm de productos fueron fabricados con materiales compuestos reforzados con fibra de carbono, absorbiendo la

industria aeroespacial y defensa el 36% y la industria de generación eólica un 33%, como sectores con mayor peso (Job, 2010).

El proceso de reciclaje de este tipo de materiales resulta complejo, la utilización de matrices de resina termoestable hace que no sean reciclables fácilmente debido a su elevada reticulación química, que no las permite ser nuevamente fundidas y posteriormente moldeadas, como si se produce en los materiales termoplásticos.

Del total de deshechos de materiales compuestos, aproximadamente 3000 Tm corresponden a materiales compuestos con fibras de carbono generados entre Europa y Estados Unidos anualmente (McConnell, 2010), Aproximadamente entre 6000 y 8000 aeronaves comerciales, actualmente fabricadas mediante laminados de epoxi y fibra de carbono, tienen un fin de vida previsto hacia el año 2030.

Como se ha expuesto con anterioridad, ni la utilización de vertederos, ni la incineración son vías sostenibles de tratar estos residuos, por lo que se han generado diferentes alternativas y estudios para su reciclado y posterior uso o tratamiento. Aunque la producción de materiales compuestos con fibras de carbono solo representa el 2% en volumen de esta familia de materiales y que la mayoría del volumen corresponde a materiales compuestos con fibra de vidrio, el residuo de fibra de carbono generado tiene un valor 10 veces superior. Este último factor, añadido a los cortos ciclos de vida de los productos generados (2-40 años) y la visibilidad de las políticas de sostenibilidad, promocionan la investigación en este campo.

Los residuos de fibra de carbono pueden generarse desde el proceso de fabricación hasta el final de la vida útil del producto fabricado, presentándose tres formas de tipo de residuo principalmente:

- Fibra seca, restos o residuos de fibra generados en el proceso de fabricación, tejido o bobinado de la fibra de carbono.

- Fibra impregnada, residuos de fibra pre-impregnada con resina provenientes de materia prima fuera de uso por degradación de la resina (reticulación de la resina por rotura de la cadena de frio o sobrepasar la fecha de caducidad del pre-impregnado).

- Productos laminados, residuos de fibra de piezas monolíticas, recortes de fabricación, sobrantes y piezas al final de su vida útil.

2.4.2.- Vías de reciclaje de la fibra de carbono

De forma básica existen dos categorías de procesos principales para el reciclaje de materiales compuestos termoestables reforzados con fibras, en este caso particular de fibras de carbono.

Estos dos procesos, tal como se muestra en la figura 2.5, son: uno, principalmente mecánico y, otro en el que además intervienen procesos térmicos, tras un primer estadio de triturado. En función del proceso de reciclado empleado, la fibra resultante puede reutilizarse en diferentes aplicaciones.

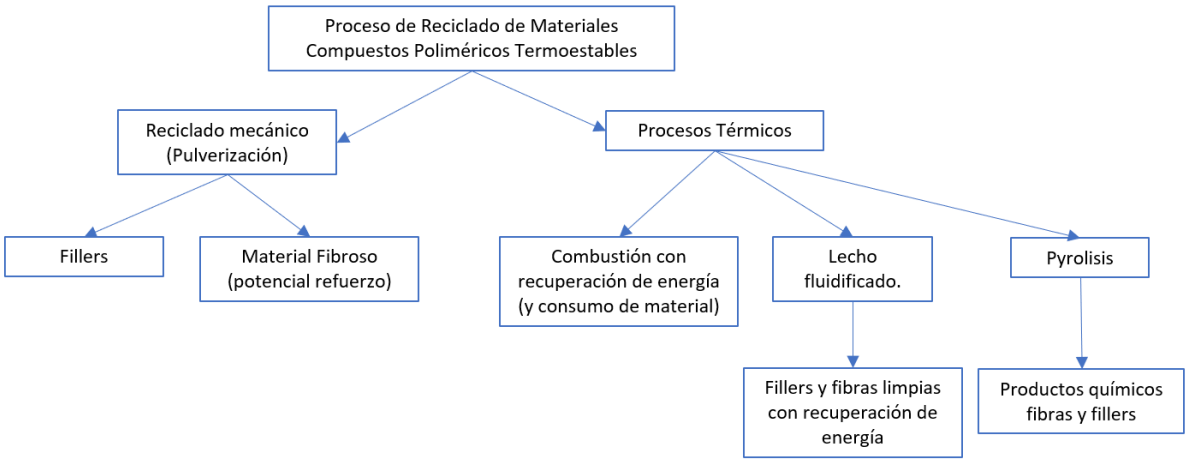

Figura 2.5: Procesos de reciclado de materiales compuestos termoestables (Pickering, 2006)

Reciclado mecánico

Consiste en reducir el tamaño de los residuos, mediante etapas sucesivas de tronzado y triturado. A mayor tamaño de residuo, la velocidad del proceso es menor, aumentando la velocidad en etapas posteriores, conforme se reduce el tamaño de partículas.

En una primera etapa se reduce el tamaño de los residuos a 50-100 mm, posibilitando la separación de insertos metálicos y otros componentes de diferente naturaleza material, consiguiendo además cierta compactación que reduce los costes de transporte por reducción del volumen.

En un proceso posterior a mayor velocidad de molido, se consiguen tamaños inferiores de residuo, con medidas entre 10 mm y 50 µm. Las fracciones más finas de tamaño están compuestas en mayor proporción, por un polvo de polímero y cargas minerales, mientras que las fracciones de mayor tamaño, cuentan con una parte más fibrosa y mayor coeficiente de forma (partículas alargadas). En este proceso se obtiene un residuo fibroso y un polvo o filler, adicionable a matrices termoplásticas como carga prácticamente mineral.

Recuperación de energía y material por combustión

Por un proceso de combustión, se extrae energía calorífica de la matriz polimérica a razón de 30000 KJ por Kg de residuo (Pickering, 2006), mientras que las fibras de vidrio o de carbono, si bien no se descomponen, sufren tal grado de degradación que no las hace aptas para un uso posterior. La degradación de las fibras, por combustión del material

compuesto, es mayor cuanto menos controlado es el proceso de oxidación que se realiza, por lo que por esta vía, la recuperación de material incombustible (las fibras), solo tiene cierto valor si la combustión se produce en los hornos de fabricación del cemento. De esta forma se incorporan al cemento los materiales incombustibles del material compuesto (fibras y minerales de carga inorgánica).

Lecho fluidificado

Las fibras de refuerzo recicladas, de carbono especialmente, tienen un mayor valor si son aptas para ser reutilizadas nuevamente en materiales compuestos de alto valor añadido. Para ello es necesario que las propiedades de las fibras se mantengan tras el proceso de reciclado y estas queden libres de impurezas. Con este fin se han desarrollado procesos de reciclaje, mediante la utilización de un lecho fluidificado de arena de sílice, en el cual se introducen los residuos hasta un tamaño aproximado de 25 mm. La arena se fluidifica con un chorro de aire a 450-550 ˚C (Ver figura 2.6) que volatiliza la resina polimérica y suspende las fibras en el gas resultante, pudiendo ser separadas en un proceso secundario, en el cual se eliminan por completo los restos de polímero.

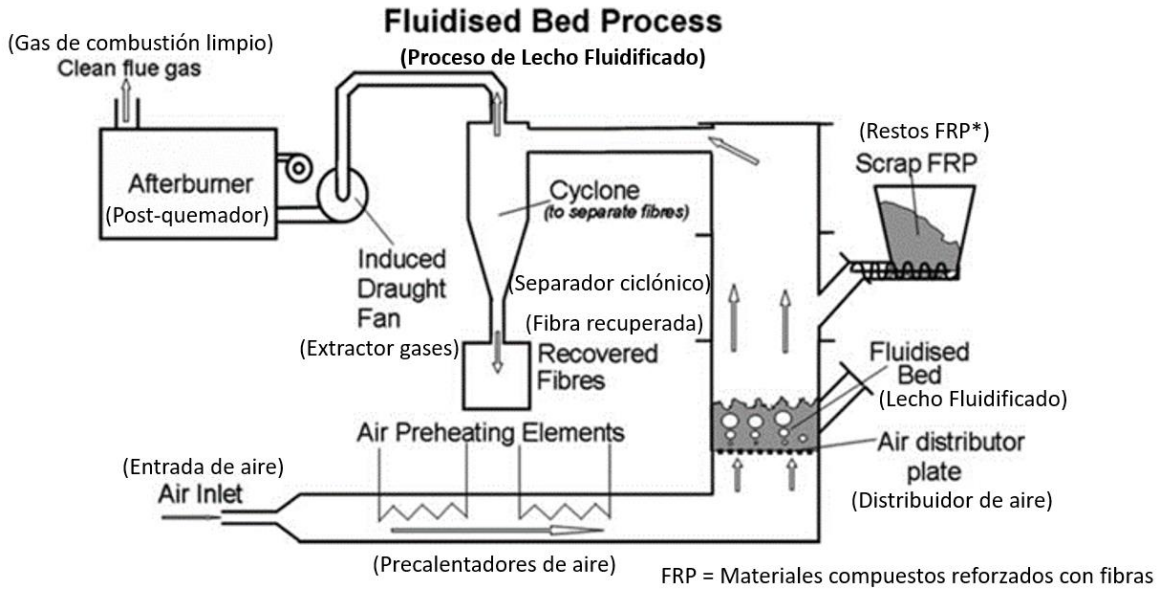

Figura 2.6.- Proceso de reciclado por lecho fluidificado (Pickering, 2006)

Las fibras de vidrio obtenidas por este proceso mantienen el 50% de la resistencia a tracción inicial, mientras que la fibra de carbono, mantiene hasta el 80% de estas propiedades. La rigidez o módulo de elasticidad inicial de las fibras se mantiene tras el procesado. Son por tanto fibras reutilizables en aplicaciones con prestaciones inferiores a las iniciales

Pirólisis

En los procesos de pirólisis, tal como muestra el esquema de la figura 2.6, el material compuesto se calienta en ausencia de oxígeno, o en cantidades limitadas. En estas condiciones. Los compuestos orgánicos que formulan la resina se descomponen en compuestos orgánicos de menor peso molecular (gases y líquidos), que son más sencillos de separar de las fibras.

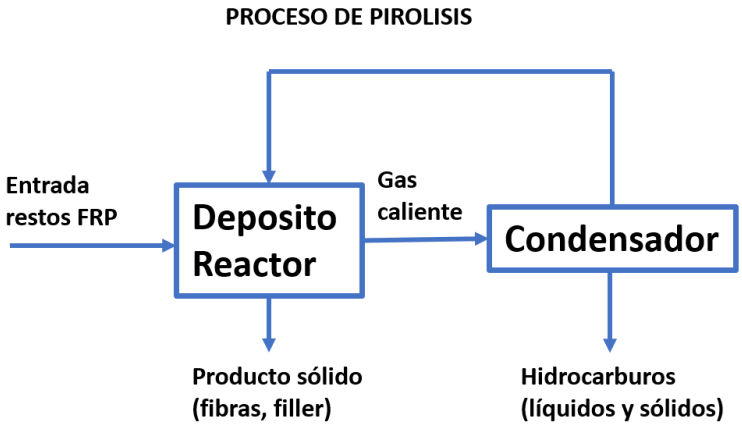

Figura 2.7.- Proceso de pirolisis (Pickering, 2006)

Cuanto menor es la temperatura a la que se produce el proceso de pirólisis, menor es la degradación de las características mecánicas de la fibra de carbono, pero mayor es el tiempo de ciclo necesario en el reactor y se necesitan de agentes catalizadores que aceleren los procesos de descomposición de la resina. Las fibras de carbono obtenidas por este proceso de reciclado pueden mantener hasta el 90% de sus propiedades mecánicas iniciales, así como obtener fibras con superficies prácticamente libres de resina, posibilitando de esta forma su uso en aplicaciones de altas prestaciones de refuerzo, con usos próximos al de la fibra original.

2.5.- CONCLUSIONES

De este repaso del estado del conocimiento, se ha podido comprobar una extensa lista de referencias de investigaciones centradas en cómo mejorar la conductividad del hormigón. Muchas de ellas enfocadas en la utilización de la fibra de carbono como fase conductora en una matriz de hormigón convencional de forma generalizada.

Contrasta en los últimos tiempos, el empleo de materiales de última generación en su nanosíntesis (nanotubos de carbono y nanofibras de carbono), con materiales de uso más extensivo como las fibras metálicas, empleadas incluso en ensayos a escala real como se ha referenciado.

Excepto para la evaluación de propiedades mecánicas, no hay estudios enfocados a la capacidad conductora asociada de las fibras de carbono recicladas adicionadas en el hormigón. La irrupción de estos tipos de fibras, genera una amplia variedad de tipologías sumada a las fibras de carbono convencionales.

La alta variedad de tipologías de fibras hace necesarios estudios comparativos de la utilización de estas, asociadas a diferentes matrices de hormigón, verificando la modificación de las propiedades conductivas en cada combinación.

Aspectos como la trabajabilidad, la rentabilidad, disponibilidad y compatibilidad con diferentes mezclas de hormigón, convencionales o más recientes, no están completamente contrastadas en las referencias consultadas o hace falta revisarlas con los últimos avances.

Esta tesis doctoral procura poner foco en estas particularidades, a la vez que se desarrolla el estudio de las propiedades conductoras de forma teórica, aplicando en test a escala real los resultados. De esta forma varias son las vías desarrolladas diferentes a las encontradas en las referencias consultadas:

- Utilización de diferentes matrices de hormigón en cuanto a tamaño del esqueleto granular y volumen de pasta.
- Introducción de la trabajabilidad como condicionante de uso, pero también como variable que se combina con la dispersión de las fibras y por lo tanto de las características conductivas.
- Búsqueda, evaluación y aplicación de fibras de carbono recicladas, con su correspondiente etiqueta sostenible, tanto ambiental como económica.
- Evaluación en condiciones industriales de la fabricación de estas tipologías de adiciones, además de la aplicación en caso real además del estudio teórico de las características funcionales añadidas al hormigón.

Capítulo 3[1]: DEVELOPMENT OF CONDUCTIVE CEMENTITIOUS MATERIALS USING RECYCLED CARBON FIBRES

Abstract

Conductive cementitious materials have gained immense attention in recent years owing to the possibility of achieving multifunctional materials. The usual approach has been to incorporate carbonaceous nanomaterials and/or virgin carbon fibres into cementitious matrices. This paper presents the first research devoted to the development of conductive cementitious materials using recycled carbon fibres (rCFs). Four different types of PAN-based rCFs were studied, by varying the aspect ratio and supplying characteristics, in two concrete dosages: conventional and ultra-high-performance concrete mixes. Two mixing methods—dry and wet—commonly used to fabricate fibre-reinforced concrete were considered. The results obtained in our result have shown that wet mix method achieves better workability of the mixes and good dispersion of the fibres. Furthermore, electrical resistivity values in the range of 3–0.6 Ω·m were obtained for rCF contents ranging from 0.2 to 0.8% in vol. The obtained results demonstrate the possibility of using rCF to develop multifunctional cementitious materials and thus enhance the possibility of using these

[1] El presente capítulo se corresponde con el artículo publicado por Faneca, G., Segura, I., Torrents, J.M. and Aguado, A. "*Development of conductive cementitious materials using recycled carbon fibres".* Cement and Concrete Composites. Vol. 92. September 2018 pp.: 135-144. https://doi.org/10.1616/j.cemconcomp.2018.06.009

materials from an industrial point of view. Furthermore, new possibilities are created for the recycling of carbon fibre composites to obtain high-added-value products.

Keywords: Conductive concrete; Recycled carbon fibre; smart cementitious materials.

3.1.- INTRODUCTION

Concrete is currently the most widely used construction material and is likely to remain the predominant material in the near future. It forms an integral part of global civil infrastructures, ranging from small buildings to large structures such as tunnels, long-span bridges, and offshore platforms. Moreover, most of the current infrastructure in the developed world is past its designed service-life. One in three railway bridges in Germany is more than 100 years old, as are half of London's water mains. In America, the average bridge is 42 years old and the average dam is 52 years old. The American Society of Civil Engineers rates approximately 14,000 of the country's dams as 'high hazard' and 151,238 of its bridges as 'deficient' (The Economist, 2015). The European Innovation Partnership on Smart Cities and Communities (EIPSCC) evaluated key urban infrastructure and most cities were described as 'aged and stressed' (European Innovation Partnership on Smart Cities and Communities, European Innovation Partnership on Smart Cities and Communities, 2013).

As most of Europe's infrastructure is already built, in the near future, efforts must be made to enhance the safety, efficiency, energy consumption, structural performance, and sustainability of new and existing buildings and infrastructure. A way forward to overcome the aforementioned problems could be the use of smart, multifunctional construction materials. The term 'multifunction' was coined to highlight the ability of a material to simultaneously exhibit specific desirable electronic, magnetic, optical, thermal, or other properties to satisfy previously unattainable performance metrics (Salonitis *et al.*, 2010). The development of smart materials and infrastructure is a hot research topic and an interesting focus for public opinion. Recently, energy-harvesting tiles were used during the Paris marathon of 2013 and helped to produce 4.7 kWh of energy (Khadilkar, 2013). Current research trends in smart cementitious materials include self-healing concrete (De Muynck, De Belie and Verstraete, 2010; Wiktor and Jonkers, 2015), enhanced bioreceptivity concrete (Manso, De Muynck, *et al.*, 2014; Manso, Mestres, *et al.*, 2014), mortars with biocide characteristics (Vaquero *et al.*, 2016), and development of conductive cementitious materials.

The incorporation of conductive phases into cementitious matrices has been one of the most popular methodologies to obtain conductive and thus multifunctional cementitious materials. The early works of Chung et al. (Chen and Chung, 1996; Shi and Chung, 1999; D D L Chung, 2000; D. D L Chung, 2000) demonstrated the possibility of developing multifunctional cementitious materials by adding carbon fibres into concrete. Several studies have considered this path and it is still a topic of interest. The incorporation

of carbonaceous materials (carbon fibres, carbon black, and carbon nanomaterials) into cement-based materials has achieved a wide range of novel functionalities. Apart from self-sensing capabilities (Chung, 2012; Xun *et al.*, 2012; Ding *et al.*, 2013, 2015; Gomis *et al.*, 2015), such an approach has resulted in cementitious materials with other properties, such as electromagnetic shielding (Zornoza *et al.*, 2010; Micheli *et al.*, 2017), self-heating (Lai, Liu and Ma, 2014; Gomis *et al.*, 2015; Wu, Liu and Yang, 2015; Galao *et al.*, 2016), cathodic protection of structures (Jing and Wu, 2011; Carmona, Garcés and Climent, 2015), and chloride removal (Cañón *et al.*, 2013; Carmona, Garcés and Climent, 2015).

Conductive cementitious materials can be obtained by incorporating different type of functional materials. Han et al (Han, Ding and Yu, 2015) identified up to ten different functional materials that have been used up to date to develop conductive multifunctional cementitious materials, including shortcut carbon fibres (CF), carbon nanotubes and nanofibers (CNT/CNF), carbon black, steel slag, and steel fibres. The use of steel fibres presents a high potential to develop conductive cementitious materials, i.e. for de-icing applications (Bai *et al.*, 2017), since they are actually been widely used in the civil engineering industry as sole reinforcement in structural concrete applications.

However, there are some drawbacks about using steel fibres to develop multifunctional cementitious materials, since the applied current may promote the corrosion of the fibres. Thus, carbon products were used to replace steel shavings in the conductive cementitious materials mixture design (Gomis *et al.*, 2015). Among all functional materials used up-to-date, cementitious matrices with either chopped CF and CNT/CNF are the most extensively and comprehensively studied in the literature (Han, Ding and Yu, 2015). More recently, other authors have also been considered the utilisation of graphene mixed with other carbonaceous materials to develop self-sensing cementitious materials (Yoo, You and Lee, 2017).

Along with the laboratory scale studies, there are some examples of real scale use of conductive cementitious materials in the literature. One of the first works was presented by Tuan in 2008 (Bai *et al.*, 2017), using a mix of carbonaceous materials and steel fibres. Most of the real-scale tests were intended for de-icing applications (Heymsfield *et al.*, 2013; Lai, Liu and Ma, 2014), and for self-sensing applications (Xun *et al.*, 2012). However, we are still far away to find multifunctional cementitious materials fully incorporated into the civil engineering industry. Recently some efforts have been made to commercialise chopped carbon fibre but the costs are significantly higher than those of other fibres used in the civil engineering industry.

A possible way to achieve low-cost multifunctional cementitious materials is the use of recycled carbon fibres (rCF). Recycled carbon fibres are mainly obtained from aerospace composite scrap. Among many different methods, most of the commercially available rCF are obtained via pyrolysis. This process allow a high retention (up to 90%) of the properties exhibited by virgin carbon fibres (Pickering, 2006; Pimenta and Pinho, 2011). The use of this kind of fibres in cementitious materials has gained attention last years, as more

companies have started worldwide to provide rCF in a commercial way. Most of recycling processes yield rCF with high retention of mechanical properties (Pimenta and Pinho, 2011) but with a 30 to 40 percent cost savings versus virgin carbon fibre.

The objective of this article is to evaluate the effect of different rCFs on the mechanical and electrical properties of cementitious materials. Accordingly, different types of rCFs were added with different contents (0.1 to 1.4% in volume) to conventional concrete (CC) and ultra-high-performance concrete (UHPC) dosages. The effect of the incorporation of rCF on the slump flow was evaluated. Furthermore, compressive and flexural strength measurements were obtained in concrete samples along with electrical measurements. Finally, rCF dispersion was evaluated via visual inspection.

3.2.- RESEARCH SIGNIFICANCE

This study is the first research devoted to the development of conductive cementitious materials using rCF. Other researchers have studied the incorporation of rCF into polymeric matrices and evaluated their mechanical and electrical properties (Wong, Pickering and Rudd, 2010; Turner, Pickering and Warrior, 2011; Akonda, Lawrence and EL-Dessouky, 2013). Only the recent work by Nguyen et al. has evaluated the effect of these kinds of fibres on the mechanical properties of cementitious materials, but the rCFs used were reclaimed carbon fibres that were not treated to eliminate polymer residue (Nguyen, Carvelli, *et al.*, 2016; Nguyen, Fujii, *et al.*, 2016). The main aim of this study is to provide insights into the use of rCF as a conductive phase to develop multifunctional cementitious materials. The research outcome might facilitate the development of novel multifunctional cementitious materials that can be employed in the civil engineering industry and thus modify the actual paradigm of our structures.

3.3.- MATERIALS AND METHODS

3.3.1.- Concrete mixing proportions and raw materials.

Two different concrete mixing proportions were used in our study (see Table 3.1): a conventional concrete mix (CC) and an ultra-high-performance concrete mix (UHPC). The main difference between both mixing proportions is the granular skeleton and cement content and they were selected to evaluate the possible presence of a double percolation phenomenon.

This phenomenon was firstly described by Wen *et al.* (Wen and D. D L Chung, 2006) and it involves fibre and cement paste percolation, as the aggregates might determine the existence of electrical conductivity through the cement paste. They demonstrated this effect in conductive cementitious materials as the aggregates might determine the existence of electrical conductivity through the cement paste. The maximum aggregate size in the UHPC

dosage is 1 mm whereas that in the CC dosage is 12 mm. The water-to-cement ratio (w/c) also differed in both mixes, 0.45 in the CC mix and 0.14 in the UHPC mix.

Component		Dosage (kg/m³)	
		CC	UHPC
Cement		400	800
Filler		260	220
Sand (0–3/0–1 mm)		500	1161
Pea gravel (2–4 mm)		520	--
Gravel (4–12 mm)		400	--
Additives	Glenium B255	16	--
	Glenium ACE425	--	30
	Meyco MS685	--	57
Water		180	110

Table 3.1. Concrete mixing proportions for conventional and ultra-high performance mixes

The cement selected to produce different mixtures was CEM I 53.5R. Filler was incorporated into the different dosages to achieve an optimum workability of the mixes with a low consumption of superplasticisers. The aggregates used for the CC mix were all granite and the filler was marble dust. The sand used for the UHPC mix was siliceous sand and the filler was calcium carbonate (Betoflow). A polycarboxylate superplasticiser (Glenium B225) was used for the CC mix and the UHPC dosage used both a polycarboxylate superplasticiser (Glenium ACE425) and nanosilica suspension (Meyco MS685) to provide self-compacting characteristics to the concrete mix.

3.3.2.- Recycled carbon fibres

The rCFs evaluated were PAN-based carbon fibres in all cases. The rCFs were provided by ELG Carbon Fibre Ltd. (CFRAN, C10/30, and CT12) and CAR FiberTec (CFTrim). The characteristics of all the rCFs are listed in Table 3.2, CFRAN and C10/30 are monofilament rCFs differing in their average length; CT12 and CFTrim are fibrillated sheets. The fibre factor, F, illustrates the effect of both the volume fraction and geometrical characteristics of the fibres and was first proposed by Narayanan and Darwish (Narayanan and Darwish, 1987) as equation 3.1:

$$F = \beta \cdot V_f \cdot L_f / d_f \qquad \text{Eq [3.1]}$$

where: β is the fibre shape factor (0.50 for round fibres), V_f is the volume fraction of fibres, and L_f and d_f are the length and diameter of the fibre, respectively (L_f/d_f: fibre aspect ratio). Both the fibre factor and mix design determine the maximum concentration of fibres in a given concrete dosage. The fibre dosage varied from 0.1% to 1.4% in volume.

Property	Value			
	CFRAN	C10/30	CT12	CFTrim
Diameter (µm)	7.5		7†	
Nominal length (mm)	6 - 60	10-30	12	12
Average length (mm)	40	20	12	12
Density (kg/m³)	1800			1760
Tensile strength (MPa)	3150		4150	4200
Young modulus (GPa)	200		252	240
Electrical resistivity (Ω·m)	0.103/0.34††			0.016
Fibre factor (-)	$4286 \cdot V_f$	$1428 \cdot V_f$	$12 \cdot V_f$	

† The effective diameter of the fibrillated sheets is 500 µm.

†† The electrical resistivity varies if the measurement is made lengthways (0.103) or across the cross-section (0.34)

Table 3.2. Properties of recycled carbon fibres as given by the suppliers.

3.3.3.- Sample fabrication

Several methods, varying in complexity, are described in the literature to disperse carbon fibres into cementitious matrices, although most of them are significantly different from the normal practice. In this study, concrete samples were intended to be produced using a fabrication procedure as close as possible to the industrial processes. Thus, the different concrete mixes were fabricated at the industrial installations of the company Escofet 1886. Specimens with dimensions 40x40x160 mm were fabricated from the mixes indicated in Table 3.1 according to UNE-EN 196-1 (AENOR, 2005). Two sets of samples were fabricated from each mix, one for the mechanical measurements and the other for the electrical measurements. The dispersion of carbon fibres is one of the most critical issues in the fabrication of carbon fibre-reinforced cementitious materials.

Many different methods are available in the literature, ranging from the surface modification of the carbon fibres, the incorporation of different admixtures (methylcellulose, water reducing agents, etc.), to the use of physical methods as ultrasonic sonication (Han, Ding and Yu, 2015; Gao *et al.*, 2017). Our aim was to work as close as possible to the real practice and the actual concrete compositions used in the precast concrete industry. In this work, rCFs were added to the mix using two methods normally used by the construction industry to manufacture fibre-reinforced cementitious materials: in the dry mix (D) after incorporating the cement and aggregates and in the wet mix (W) after incorporating the water and additives. Furthermore, reference samples were obtained with no addition of rCF.

The electrodes used for the electrical measurements were stainless steel set screws of length 5 cm, which were dipped 3.5 cm into the concrete samples. Figure 3.1 shows a scheme on the electrodes positioning on the specimens.

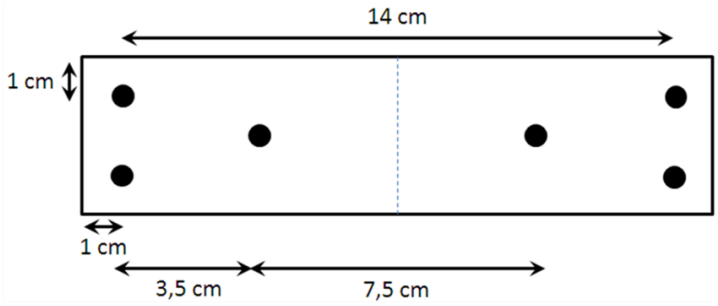

Figure 3.1. Location of the electrodes in the specimens

The samples were cured in a curing chamber (20 ± 2 °C; 95 ± 5% relative humidity) for 28 days. The sample notation was carried out according to the following code: CC/U distinguishes between CC and UHPC (denoted as U) mixes, C_f indicates the fibre content (varying from 00 for the reference sample to 14 for the sample with 1.4% fibre content), f indicates the fibre type, and M indicates the mixing method of the fibres (D or W).

$$\{CC/U\} - C_f - f - M$$

3.3.4.- Characterisation methods

The slump flow was measured according to UNE-EN 1015-3 (AENOR, 2000) prior to the elaboration of the specimens for all the mixes except CFRAN fibres. Flexural and compressive strength measurements were obtained in the concrete samples according to UNE-EN 196-1 (AENOR, 2005); three and six replicates were made for each dosage. The electrical characterisation of the samples was performed using an Agilent HP 4192A impedance analyser and using an instrumentation amplifier as the front-end to allow 4-probe measurements (Gersing, 1991) with an effective voltage of 1 V AC to avoid polarisation effects in the electrodes (Wen and D D L Chung, 2006; Wen and Chung, 2007). The measurements were obtained with the frequency scanning from 10 Hz to 1 MHz, providing electrical impedance (Z, in Ω) and phase (ϕ, in °). The electrical impedance is described by equation 3.2 and is composed of a real part (electrical resistance, *R*) and an imaginary part (reactance, *X*). *R* and *X* are obtained from equations 3.3 and 3.4:

$$Z = R + j \cdot X \qquad \text{Eq [3.2]}$$

$$R = Z \cdot \cos\left(\frac{\phi \cdot \pi}{180}\right) \qquad \text{Eq [3.3]}$$

$$X = Z \cdot \sin\left(\frac{\phi \cdot \pi}{180}\right) \qquad \text{Eq [3.4]}$$

Finally, the electrical resistivity (ρ, in Ω·m) is obtained using equation 3.5:

$$\rho = R \cdot \frac{S}{l} \qquad \text{Eq [3.5]}$$

where S is the effective transverse section (0.0016 m2 in our study) and l is the measurement length (0.07 m in our study). All the samples were allowed to reach hygrothermal equilibrium by maintaining them under laboratory conditions for 15 days after the completion of the curing period. The rCF dispersion in the cementitious matrix was evaluated by visual inspection.

3.4.- RESULTS

3.4.1.- Physical and mechanical properties

The slump flow variation evaluated for different rCFs is shown in Figure 3.2. The slump flow was not measured in the CC-CFRAN-D samples owing to the difficulties observed during the mixing of the samples. The excess length of this rCF (which was larger than the maximum size of 60 mm provided by the supplier) and the characteristics of the concrete dosage resulted in a significant reduction in the mix workability. The data were grouped into two sets according to the mixing method. The samples with the rCF incorporated into the wet mix (W samples) exhibited slightly larger slump flow for different fibre contents. Furthermore, the rCFs provided as fibrillated sheets (CT12 and CAR) exhibited larger slump flow and thus better dispersion of the fibres in the cementitious matrix than those presented as single fibres (CFRAN and C10/30). For all the samples, it was observed that the slump flow was reduced as the content of rCF was increased, which is consistent with the results presented in other studies with virgin carbon fibres, although the mixing methods were different ((Ding *et al.*, 2013; Yakhlaf, Safiuddin and Soudki, 2013).

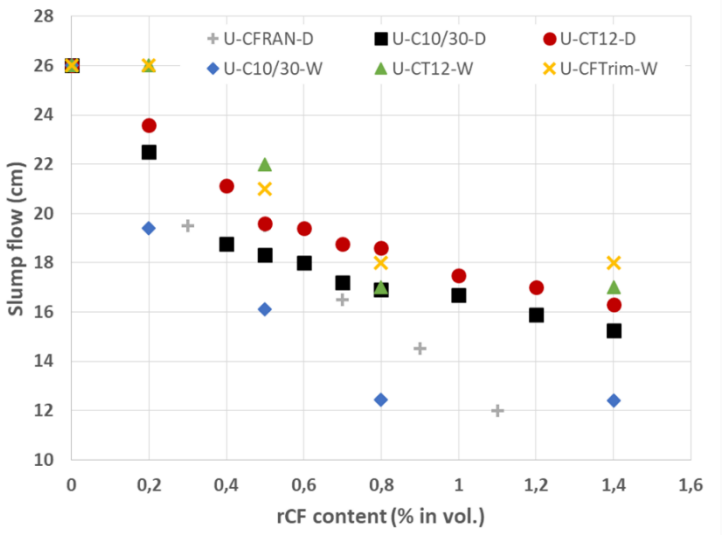

Figure 3.2. Variation of slump flow with the content of rCF for different mixes.

Considering the difficulties observed during the fabrication of the conventional concrete mixes for CFRAN carbon fibres, the rest of the mixes were obtained only with the UHPC mix. The fibre factor *F* of the different rCFs, as detailed in Table 3.2, influences the workability of the mixes. There are no reported values of the fibre factor in the literature, although Grunewald provided maximum values between 0.3 and 1.9 for steel-fibre-reinforced concrete (Grünewald, 2004). Considering only the rCF characteristics and volume fractions, the fibre factor F varies between 428 and 6000 for CFRAN, 143 and 2000 for C10/30, and 1.2 and 16.8 for CT12 and CFTrim.

The results of the compressive and flexural strength measurements (Figure 3.3 a and b, respectively) showed different behaviours of the rCF concrete samples. First, concretes made with CFRAN carbon fibres exhibited a clear influence of the granular skeleton as UHPC concretes exhibited larger mechanical properties than the CC concretes. As mentioned previously, the incorporation of CFRAN fibres into the conventional concrete mixes resulted in a large reduction in the workability.

The difficulty in mixing the CC dosages influenced the compactation of the samples and thus, more porosity was incorporated into the mix. Therefore, these samples exhibited lower mechanical performance. Second, the mixes that incorporated rCFs into the wet mix exhibited larger compressive strength than the dry mix samples. This result is also consistent with the results of workability and those of previously published research works (Wang *et al.*, 2008).

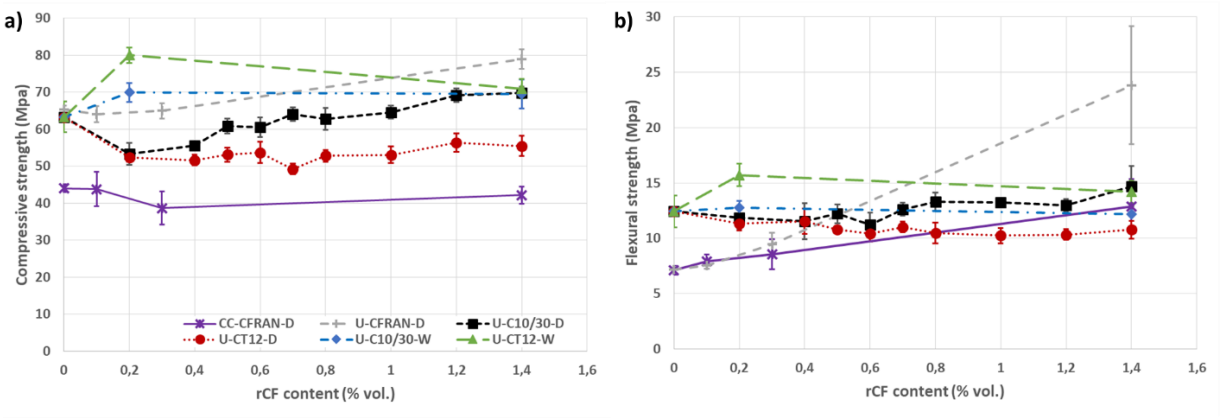

Figure 3.3. Variation of a) compressive and b) flexural strength with the rCF content for different mixes

Finally, regarding the format of the rCF (single fibre or fibrillated sheets) and considering the slump test results, larger mechanical response of CT12 samples is expected. Further, when the rCFs were incorporated into the dry mix, C10/30 samples exhibited larger mechanical response both in compressive and flexural strength measurements. When the rCFs were incorporated into the wet mix, the trend shifted and CT12 samples exhibited larger compressive and flexural strength.

This result might be explained in view of the critical pull-out length (L_f^{crit}) and number of fibres per unit volume (N), as recently presented by Han et al. (Han *et al.*, 2016). In that work, critical pull-out length of carbon fibres can be got when the carbon fibres are snapped. The authors demonstrated that, as the length of the carbon fibre decreases, N increases but L_f^{crit} decreases.

Figure 3.4 presents the variation of N and L_f^{crit} with the rCF content for C10/30 and CT12 fibres. More carbon fibres in the bulk matrix indicate better mechanical performance up to a certain rCF content given by the fibre factor. Once this value is reached, a further increase in the carbon fibre content might have a weakening effect owing to the presence of air voids and low dispersion of the carbon fibres. Thus, N mainly influences the compressive strength. As shown in Figure 3.3a C10/30 and CT12 samples exhibit almost similar compressive strength for low rCF content, because the number of fibres per unit volume is very similar (see Figure 3.4a). As the rCF content increases, the difference between N of C10/30 and CT12 increases, and thus more defects (air voids and bundles of carbon fibres) might be present in the cementitious matrix.

Furthermore, the value of L_f^{crit} will determine the mechanical behaviour of the carbon fibre reinforced cementitious composites. As L_f increases and exceeds L_f^{crit}, the carbon fibre maximum stress also increases until $L_f = L_f^{crit}$. Further increases of L_f are not related to larger increases in the fibre maximum stress since the carbon fibre will be snapped from the cementitious matrix when the material is damaged. The length of both C10/30 and CT12 carbon fibres is larger than the value of L_f^{crit} for almost all rCF contents (see Figure 3.4b). Therefore, no significant differences are expected in the flexural behaviours of the specimens as shown in Figure 3.3b.

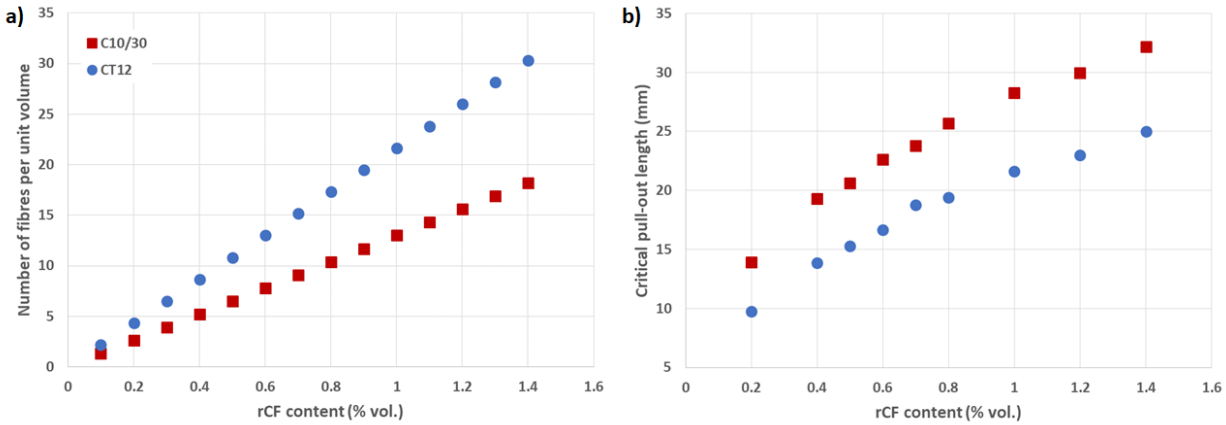

Figure 3.4. Variation of (a) N and (b) Lfcrit with the rCF content for C10/30 and CT12 fibres

3.4.2.- Electrical charactrization

3.4.2.1.- Effect of CFRAN fibres and influence of granular skeleton

First, the influence of the granular skeleton was verified for CFRAN fibre contents of 0.1, 0.3, and 1.4%. The Bode diagrams (impedance versus frequency) for these samples are illustrated in Figure 3.5. A line is drawn at 50 Hz as it is the standard frequency of electrical mains.

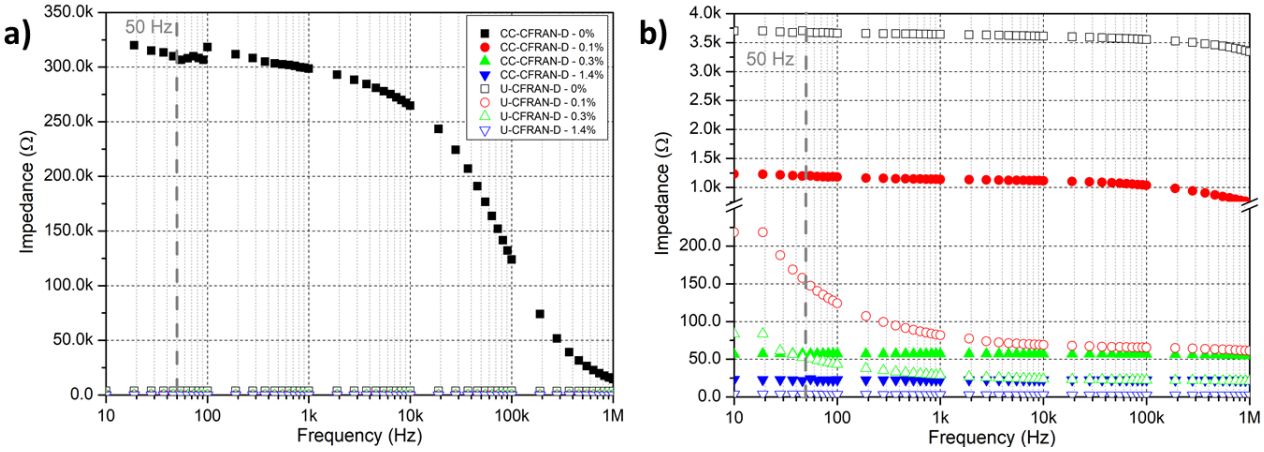

Figure 3.5. Bode diagrams for CC and UHPC mixes with CFRAN fibres: a) complete impedance scale, and b) 0–1300 Ω

The electrical patterns of both CC and UHPC concrete samples exhibit large differences. The plain CC specimens with no rCF addition evidence and impedance variation with frequency characteristic of an insulator material. There is almost no variation of the impedance with the increasing frequency up to 10 kHz. Once this value is reached, a large reduction on the impedance is observed.

The plain UHPC concrete samples also behave as an insulator, but the variation of the impedance with frequency is different from the CC samples. Firstly, for the same frequency value, UHPC samples exhibit impedance values that are 100 to 10 times lower than the CC ones; as the frequency increases, the differences between CC and UHPC samples reduces. Secondly, the electrical pattern of the plain UHPC samples do not exhibit a drastic reduction of the impedance for frequency values above 10 kHz, but just a slight reduction in the impedance for frequencies larger than 100 kHz.

The reduction of impedance observed in the plain CC specimens are related to polarization effects. Some authors have suggested that polarization effects are not eliminated by the use of AC but are rather manifested in the form of introduction of a capacitance in parallel with the electrical resistance. As the frequency of the applied current is increased, the effect of the capacitance is reduced. The differences observed between the plain concrete samples of both CC and UHPC mixes are related to the different granular

skeletons of the mixes and the percolation of the cementitious paste (Wen and Chung, 2007).

The differences between the maximum aggregate sizes of the CC and UHPC mixes (1mm in the UHPC mix vs. 15 mm in the CC mix) explain the different electrical patterns observed. Considering the differences observed in the electrical behaviour and the difficulties in the mixing process of the CC-CFRAN dosage, only the UHPC mix was used in the rest of this study.

Figure 3.6 shows the Bode diagrams for CFRAN fibre contents from 0 to 1.4% for the UHPC mix. The incorporation of rCF into the cementitious matrix drastically modifies the electrical behaviour of the material.

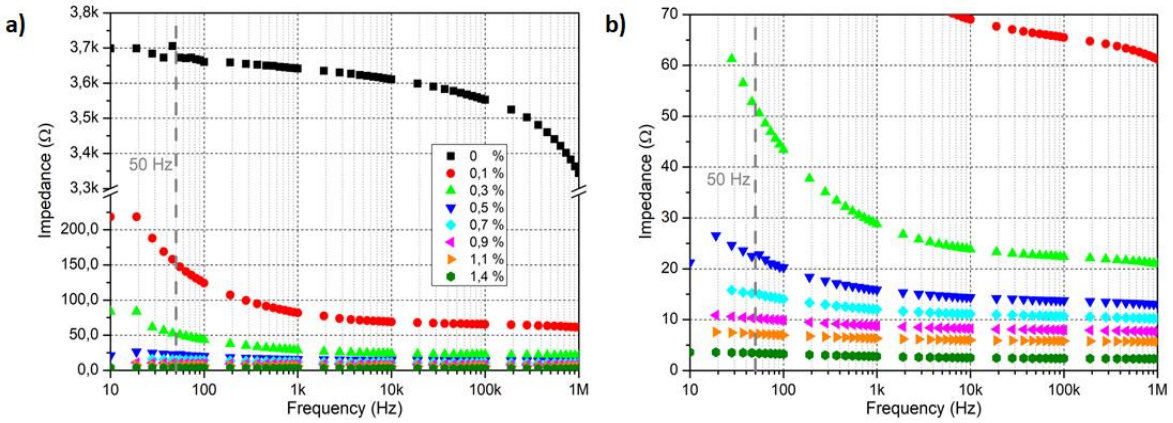

Figure 3.6. Bode diagrams for UHPC mixes with CFRAN fibres: a) complete impedance scale, and b) zoom-in the 0–70 Ω range of impedance

The reference samples behave as an insulator with almost no variation in the impedance with the frequency. A small reduction in the impedance can be observed only for frequencies up to 100 kHz. However, the incorporation of the rCF modifies the electrical pattern of the samples. It can be observed that the impedance is reduced as the frequency of the applied current is increased.

Large reductions in the impedance values are observed as the frequency is increased up to 1–10 kHz such that the plateau appears in accordance with previous studies (Chen, Wu and Yao, 2004). This frequency helps overcome the effects appearing in the samples owing to the ionic conductivity of the cementitious matrix, and is referred to as the capacitance threshold (C_t). Second, the incorporation of the CFRAN fibres drastically reduces the impedance of the samples up to the rCF content of 0.6%. Further increments in the CFRAN content do not lead to larger decreases in the electrical impedance. This electrical behaviour may demonstrate a continuous electrical path between the electrodes.

The visual inspection of the fracture interfaces of the CC and UHPC concrete samples (see Figure 3.7) shows that CFRAN fibres tend to form bunches after mixing. The

characteristics of these fibres (very high aspect ratio and supplying characteristics) did not allow good dispersion of the fibres with the standard mixing procedures used by the industry.

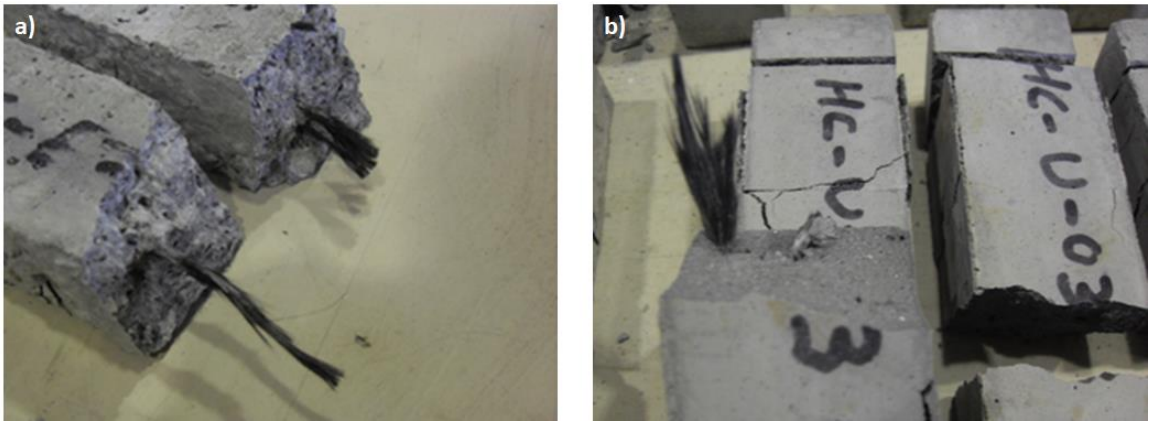

Figure 3.7. Presence of bunches in the CFRAN samples: a) CC mix and b) UHPC mix

3.4.2.2.- Effect of C10/30 and CT12 fibres

In the case of C10/30 and CT12 fibres, the general electrical patterns obtained are similar to those observed for CFRAN fibres, as shown Figure 3.8. Nevertheless, an inversion phenomenon is observed for both types of fibres. The incorporation of both types of rCFs reduces the impedance of the samples until the rCF content of 0.4–0.5% is reached.

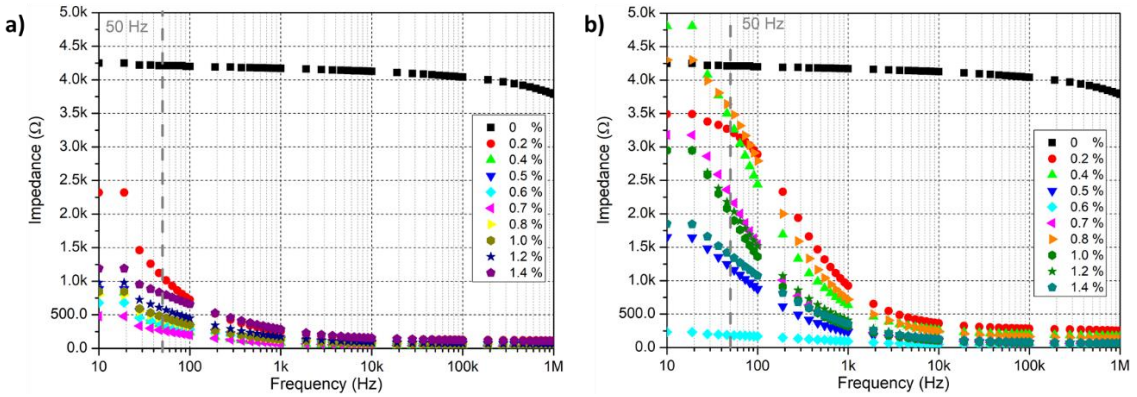

Figure 3.8. Bode diagrams for UHPC mixes with: a) C10/30 fibres and b) CT12 fibres

Further increases in the rCF content produce an inversion phenomenon and the impedance values increase again. In the case of C10/30 fibres (Figure 3.8a), the maximum impedance reduction is achieved for 0.5% content of rCF; a further increase in the rCF content results in a slight increase in the measured impedance. The CT12 fibres exhibit a more evident inversion phenomenon for rCF contents larger than 0.6% (see Figure 3.8*Figure 3.*b). These inversion phenomena clearly highlight the inadequate dispersion of rCF in the concrete samples.

The visual inspection of the cross-section of the samples (Figure 3.9) also shows the presence of bunches of rCF. The distribution of rCF in the C10/30 concrete samples correlates with the impedance variation shown in Figure 3.a. The number of fibres in the cross section increases up to a content of 0.6% of rCF. Bunches of rCF are observed in the cross section as the rCF content increases.

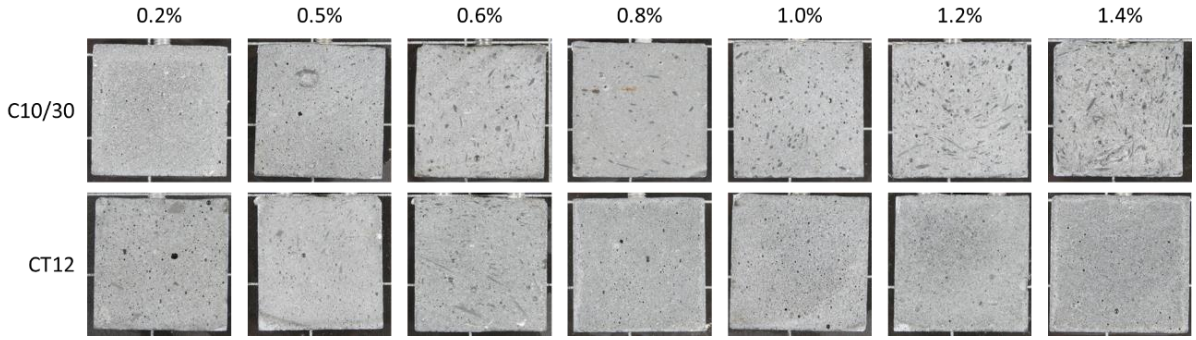

Figure 3.9. rCF dispersion in C10/30 and CT12 concrete samples

The distribution of rCF in the CT12 samples presents some differences. The agglomerations of carbon fibres are observed for low contents of rCF. Nevertheless, for rCF contents larger than 0.6% no evidence of rCF can be detected in the cross section of the samples. The CT12 carbon fibres were provided as fibrillated sheets.

A possible explanation for this result is the separation of the rCF sheets into individual carbon fibres or the degradation of the carbon fibres. The impedance variation for these samples (Figure 3.8b) may also be in accordance with a deterioration of the carbon fibres.

3.4.2.3.- Influence of rCF mixing method

Notably, all the electrical patterns shown above correspond to rCF added to the dry mix after the cement and aggregates. The effect of the mixing method on the electrical patterns is illustrated in Figure 3.10. The incorporation of rCF into the wet mix after incorporating the water and additives modifies the electrical behaviour of the samples significantly.

The modification affects both the impedance value and the frequency at which the impedance stabilises. First, the impedance of the samples is drastically reduced when the mixing method is modified. Furthermore, no inversion effect appears in the samples in the wet mix, thus demonstrating good dispersion of the rCF into the cementitious matrix. The presence of bunches of rCF could not be observed in the analysis of the cross-section of the

concrete samples (see Figure 3.11). Furthermore, no evidence of fibre deterioration is observed in the cross section of CT12 concrete samples.

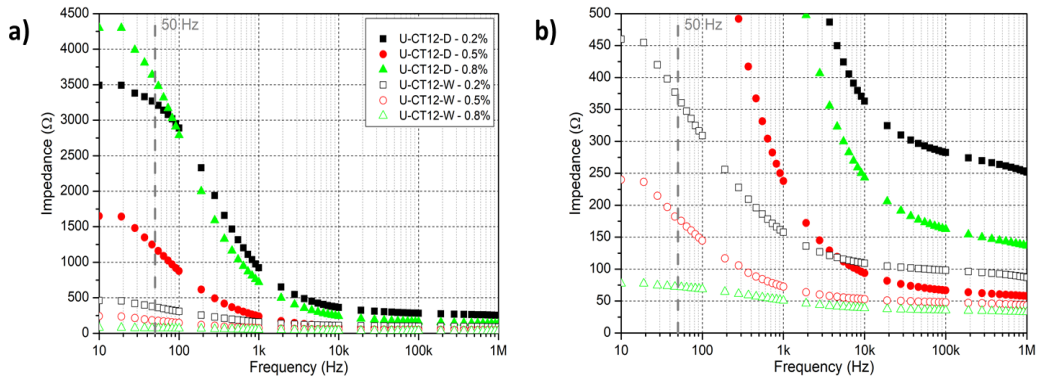

Figure 3.10. Effect of the mixing method on the electrical pattern of CT12 mixes: a) complete impedance scale and b) zoom-in the 0–500 Ω range of impedance.

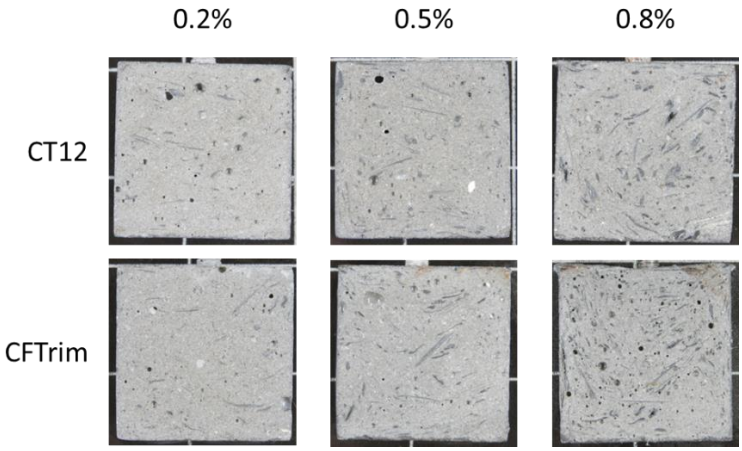

Figure 3.11. rCF dispersion in wet mix concrete samples.

Figure 3.12 illustrates the variation of $Z_{CT12\text{-}D}Z_{CT12\text{-}W}$ ratio with the frequency that helps to identify the effect of the mixing method on the dispersion of rCF in the cementitious matrix. For rCF contents below the percolation threshold (rCF contents of 0.2 and 0.5%), the influence of fibre dispersion results in a difference in impedance of the order of ten times. Nevertheless, when the rCF is approximately equal to or more than the percolation threshold (rCF content of 0.8%), the better fibre dispersion in the wet mix samples facilitates larger differences in the electrical behaviour of the samples. Notably, once the frequency surpasses the C_t value, the ratio $Z_{CT12\text{-}D}Z_{CT12\text{-}W}$ stabilises at an average value of 3. Second, the incorporation of the rCF into the wet mix also reduces the value of C_t for different concrete samples to approximately 100 kHz for the dry mix samples and 1 kHz for the wet mix samples.

Furthermore, the incorporation of the rCF into the wet mix also facilitates the comparison between the electrical patterns of CT12 and CFTrim (see Figure 3.12). Although CT12 and CFTrim rCFs exhibit different electrical properties (see Table 3.2), the electrical behaviours of their equivalent concrete samples are quite similar. For rCF content of 0.8%, the percolation threshold value is reached and a continuous network of rCFs is formed in accordance with the previous studies (Chen, Wu and Yao, 2004). The similarities observed between the electrical patterns of CT12 and CFTrim concrete samples demonstrate that the electrical resistivity is determinate at the end by the cementitious paste that surrounds the rCF rather than by the electrical resistivity of the later.

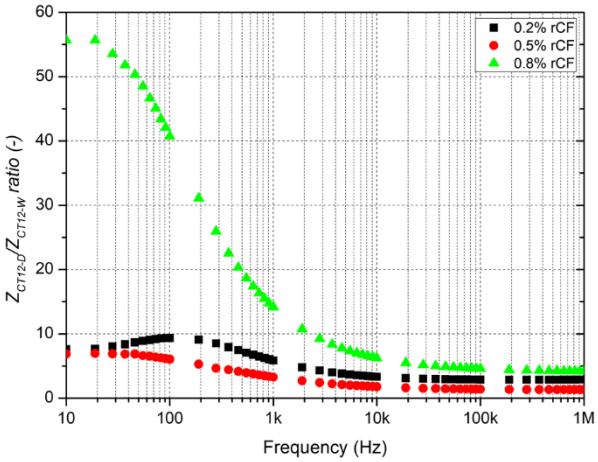

Figure 3.12. Variation of $Z_{CT12\text{-}D}/Z_{CT12\text{-}W}$ ratio with frequency

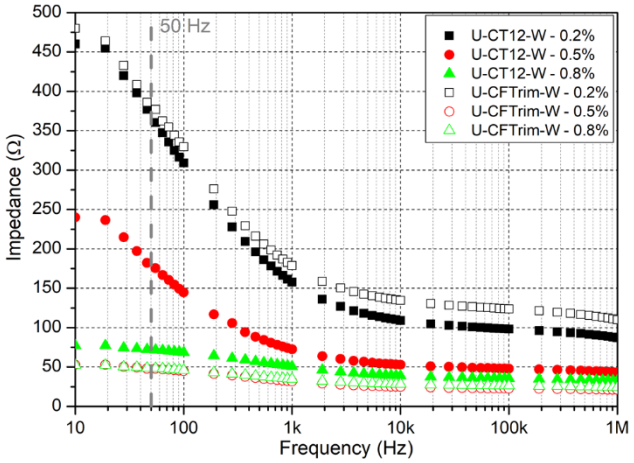

Figure 3.13. Comparison of the electrical behaviour of UHPC mixes with CT12 and CFTrim fibres added to the wet mix

3.4.2.4.- Electrical resistivity calculation

The electrical resistivity of different concrete samples can be calculated from the measured impedance. The impedance measured, Z, is a complex number and thus cannot be used to determine the electrical resistivity of the samples. The electrical resistance is used instead, as described by equation [3.5]. As AC measurements were obtained at different frequencies, a non-trivial question is to determine the frequency at which the electrical resistivity must be calculated. Many authors achieved the AC characterization of carbon fibre-reinforced concrete (F J Baeza *et al.*, 2013; Gomis *et al.*, 2015; Han *et al.*, 2016) but the authors only found one reference that provided the nominal frequency at which the electrical resistivity was calculated. Chen et al. (Chen, Wu and Yao, 2004) chose 100 kHz as the value of Ct in their experiments. Therefore, in this work, two electrical resistivity values are obtained: ρ50 Hz and ρ100 kHz. As stated previously, ρ50 Hz is of high technical importance as the standard frequency for AC is 50 Hz.

The frequency selected for the electrical resistivity measurements affects the electrical resistivity values as shown in Figure 3.14. The measurements obtained at 50 Hz clearly demonstrate the influence of the fibre dispersion on the electrical resistivity of the

samples (see Figure 3.14 a and b). This situation was clearly observed with U-CT12-D samples. These samples exhibited inadequate dispersion of the fibres and bunches appeared after the visual inspection. This was also reflected in $\rho_{50\ Hz}$ as they exhibited larger electrical resistivity values. Nevertheless, the electrical resistivity of these samples measured at 100 kHz is approximately 1.5 Ω·m.

The lowest electrical resistivity is obtained for the wet mix rCF samples (U-CT12-W and U-CFTrim-W). Furthermore, these samples are the ones less affected by the chosen frequency owing to the good dispersion of fibres in the cementitious matrix. The values of $\rho_{50\ Hz}$ obtained for the wet mix rCF samples are in the range of 3 to 0.6 Ω·m, which is consistent with the reported values for virgin carbon fibres (Chen, Wu and Yao, 2004; F J Baeza *et al.*, 2013; Galao *et al.*, 2016).

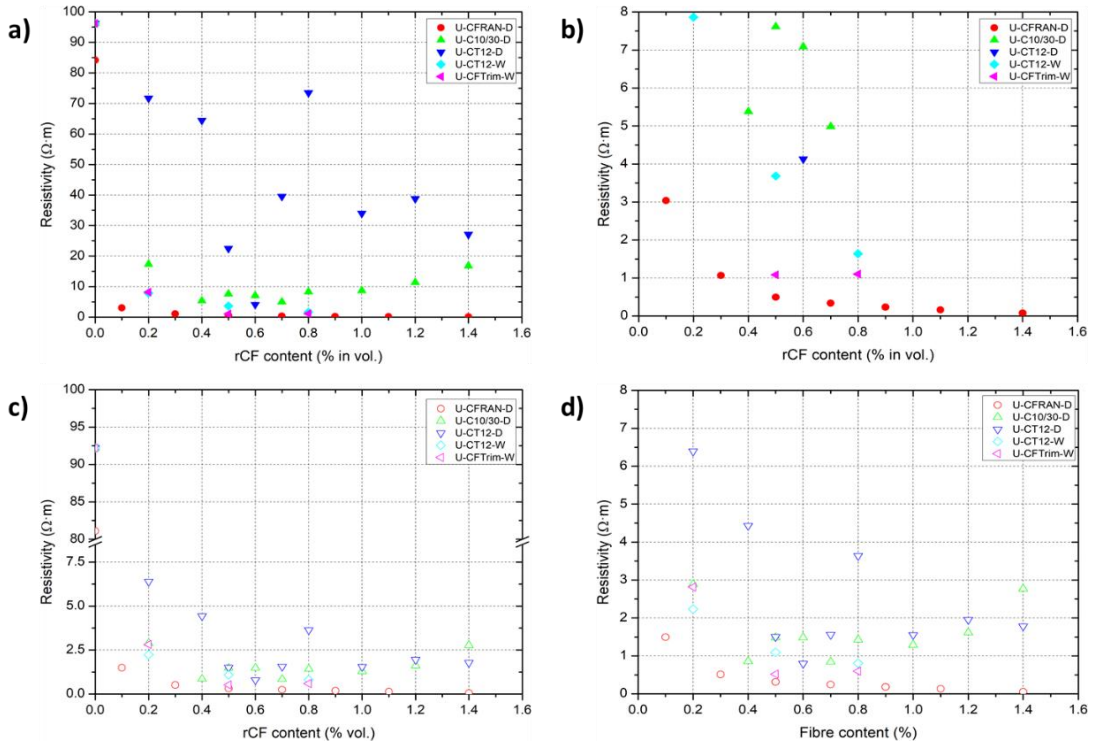

Figure 3.14. Electrical resistivity variation with the rCF content of different concrete samples obtained at 50 Hz (a and b) and 100 kHz (c and d).

3.4.2.5.- Estimation of C_t

In the different samples analysed, we have identified a 'cut-off' frequency: the *capacitance threshold*, C_t. For frequency values between 10 Hz and C_t, there is a large variation in the impedance of the samples. For frequency values above C_t, the impedance reaches a plateau and stabilises. The values of C_t vary in the range of 1 to 100 kHz depending on the type and content of fibre and the mixing method. The complex impedance spectra (Nyquist diagrams) of different concrete samples will be analysed to understand this question more clearly. The Nyquist diagrams of cementitious materials with conductive

inclusions normally exhibit three individual arc/features, accounting for the electrochemical reactions and product layer deposition at the electrodes and bulk-related features (Ford, Shane and Mason, 1998).

Figure 3.15 illustrates the Nyquist diagram for the neat UHPC concrete sample in which only two arcs can be observed. The spur element on the right side is related to the polarisation effects at the electrode (McCarter *et al.*, 2009). The rest of the diagram is part of the arc related to the bulk response of the sample. The incorporation of the rCF modifies the diagram as shown in Figure 3.16.

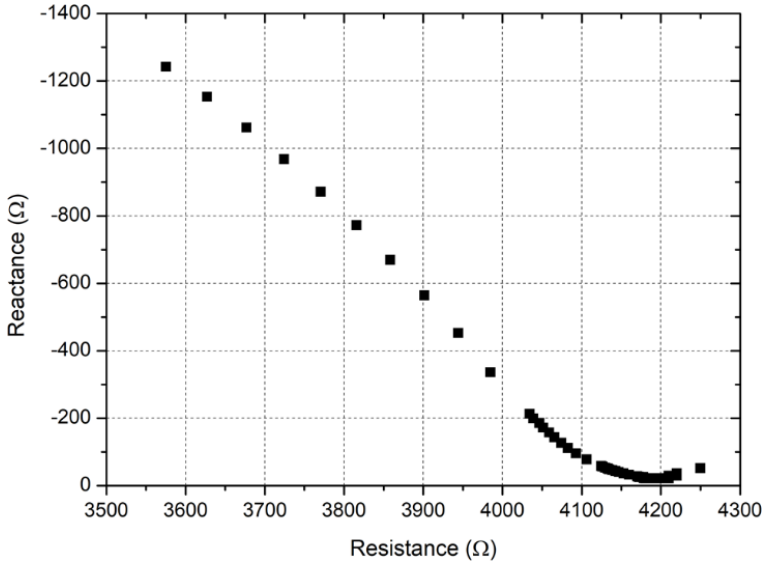

Figure 3.15. Nyquist diagram for the reference UHPC concrete

Both the reactance and electrical resistance values decrease and the feature attributed to the electrode polarization effects is not discernible, as described by previous researchers (McCarter *et al.*, 2009). Ford et al. (Ford, Shane and Mason, 1998) demonstrated that the Nyquist diagram of cementitious samples is affected by the inclusion of conductive phases. The emerging high-frequency arc that appears on the left side of the diagram is related to the bulk features of the sample. The other arc is characteristic of the conductive fibres (Ford, Shane and Mason, 1998; Torrents, Mason and Garboczi, 2000).

The Nyquist diagrams can also account for the rCF dispersion on the cementitious matrix as shown in Figure 3.17. The incorporation of CT12 fibres into the dry mix results in large increases in both the reactance and electrical resistance as compared with the wet mix samples (see Figure 3.16). Furthermore, the inversion phenomena caused by the build-up of the rCF is also evidenced.

Two parameters can be obtained from the Nyquist diagrams: the frequency of the maximum of the arc (f_{max}), and the frequency and electrical resistance at the cusp-point between two arcs (f_{cusp}, R_{cusp}) as presented in Table 3.3 for CT12 and CFTrim concrete

samples. The values of f_{max} are very similar for different samples and vary between 28 Hz and 370 Hz, and are related to the rCF inclusion in the cementitious matrix.

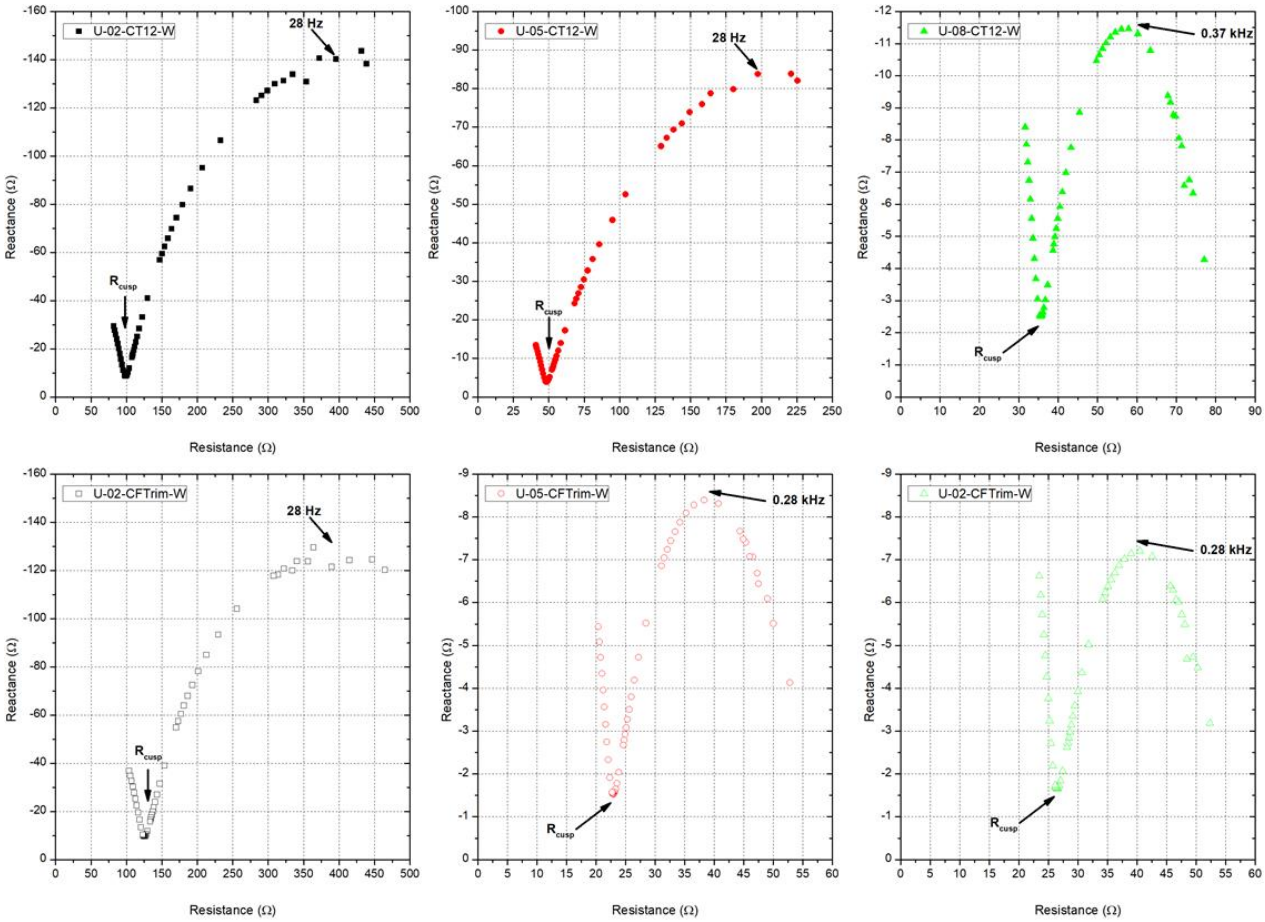

Figure 3.16. Nyquist diagrams for the UHPC concretes wit rCF fibres added to the wet mix

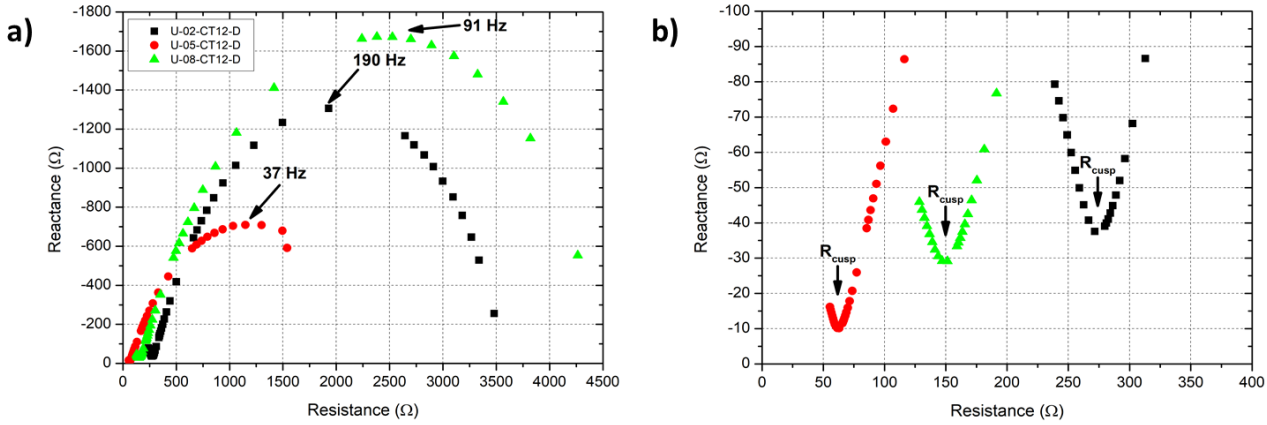

Figure 3.17. Nyquist diagrams for the UHPC concretes with CT12 fibres added to the dry mix

The analysis of the characteristic values of the cusp-point is also of interest. Mason et al. identified the *cusp frequency* (f_{cusp}) as the frequency value required to bypass the cementitious matrix that surrounds the rCF (Mason *et al.*, 2002). There is a clear shift of the

cusp electrical resistance as the rCF increases. The reduction in R_{cusp} corresponds to the reduction in the outer bulk contributions to the fibre current path. Furthermore, the values obtained for f_{cusp} are very close to those indicated as the *capacitance threshold* (C_t). C_t can be estimated from the reactance value at the cusp-point according to equation 3.6.

$$C_t = \frac{1}{2 \cdot \pi \cdot f_{cusp} \cdot X_{cusp}} \qquad \text{Eq [3.6]}$$

The values obtained for C_t can be related to the '*frequency switchable model*' described by several authors (Torrents, Mason and Garboczi, 2000; Mason *et al.*, 2002; Hixson *et al.*, 2003). Therefore, the *capacitance threshold* can be related to the cementitious paste that coats the carbon fibres. Two adjacent carbon fibres will always be surrounded by cementitious paste. This situation can be simplified and consider the system of the carbon fibres and the cementitious paste equivalent to a parallel-plate capacitor with its capacitance *C* defined by equation 3.7, where ε is the permittivity, *A* is the area of the plates, and *d* the distance the distance between them. If ε and A are assumed constant values, reductions in the distance between the plates produce an increase in the capacitance value of the system.

$$C = \frac{\varepsilon \cdot A}{d} \qquad \text{Eq [3.7]}$$

Consequently, as the rCF content increases and the dispersion of carbon fibres is enhanced, the distance between the fibres is reduced, as reflected by the increasing Ct values shown in Table 3. Finally, the overall electrical resistance of the concrete sample is reduced.

Sample	rCF content (% in vol.)	Parameter			
		f_{max} (Hz)	R_{cusp} (Ω)	f_{cusp} (kHz)	C_t (nF)
U-CT12-D	0.2	190	271.6	190	22.3
	0.5	37	62.9		82.6
	0.8	91	151.3		28.7
U-CT12-W	0.2	28	99.2	64	284.7
	0.5	28	48.5		637.2
	0.8	370	35.6	73	868.2
U-CFTrim-W	0.2	37	125.4	55	301.9
	0.5	280	22.9	64	1629.3
	0.8	280	26.4		1508.2

Table 3.3. Parameters obtained from the Nyquist diagrams of CT12 and CFTrim concrete samples

3.5.- CONCLUSIONS

This paper has demonstrated the possibility of developing conductive cementitious materials with recycled carbon fibres. This research facilitates the incorporation of multifunctional cementitious materials in the civil engineering industry, as the cost of the rCF is much lower than that of previously used carbonaceous materials. Thus, the use of multifunctional cementitious materials can be extended in actual concrete structures and not only in laboratory and small scale test applications.

Four different types of rCF were evaluated in this work. The best dispersion of the rCF was achieved for the fibrillated samples with the length of 12 mm (CT12 and CFTrim). The workability of the fresh concrete samples was significantly modified by the incorporation of the rCF, although acceptable values were obtained for the concrete samples that incorporated the rCF using the wet mix method. In terms of the mechanical performance, a reduction in both flexural and compressive strength was observed with the adding of the rCF using the dry mix method.

The electrical behaviours of different concrete samples with rCF did not differ significantly from the electrical characteristics described in the literature for concrete samples with virgin carbon fibres. The Bode diagrams of different concrete samples exhibited a common pattern. The impedance of the samples decreased as the frequency increased up to a threshold value and thereafter stabilised in a plateau. This frequency is sensitive to the fibre dispersion and is required to bypass the cementitious matrix that surrounds the rCF. The electrical resistivity values obtained for the wet mix rCF samples were between 3 and 0.6 Ω·m, which is consistent with the reported values for virgin carbon fibres.

Furthermore, we have evaluated in this work presence of a *capacitance threshold* value (C_t) in conductive cementitious materials. that is related with the cementitious paste that coats the carbon fibres.

Lastly, the results presented in this article may also help boost the recycling industry of carbon fibre composites, providing new added-value applications that may be used in large structures. We are facing a world-wide problem on the recycle of obsolete aircrafts that are actually been stored in large airfields. The incorporation of rCF in multifunctional concrete structures may be good contribution and will allow to enhance the sustainability of our infrastructures.

Capítulo 4[2]: SELF-SENSING CONCRETE MADE FROM RCF

Abstract

The electrical and piezo-resistive responses of recycled carbon fibre (rCF)-reinforced concrete is analysed in this article. Two different PAN-based rCFs (monofilament rCF and fibrillated rCF sheets) incorporated into dry concrete mix were investigated. Piezo-resistivity was evaluated by simultaneously monitoring the variation in the applied DC voltage during both flexural and compressive tests. Although both plain and rCF-reinforced concrete samples showed piezo-resistive responses, the latter show increased signal-to-noise-ratio and thus behave like self-sensing materials. The electrical behaviour suggests a mixed control owing to both ionic and electronic conductivity, with the dominant one depending on the rCF content and rCF dispersion. This work enhances the possibility of generalising the use of smart cementitious materials in the civil engineering industry.

Keywords
Self-sensing concrete; strain sensing; recycled carbon fibre; smart material

2 El presente capítulo se corresponde con el artículo publicado por, Segura, I., Faneca, G., Torrents, J.M. and Aguado. A., "Self-sensing concrete made from recycled carbon fibres". Smart Materials and Structures 28 (2019) 105045.http://dx.doi.org/10.1088/1361-665X/ab3d59

4.1.- INTRODUCTION

Since the last 15 years, there is a revolution to turn civil infrastructures and buildings all over the world into smart structures. Our current society is increasingly demanding that the infrastructures and cities become smart and provide other functionalities in addition to their mechanical performance and durability. Furthermore, the recent failures in the summer of 2018 of a motorway bridge in Genova, Italy and of a concrete pier in Vigo, Spain, have brought the focus on how our society deals with infrastructure monitoring and maintenance. Moreover, there is a need to reduce monitoring costs and to avoid further collapse of existing infrastructures.

This revolution has mainly considered the incorporation of multi-functional devices and sensors into civil infrastructures and architectural heritage. Nowadays, optical fibres are widely employed for monitoring civil infrastructures (Barrias, Casas and Villalba, 2016), and wireless sensor networks (WSN) are being extensively used to help preserve the building heritage (Zonta *et al.*, 2010). One of the main challenges of this approach is the durability of the sensors since they may become *external agents* in the structures. Experience reminds us of the lack of durability of such sensors, as evidenced by dam auscultation and WSN systems. The inconvenient truth is that almost 70% of the sensors fail or are inoperative after 1 year of operation (Ceylan, 2014). To describe this situation in medical terminology, we are facing a serious problem of "*transplant rejection*" by our infrastructures.

However, a very promising alternative to the use of conventional sensors is the development of smart cementitious materials with self-sensing abilities, which would allow detection of strain and damages in new and existing infrastructures. The incorporation of conductive phases into cementitious matrices has been one of the most popular methodologies to develop self-sensing cementitious materials. In 1993, Chen and Chung first reported the piezo-resistive effects of carbon fibre-reinforced cementitious materials (Chen and Chung, 1993).

The incorporation of conductive phases into the cementitious matrix modifies its conductive characteristic. Thus, piezo-resistive effect appears when stress is applied to the material, owing to the modification of the conductive characteristics of the material. For carbon fibre-reinforced composites, piezo-resistivity is considered to originate from the slight pull-out of crack-bridging fibres during crack opening and the consequent increase in the contact electrical resistivity of the fibre–matrix interface (Wen and D. D L Chung, 2006), or the conduction network degeneration resulting from fibre reorientation under finite strain (Taya, Kim and Ono, 1998).

The piezo-resistivity of carbon fibre cementitious materials has been extensively investigated until now (Chen and Chung, 1996; Shi and Chung, 1999; D D L Chung, 2000; D. D L Chung, 2000; Baeza *et al.*, 2011; Francisco Javier Baeza *et al.*, 2013), and nowadays, it is being explored through the incorporation of graphene (Liu *et al.*, 2016), carbon nanotubes

(CNTs) and nanofibers (Coppola, Buoso and Corazza, 2011; Han *et al.*, 2011; Francisco Javier Baeza *et al.*, 2013; Konsta-Gdoutos and Aza, 2014; Galao *et al.*, 2017), multiphasic mixes of conductive additives (Ding *et al.*, 2013, 2015, 2016; Dong *et al.*, 2016), and CNT-coated aggregates (Loh and Gonzalez, 2015). An interesting review on the development of self-sensing cementitious materials was published by Chan et al. (Han, Ding and Yu, 2015). However, the incorporation of smart materials into novel or existing infrastructures has not taken off, and has been limited to some pilot studies only (Shi and Chung, 1999; Han, Yu and Kwon, 2009; Han *et al.*, 2011, 2013). One key reason for this situation is the high cost of the conductive phases that are being used in the development of smart cementitious materials.

The use of recycled carbon fibres (rCF) is a very promising alternative in the development of sustainable smart cementitious materials. Recycled carbon fibres are mainly obtained from aerospace composite scrap. Among many different methods, most of the commercially available rCF are obtained via pyrolysis. This process allow a high retention (up to 90%) of the properties exhibited by virgin carbon fibres (Pickering, 2006; Pimenta and Pinho, 2011). The use of rCF may allow to design economically affordable smart cementitious materials since most of recycling processes yield rCF with high retention of mechanical properties (Pimenta and Pinho, 2011) but with a 30 to 40 percent cost savings versus virgin carbon fibre (cost of commercial chopped carbon fibres: 15 €/kg vs cost of rCF: 7-8 €/kg). In a recent paper (Faneca *et al.*, 2018), we demonstrated the possibility of using recycled carbon fibres to develop conductive cementitious materials, and realized electrical resistivity in the range of 3–0.6 Ω•m for rCF contents ranging from 0.2 to 0.8% in vol.

As a continuation of this research, in this study, we explore the capability of recycled fibre cementitious composites as smart materials for self-sensing applications. Two different types of rCF (fibrillated and sheet-type) were evaluated as additives; these two were incorporated at different contents (0.1 to 1.4% in volume) in ultra-high-performance concrete (UHPC) mix. Piezo-resistivity of the prepared concrete samples was evaluated under both flexural and compressive conditions, by taking into account the effect of the moisture content of the samples.

4.2.- MATERIALS AND METHODS

4.2.1.- Concrete dosage and raw materials

The concrete dosage used in our study is shown in Table 4.1; this is characteristic of a UHPC dosage. This concrete dosage was selected because it is expected to enhance the electrical conductivity owing to the presence of a double percolation phenomenon, as described by Wen et al. (Wen and D. D L Chung, 2006). The cement selected to produce the UHPC mixtures was a CEM I 53.5R. The sand used was siliceous sand and fine calcium carbonate powder (Betoflow) was incorporated into the different dosages to achieve an optimum workability of the mixes with a low consumption of superplasticisers. Both a

polycarboxylate superplasticiser (Glenium ACE425) and nanosilica suspension (Meyco MS685) were used as additives to provide self-compacting characteristics to the concrete mix.

Component		Dosage (kg/m³)
Cement		800
Betoflow		220
Sand (0-3/0-1 mm)		1161
Additives	Glenium ACE425	30
	Meyco MS685	57
Water		110

Table 4.1. Concrete dosage used for the mixes

The water to cement (w/c) ratio of the concrete mixes was 0.14. Two different PAN-based rCF samples provided by ELG Carbon Fibre Ltd (C10/30, and CT12) were used in this study. The characteristics of the rCF are described in Table 4.2; C10/30 are monofilament rCF and CT12 are fibrillated sheets of rCF.

Property	Value	
	C10/30	CT12
Diameter (μm)	7.5	7†
Nominal length (mm)	10–30	12
Average length (mm)	20	12
Fibre factor *F*	1428	12
Density (kg/m³)	1800	1760
Tensile strength (MPa)	3150	4150
Young modulus (GPa)	200	252
Electrical resistivity (Ω·m)	0.103/0.34††	0.016

† The effective diameter of the fibrillated sheets is 500 μm.

†† The electrical resistivity value varies depending on whether the measurement is made lengthways (0.103) or along the cross-section (0.34)

Table 4.2. Properties of recycled carbon fibres

The fibre factor F given by Eq. 4.1, as proposed by Narayanan and Darwish, allows to account for the effect of both the geometrical characteristics of the fibres, length (Lf) and diameter (df) (Narayanan and Darwish, 1987).

$$F = \beta \cdot L_f / d_f \qquad \text{Eq (4.1)}$$

where, β is the fibre shape factor (0.50 for circular fibres), and the fibre was dosage varied from 0.1% to 1.4% in volume.

4.2.2.- Sample fabrication

UHPC samples with dimensions of 40 × 40 ×160 mm were fabricated with the dosages indicated in Table 4.1, according to UNE-EN 196-1 (AENOR, 2005). The concrete samples were produced at the industrial installations of the company, Escofet 1886, with a fabrication procedure replicating the industrial process as closely as possible. Two sets of samples were fabricated from each mix, one set for mechanical measurements and another for electrical measurements. In this work, rCFs were added to the dry mix (D) after incorporating the cement and aggregates. No specific dispersion procedure was implemented since our main aim was to work as close as possible to the real practice and use the actual concrete compositions used in the precast concrete industry. Reference samples were prepared without adding rCF.

The electrodes for the electrical measurements were stainless steel set screws of 5 cm length that were introduced 3.5 cm deep into the concrete samples. The samples were cured in a humid chamber (20° ± 2 °C; relative humidity of 95 ± 5%) for 28 days. The samples are designated according to the following code: U-Cf-f-M where, U stands for UHPC mixes, Cf indicates the fibre content (which varies from 0 for the reference sample to 14 for the 1.4% fibre content), f indicates the fibre type, and M indicates the mixing method of the fibres (D).

4.3.- CHARACTERISATION.

Slump flow was measured according to UNE-EN 1015-3 (AENOR, 2000) prior to the development of the concrete samples. Flexural and compressive strength measurements were performed on the concrete samples in compliance with UNE-EN 196-1 (AENOR, 2005); three and six replicates were made for each dosage, respectively. The electrodes used for the electrical measurements were stainless steel set screws of length 5 cm, which were dipped 3.5 cm into the concrete samples. The samples for mechanical strength measurements did not included steel electrodes. Figure 4.1 shows a scheme on the electrodes positioning on the specimens.

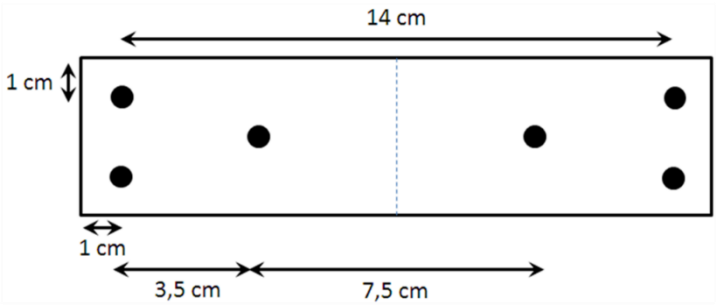

Figure 4.1. Location of the electrodes in the specimens

The electrical properties of the samples were characterized with an Agilent HP 4192A impedance analyzer, using an instrumentation amplifier as a front-end to allow 4-probe measurements (Gersing, 1991), with an effective voltage of 1 V AC to avoid polarization effects in the electrodes (Wen and D D L Chung, 2006; Wen and Chung, 2007). The measurements were conducted in the frequency scanning range of 10 Hz to 1 MHz providing electrical impedance (Z, in Ω) and phase (ϕ, in degrees). The electrical impedance is described by equation 4.2 and is composed of a real part (resistance, R) and an imaginary part (reactance, X); R and X are given by Equation 4.3 and 4.4:

$$Z = R + j \cdot X \qquad \text{Eq (4.2)}$$

$$R = Z \cdot \cos\left(\frac{\phi \cdot \pi}{180}\right) \qquad \text{Eq (4.3)}$$

$$X = Z \cdot \sin\left(\frac{\phi \cdot \pi}{180}\right) \qquad \text{Eq (4.4)}$$

The electrical resistivity (ρ, in Ω•m) was calculated from the impedance data using Eq. 4.5, where, S is the effective transverse section (0.0016 m2 in our study), and l is the measurement length (0.07 m in our study). All the samples were allowed to reach a hygrothermic equilibrium by storing them under laboratory conditions for 15 days after finishing the curing period. Lastly, the electrical conductivity (σ, S/m) of the samples was easily calculated as the inverse of the resistivity, using Eq. 4.6. The electrical conductivity values are expressed as the mean of values determined for three different specimens.

$$\rho = R\frac{S}{l} \qquad \text{Eq (4.5)}$$

$$\sigma = \frac{1}{\rho} \qquad \text{Eq (4.6)}$$

Piezo-resistivity tests were performed on 40×40×160 mm specimens to evaluate the characteristics of the different conductive concrete samples. Samples were loaded both under flexural and compression conditions. Electric current was passed through the samples using an external DC current source (Keithley Model 6020) to monitor the resistivity variation during the mechanical tests, by fixing the output current to 3 V. Piezo-resistivity measurements were performed on one specimen of each dosage.

4.4.- RESULTS

4.4.1.- Physical and mechanical properties

The influence of the rCF type and content, as well as the mixing method on the slump flow is depicted in Figure 4.2a. The rCF fibres supplied as fibrillated sheets (CT12) exhibited

a larger slump flow compared to that of monofilament rCF (C10/30) at all fibre dosages. A larger slump flow is usually related with better dispersion of the rCF in the cementitious matrix and is strongly affected by the geometrical parameters of the fibre (fibre factor, F).

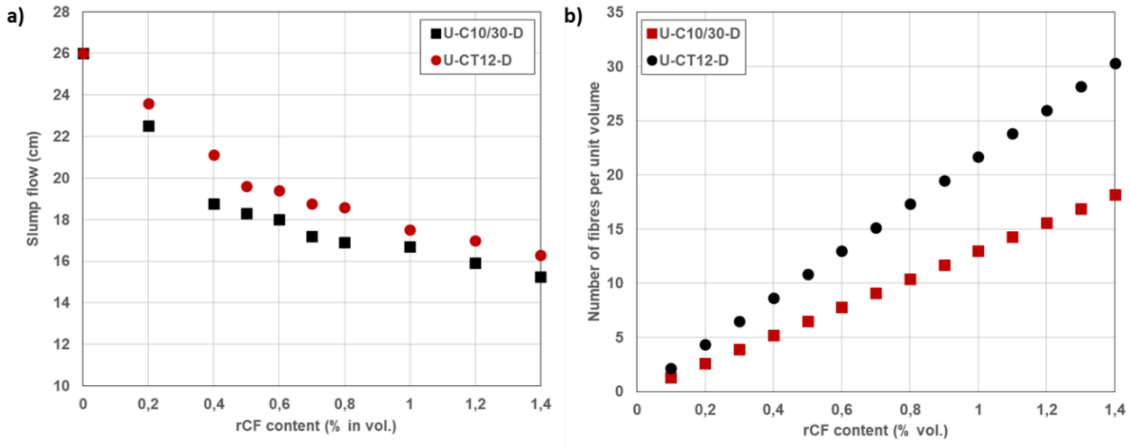

Figure 4.2. Variation of: (a) slump flow with the content of rCF for the different mixes, and (b) N per unit volume with the rCF content for C10/30 and CT12 fibres

Considering the differences in the properties of the two types of rCF shown in Table 4.2, larger differences would be expected in the slump flow of concrete with C10/30 and CT12 samples. However, the fibre dispersion in cementitious materials is affected not only by the fibre factor but also by the number of fibres per unit volume, N. This parameter can be calculated according to Eq. 4.7,

$$N = \frac{V_f}{\pi \cdot \left(d_f/2\right)^2 \cdot L_f} \qquad \text{Eq (4.7)}$$

where, Vf is the volume fraction, df is the diameter (in mm), and Lf is the length of carbon fibres (in mm). Figure 1b shows the variation of N with the rCF content for concrete samples containing C10/30 and CT12. For low rCF contents, the number of fibres per unit volume is very similar for both samples. As the rCF content increases, the difference between the N values of C10/30 and CT12 samples increases. Thus, the results of slum flow reflect this relationship between the geometrical factor of the fibres and the number of fibres per unit volume.

The mechanical properties of the specimens shown in Figure 4.3 also reflect the relationship between the geometrical factor of the fibres and the number of fibres per unit volume. Considering the slump test results shown in Figure 4.2, a larger mechanical response of CT12 samples is expected. However, an inverse trend is observed with the C10/30 specimens exhibiting a larger mechanical response both under compressive and flexural conditions.

This result might be explained again in view of the number of fibres per unit volume (N). More carbon fibres in the bulk matrix can result in better mechanical performance up to a certain rCF content given by the fibre factor. Once this value is reached, a further increase in the carbon fibre content might have a weakening effect owing to the presence of air voids and low dispersion of the carbon fibres. As shown in Figure 4.3a, C10/30 and CT12 samples exhibit almost similar compressive strengths at a low rCF content, because the number of fibres per unit volume is very similar. As the rCF content increases, the difference between the N value of C10/30 and CT12 increases, and thus more defects (air voids and bundles of carbon fibres) might be present in the cementitious matrix.

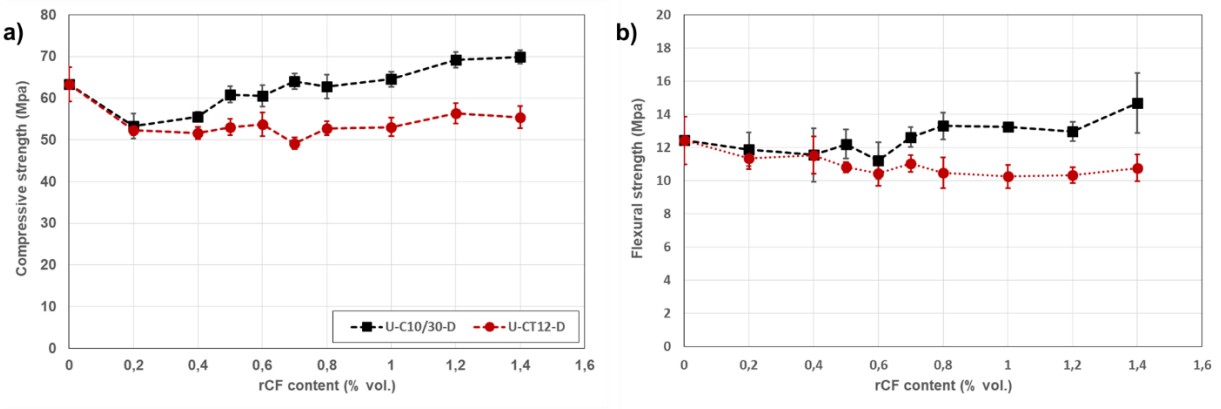

Figure 4.3. Variation of the a) compressive and b) flexural strengths with the fibre content for different concrete mixes.

4.4.2.- Electrical conductivity

The electrical characteristics of carbon fibre-reinforced cementitious composites are strongly influenced by the applied frequency in AC measurements. Figure 4.4 shows the Bode diagrams of a reference sample and a sample containing rCF.

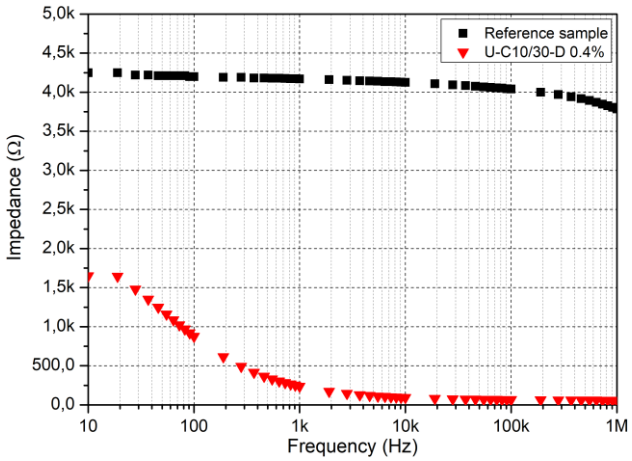

Figure 4.4. Bode diagrams for a reference concrete sample and an rCF-reinforced sample

The reference sample behaves like an insulator with almost no variation in the impedance with the frequency. The incorporation of the rCF modifies the electrical behaviour of the samples, and the impedance reduces as the frequency of the applied current is increased. As stated by several researchers, there is a cut-off frequency that permits bypassing of the cementitious matrix that surrounds the fibres in carbon fibre-reinforced materials (Mason *et al.*, 2002), referred to as cusp frequency. This cut-off frequency is also displayed when rCF is used (Faneca *et al.*, 2018), and the values are 100 and 190 kHz, respectively, for C10/30 and CT12 samples. The electrical resistivities were determined at two different frequency values: 50 Hz and 190 kHz. The first value coincides with the standard frequency for AC, and the second was selected to perform the measurements above the capacitance threshold (Ct) value, and thus bypass the cementitious matrix that surrounds the rCF (Mason *et al.*, 2002; Faneca *et al.*, 2018).

The variation of the electrical conductivity with the fibre content for specimens with C10/30 and CT12 is shown in Figure 4.5, where the y-axis presents different limits to accommodate the different limits of both σ50Hz and σ190kHz. For low frequencies (see Figure 4.5a), specimens with C10/30 exhibit larger electrical conductivity and CT12 specimens present electrical conductivities that are quite similar to that of the reference sample without rCF. Furthermore, the electrical conductivity of samples with C10/30 decreases for fibre contents larger than 0.6% vol. This electrical behaviour is related to the presence of carbon fibre bunches in the cementitious matrix (Faneca *et al.*, 2018).

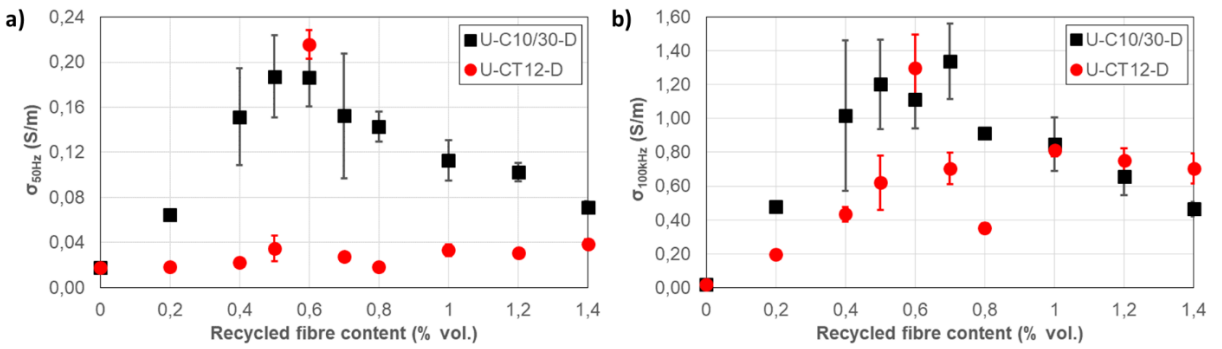

Figure 4.5. Variation of the electrical conductivity with the fibre content: a) at 50 Hz, and b) at 190 kHz.

However, when the capacitance threshold is surpassed (Figure 4.5b), the electrical behaviour is modified. Whereas the electrical conductivity of the reference sample remains almost invariant (it varies from 0.0178 S/m at 50 Hz to 0.0185 at 190 kHz), there is a strong increase in the electrical conductivity of the specimens containing rCF. The samples with C10/30 fibres present a seven-fold increase in the electrical conductivity on average, while the samples with CT12 fibres show a nineteen-fold increase on average. Although the number of fibres per unit volume of CT12 samples is larger than that of C10/30 samples, the presence of fibre bunches limits the electrical properties of the former. However, for frequencies above the capacitance threshold, the effect of the fibre bunches on the electrical

conductivity is diminished and the electrical conductivity of both C10/30 and CT12 samples becomes equal.

The electrical properties of carbon fibre-reinforced cementitious composites depend mostly on two different parameters: the dispersion of the fibre in the cementitious matrix and the waviness of the carbon fibres. The goodness of fibre dispersion in the cementitious matrix will determine the presence of fibre agglomerates (clusters). Furthermore, the characteristics of the carbon fibres usually utilised in cementitious composites may affect its waviness and thus its actual length. Both parameters will determine the presence of a continuous path of fibres and thus the electrical conductivity of the composite. García-Macías (García-Macías, Alessandro and Castro-triguero, 2017) studied both the effect of clustering and waviness on the electrical conductivity of CNT cementitious composites. The results shown in Figure 4.5 are consistent with the combined effect of clustering and waviness.

4.3.3.- Piezo-resistive response of specimens under laboratory conditions

Figure 4.6 shows the load-voltage curves obtained for different concrete specimens made with different contents of C10/30 rCF during compression tests. First, it is noticeable that the reference specimen without rCF also shows a piezo-resistive effect. A small variation in the voltage curve can be observed repeatedly, coinciding with the maximum and minimum values of the applied load. The piezo-resistive responses were also observed using DC, and thus ionic effects can be observed in the voltage curve represented by the voltage drop from the start to the end of the test.

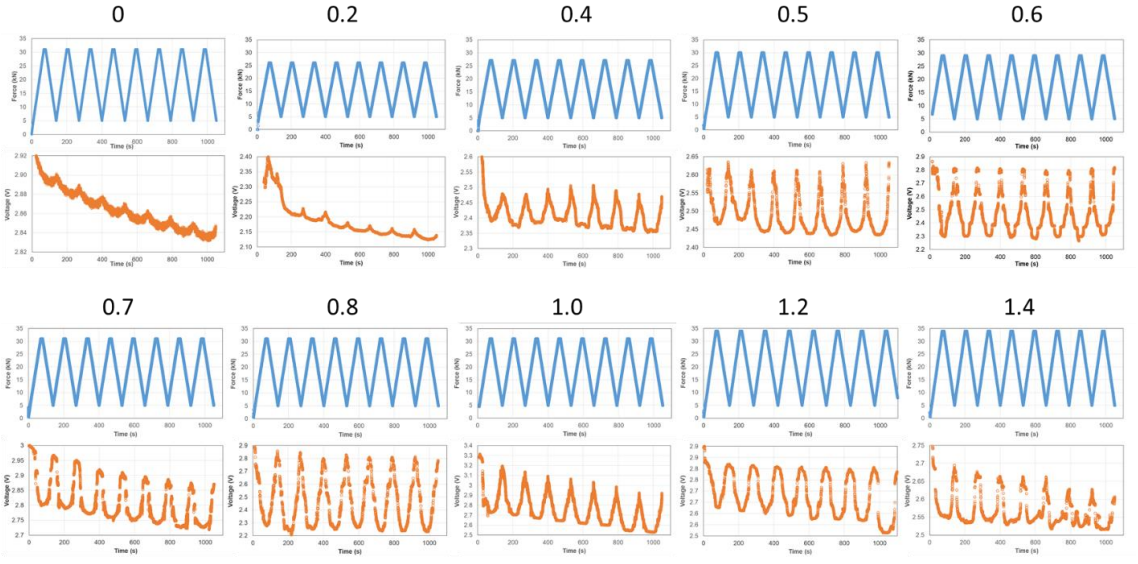

Figure 4.6. Load-voltage curves for the concrete specimens prepared with C10/30 rCF during the compression tests. The numbers above the curves indicate the rCF content of the concrete specimens.

The introduction of the rCF has a remarkable effect on the voltage curve; it increases the amplitude of the voltage variation. The amplitude of the voltage variation depends on the rCF content and increases up to a fibre content of 0.8 %. However, the introduction of rCF also affects the stability of the voltage curve and for fibre contents above 0.2 %, the initial and final voltage is almost the same for different specimens. No evidences of the piezo-resistive effect were observed upon analysing the load-voltage curves obtained from flexural tests (see Figure 4.7).

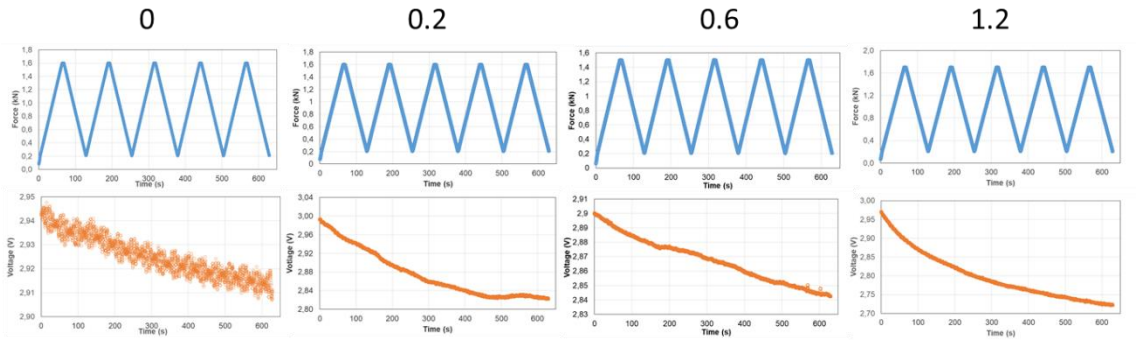

Figure 4.7. Load-voltage curves for the concrete specimens containing C10/30 rCF during the compression tests. The numbers above the curves indicate the rCF content of the concrete specimens.

Similar load-voltage curves were obtained for the specimens containing CT12 fibres, indicating a piezo-resistive phenomenon during the compression tests (see Figure 4.8), but no clear evidence of it was found during the flexural tests. The load-voltage curves in Figure 8 present some distinctive features presenting more noise and more irregular patterns that those shown in Figure 4.6. The different data obtained from the load-voltage curves during the compression tests are collected in Table 4.3.

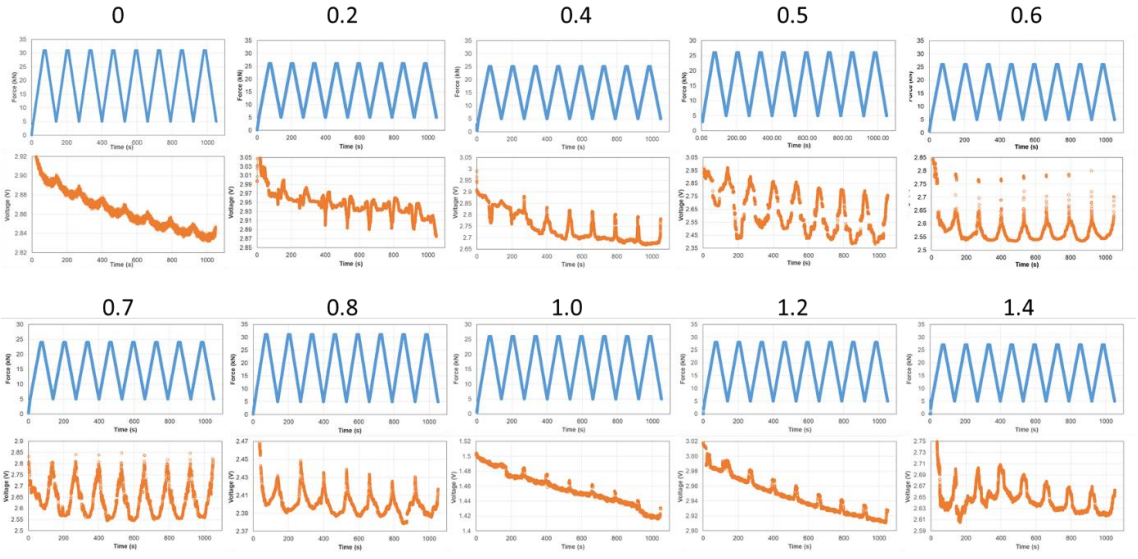

Figure 4.8. Load-voltage curves for the concrete specimens containing CT12 rCF during the compression tests.

rCF Content (%)	C10/30		CT12	
	Voltage drop (V)	$\Delta V_{peak-peak}$ (V)	Voltage drop (V)	$\Delta V_{peak-peak}$ (V)
0	- 0.09	0.005	- 0.09	0.005
0.2	- 0.89	0.02	- 0.20	0.04
0.4	- 0.66	0.11	- 0.21	0.10
0.5	- 0.35	0.38	- 0.22	0.17
0.6	- 0.06	0.50	- 0.30	0.24
0.7	- 0.13	0.15	- 0.20	0.27
0.8	- 0.32	0.57	- 0.16	0.04
1	- 0.37	0.41	- 0.07	0.009
1.2	- 0.09	0.21	- 0.09	0.01
1.4	- 0.16	0.12	- 0.05	0.05

Table 4.3. Parameters obtained from the load-voltage curves of concrete specimens with C10/30 and CT12 during the compression tests

One of the parameters affected by the type of rCF used is the voltage drop measured during the piezo-resistive tests, as shown in Figure 4.9. The voltage drop is related to the presence of the polarisation phenomenon because of the movement of electrical charges during the test. The polarisation phenomenon usually appears in cementitious materials when they are subjected to an electrical field. Wen et al. have already shown that electrical polarisation diminishes when carbon fibres are incorporated into cementitious matrices (Wen and Chung, 2001).

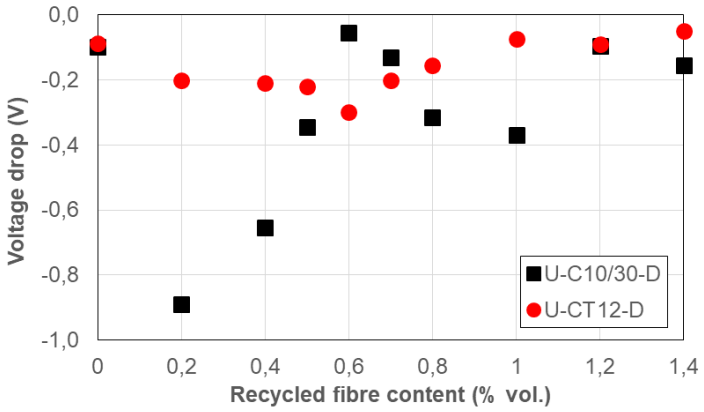

Figure 4.9. Voltage drop measured during the piezo-resistive tests.

Samples incorporated with C10/30 fibres present very large voltage drops for low fibre contents, and the voltage drop diminishes with an increase in the rCF content. The voltage drop stabilises at approximately −0.1 to 0.2 V. A further increase in the voltage drop in C10/30 samples may be related to the presence of fibre bunches (Faneca *et al.*, 2018). Samples incorporated with CT12 fibres present a voltage drop that almost shows no variation with the rCF content. For rCF contents below the percolation threshold value (~0.6% vol.), the voltage drop of CT12 specimens is lower than that of C10/30 samples.

The second parameter influenced by the type and content of rCF is the amplitude of the voltage variation (ΔVpeak-peak). The variation of ΔVpeak-peak with the rCF content is very similar for concrete samples with both rCF types, C10/30 and CT12, as shown in Figure 4.10, where three different zones can be identified. In zone I, for low rCF contents (below 0.2% vol.), the ΔVpeak-peak values are very similar to that observed for the reference sample without rCF. Further increase in the rCF content results in a linear increase in ΔVpeak-peak up to the percolation threshold value. The slope of the linear variation in zone II is different for C10/30 and CT12 fibres, with the corresponding slopes being 1.02 and 0.49, respectively.

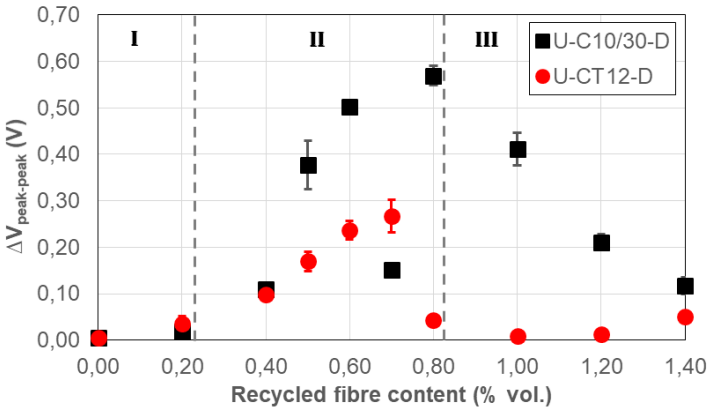

Figure 4.10. Variation of ΔVpeak-peak with the rCF content

The observed behaviour can be explained considering the number of fibres per unit volume, N. For rCF contents below 0.4%, the differences in the numbers of fibres per unit volume of CT12 and C10/30 fibres are small, and thus low differences in is expected in the fibre dispersion. However, as the rCF content increases, so does the difference in N. Lastly, in zone III, ΔVpeak-peak diminishes with the fibre content because of the formation of fibre bunches in the cementitious matrix, although the variation is clearly influenced by the fibre type. The samples incorporated with CT12 fibre display a more drastic reduction in ΔVpeak-peak for rCF contents above the percolation threshold. Thus, the number of fibres per unit volume seems to play a specific role in the conductivity of the concrete, and thus on the observed piezo-resistive phenomenon.

However, some differences are observed when ΔVpeak-peak is analysed considering the conductivity of the samples (see Figure 4.11). Considering the hypothesis presented, ΔVpeak-peak could be expected to increase with the conductivity of the specimens up to a maximum value related to the percolation threshold. The samples incorporated with C10/30 fibres agree with this hypothesis at both 50 Hz and 190 kHz, with some outlier values (clearly identified in Figure 4.11 by shaded areas), which will be analysed further. However, samples incorporated with CT12 fibres do not agree with this behaviour when analysed at 50 Hz, but they agree when the values of ΔVpeak-peak are compared for σ190kHz, with some outlier values.

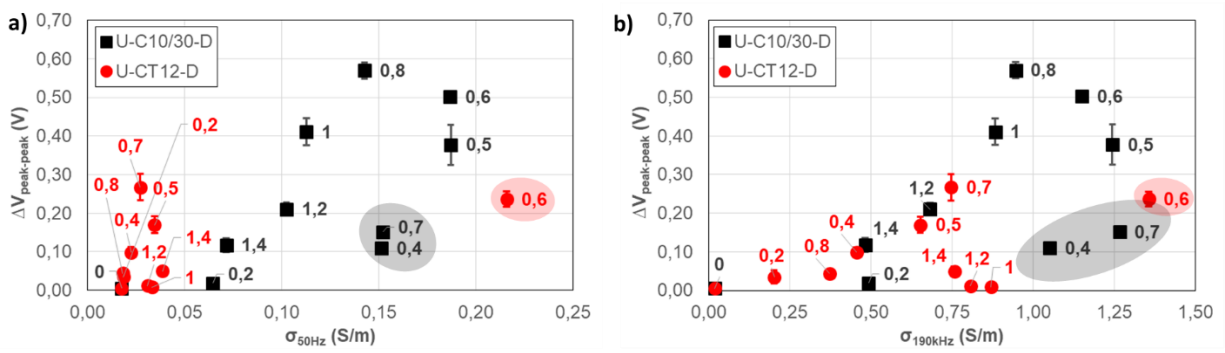

Figure 4.11. Variation of ΔVpeak-peak with the conductivity for each rCF type: a) σ50Hz, and b) σ190kHz (outliers identified by shaded areas).

The two values identified as outliers in the ΔVpeak-peak vs σ curve of the C10/30 samples were also outliers in the ΔVpeak-peak–Vf curve and correspond respectively to the values immediately below and above the percolation threshold (0.4 and 0.7% vol.) Similarly, the outlier in the ΔVpeak-peak–σ curve of the C10/30 sample corresponds to the rCF content at the percolation threshold (0.6% vol.). However, the trends observed in the ΔVpeak-peak–σ (Figure 11) curves do not correlate completely with the σ–Vf curves (Figure 4.5).

4.- DISCUSSION

Several researchers have proposed models to account for the piezo-resistive responses of conductive cementitious materials. The first studies on this topic were presented by Sun et al. (Sun *et al.*, 2000)] and Wen & Chung (Wen and D. D L Chung, 2006). More recently, García-Macías et al. (García-Macías, Alessandro and Castro-triguero, 2017) presented a very detailed review on the available models and proposed a new three-dimensional mixed micromechanics-FEM modelling of piezo-resistive CNT smart concrete. Sun et al. (Sun *et al.*, 2000) described the observation of piezo-resistive effects in plain cementitious materials and explained it in terms of a solid-liquid interface double-layer model. In this situation, when a compressive force is applied, the ions in the double-layer are transported to the cement pore solution because of the interface shear stress. Thus, charges accumulate and a streaming potential difference arises.

The load–voltage curve of the reference samples (Figure 4.6) presents two different phenomena during loading and unloading. During the loading of the sample, the voltage decreases because of a leakage of charges through the conductive paths of the cementitious matrix and the flow of the cement pore solution. During unloading, a part of the solution refills the vacated pores and the voltage is increased. When the rCFs are incorporated into the cementitious matrix, the mechanism is mostly similar because of the cementitious paste that coats the carbon fibres. Two adjacent carbon fibres will always be surrounded by cementitious paste, but the thickness of this interface reduces as the rCF content is increased.

Thus, the incorporation of rCF does not alter the main mechanism of piezo-resistivity but amplifies the effect by increasing the signal-to-noise ratio. The signal-to-noise ratio, SNR, (in dB) is estimated by Eq. 8, as the ratio of the value of a given parameter (σ50Hz, σ190kHz, or ΔVpeak-peak) for a concrete sample with a given rCF content to that of the same parameter for the plain concrete sample:

$$SNR = 10 \cdot log\left(P_{signal} / P_{noise}\right) \qquad \text{Eq (4.8)}$$

The influence of the rCF content on the SNR is presented in Figure 4.12, where two different behaviours can be identified. First, the SNR of σ50Hz and σ190kHz presents a slight increase for rCF contents below the percolation threshold and stabilizes for further increases in the rCF. The average SNR values of σ50Hz and σ190kHz differ significantly for a given fibre type, as shown in Table 4.4. Moreover, the average SNR values σ50Hz also differ significantly for C10/30 and CT12 fibres, however, on the contrary, the SNR values of σ190kHz are very similar. The conductivity measurements for frequencies below the capacitance threshold (50 Hz) are controlled by the fibre-matrix interface, and thus by the dispersion of the carbon fibres.

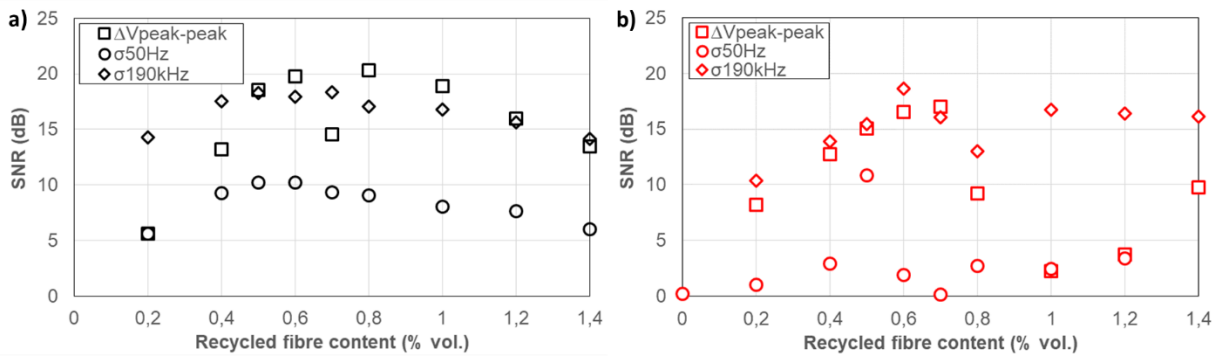

Figure 4.12. Variation of the SNR of σ50Hz, σ190kHz, and ΔVpeak-peak for a) U-C10/30-D specimens, and b) U-CT12-D specimens

As discussed previously, the specimens incorporated with CT12 fibres in our study are more likely to present fibre bunches than the ones incorporated with C10/30 fibres, because of the larger number of fibres per unit volume of the former. Therefore, the SNR of σ50Hz reflects the influence of the fibre-matrix interface. However, for frequency values above the capacitance threshold (190 kHz), the conductivity values are mainly influenced by the electronic conduction and the effects of the fibre-matrix interface are reduced. Thus, the SNR of σ190kHz is very similar for both fibre types. The variation in the SNR of ΔVpeak-peak with the rCF content presents a mixed behaviour between σ50Hz and σ190kHz.

For values below the percolation threshold, the SNR values of ΔVpeak-peak are similar to those of σ50Hz. This behaviour is observed in the samples incorporated with both C10/30 and CT12 fibres. For rCF contents above the percolation threshold, the SNR of ΔVpeak-peak varies depending on the fibre type: for the C10/30 samples, the SNR almost

shows no variation with increasing rCF content, whereas for the CT12 specimens, there is a strong decrease in the SNR followed by an increase for larger rCF contents. This mixed behaviour may be attributed to a mixed control of the piezo-resistive phenomena in these samples. For rCF contents below the percolation threshold, the main controlling factor is the fibre-matrix interface, whereas for larger rCF contents, the controlling factor varies between the electronic transfer mechanism and the fibre-matrix interface, depending on the characteristics of the fibre dispersion in the cementitious matrix.

SNR (dB)	Fibre type	
	C10/30	CT12
σ_{50Hz}	8.4	2.8
σ_{190kHz}	16.7	15.2
$\Delta V_{peak-peak}$	15.6	10.5

Table 4.4. Average values of SNR for different parameters and rCF types

The observed behaviour is in agreement with previous observations by Sun et al. (Sun *et al.*, 1998), which were more recently confirmed by Baeza et al. (Baeza *et al.*, 2018), who proposed a constitutive model for the electrical behaviour of carbon fibre-reinforced composites. This model includes four possible conductive mechanisms: 1) ionic conductivity, 2) conductivity due to electronically conductive fibres in the cement matrix and conductive holes, 3) conductivity due to electronically conductive paths between the fibres and the continuous conductive holes, and 4) conductivity due to electronically conductive fibres passing through the conductive network past the conductive hole.

For a sample with low carbon fibre content, the main conductive mechanisms are 1) and 2). As the fibre content increases, electrical conduction occurs mainly via mechanisms (2) and (3). When the fibre content is increased above the percolation threshold, mechanism 4) becomes the main pathway. Therefore, the piezo-resistive phenomena shown in Figure 4.6 and Figure 4.8 reflect both the influence of the fibre-matrix interface and the electronic transfer mechanism. For low rCF contents, the thickness of the fibre-matrix interface is large and so is the distance between the carbon fibres.

Thus, for low rCF contents the fibre-matrix interface in the cementitious matrix will control the piezo-resistive response of the composite. As the rCF content is increased up to the percolation threshold, the thickness of the cementitious matrix surrounding the fibres reduces, and thus the electronic transfer mechanism becomes dominant in the piezo-resistive phenomenon. For rCF contents above the percolation threshold, the presence of fibre bunches and the effect of the fibre waviness will determine the observed behaviour, and thus the fibre-matrix interface increasingly influence the piezo-resistive behaviour.

4.5.- CONCLUSIONS

The piezo-resistive phenomenon observed in cementitious materials is inherent to their porous structure and the enclosed aqueous solution. The piezo-resistive effect in these materials could be increased by incorporating carbon fibres. In this article, we demonstrated that rCFs can also be incorporated in cementitious composites to increase their piezo-resistive responses. Furthermore, we showed that the main parameters that control the electrical behaviour of carbon fibre-reinforced cementitious composites (fibre dispersion and fibre waviness) also determine the piezo-resistive responses of our cement composites.

For rCF contents below the percolation threshold, the piezo-resistive response is mainly controlled by the thickness of the cementitious paste surrounding the rCF, and thus small piezo-resistive response was obtained. When the rCF was increased, the electronic transfer mechanism started to control the electrical behaviour, and thus the piezo-resistive response increased. However, for rCF contents above the percolation threshold, the presence of fibre bunches and the waviness of the carbon fibres determine the main parameter that controls the electrical behaviour: (i) the fibre-matrix interface and thus the ionic conductivity or (ii) the electronic conduction.

The results presented in this paper open new possibilities for the development of smart cementitious materials that can be introduced into civil engineering structures. The use of recycled carbon fibres and of fabrication procedures similar to those used by the civil engineering industry allow the development of cementitious composites with properties that are equivalent to those of materials fabricated with expensive carbonaceous materials or using sophisticated fabrication and dispersion protocols.

Capítulo 5[3]: CONDUCTIVE CONCRETE MADE FROM RCF FOR SELF-HEATING AND DE-ICING APPLICATIONS

Abstract

This paper presents a broad experimental study performed at laboratory and industrial facilities to develop conductive concrete for self-heating and de-icing applications in urban furniture. Self-heating capacity is achieved by the application of electric current through a highly dense matrix containing recycled carbon fibers and graphite flakes. Prisms and slabs were fabricated with two different conductive concretes and electrode configurations to characterize the electrical properties and heating performance. Finally, 3 benches with different electrode disposals were fabricated to assess the heating capacity in real-scale applications.

The results presented indicate promising results about the use of recycled carbon fibers for electrothermal concrete applications and identify the electrode configuration that allows the most efficient heat transfer and reduction of temperature gradients within the heated element. Real-scale tests show that the current technology developed is potentially applicable at de-icing applications in climates where temperatures remain within the range of -3 or -5 ºC.

3 El presente capítulo se corresponde con el articulo aceptado para su publicación por Faneca, G., Ikumi, T., Segura, I., Torrents, J.M. and Aguado. A. "Conductive concrete made from recycled carbon fibres for self-heating and de-icing applications in urban furniture". Materiales de Construcción. 10 Marzo de 2020. https://doi.org/10.3989/mc.2020.17019

Keywords: Thermal Analysis; Electrical properties; Temperature; High Performance Concrete; Fibre reinforcement

5.1.- INTRODUCTION.

The concept of smart cities have emerged from the opportunities created by the digital era to face the challenges associated with the new urban context. Digital innovation opens up the possibility to be more efficient and more effective, better combating challenges in individual infrastructures, across infrastructure systems, and throughout society as a whole (WEF, 2013; ARUP and UCL, 2017; ICE, 2017). As "smart solutions", or digital technologies, become more commonplace in our cities, the so-called "smart materials" have received increasing attention within the scientific community (D'Alessandro *et al.*, 2016). Their potential is perceived as a key element to bring value to our urban areas and translate it into a profitable commercial practice.

Research on cementitious materials used for civil and building construction has been traditionally focused on mechanical performance and durability characteristics to cover its main functionality, which is structural. However, nowadays there is a demand of multifunctional materials that are not only able to cover the structural requirements but also incorporate additional features that provide the resulting material with an increased range of applications. Most current functional properties in smart concrete are based on the incorporation of functional fillers or aggregates to generate conductive properties in the material.

Conductive concrete has been used as anode for electrochemical chloride extraction (Westhof, 2006; Xu and Yao, 2009; Pérez *et al.*, 2010; del Moral *et al.*, 2013), electromagnetic wave shielding (Singh *et al.*, 2011; Han *et al.*, 2017a), self-sensing concrete (Chen and Chung, 1993; Park *et al.*, 2006; Han, Yu and Ou, 2014; Han, Ding and Yu, 2015), cathodic protection (Carmona, Garcés and Climent, 2015), energy harvesting (Lee *et al.*, 2014; Wei *et al.*, 2014) and electrothermal control (Chung, 2004; Baeza *et al.*, 2010; Zhao *et al.*, 2011, 2019; Lai, Liu and Ma, 2014; Wu, Liu and Yang, 2015; Zhang *et al.*, 2016; Galao *et al.*, 2016; Hambach *et al.*, 2016; Kim *et al.*, 2016; Bai *et al.*, 2017; Sassani *et al.*, 2018; Wang *et al.*, 2019), among others.

Electrothermal concrete refers to the material achieving electrical resistance heating based on the Joule effect. Research on electrothermal concrete has been mainly focused on deicing and snow melting applications in roadways (Zhao *et al.*, 2011; Lai, Liu and Ma, 2014; Wu, Liu and Yang, 2015; Zhang *et al.*, 2016; Bai *et al.*, 2017; Sassani *et al.*, 2018; Wang *et al.*, 2019), and indoor electrical floor heating (Hambach *et al.*, 2016; Bai *et al.*, 2017; Sassani *et al.*, 2018; Wang *et al.*, 2019; Zhao *et al.*, 2019). Since conventional concrete behaves as a dielectric material, electrically conductive fillers such as carbon

fibers, steel fibers, steel shaving, nickel powders and graphite are incorporated to reduce the resistivity of concrete (Han *et al.*, 2017b).

The use of steel fibers presents a high potential to develop conductive cementitious materials since these are already been widely adopted in a broad range of structural and non-structural concrete applications (Faneca *et al.*, 2018). However, the flow of electric charges through steel fiber reinforced concrete promotes fiber corrosion and thus, the degradation of both the structural and thermal functionality of the material. Nowadays, carbonaceous products are mainly used instead of steel fibers or shavings in the conductive cementitious materials mixture design (Gomis *et al.*, 2015) since these present high thermal conductivity, low thermal expansion and are highly resistant to corrosion.

However, the world-wide demand for virgin carbon fibers often surpasses supply capacity (Roberts, 2006, 2007), which causes an increase of cost both in terms of energy consumed during manufacturing (up to 165 kWh/kg) and material price (up to 40 £/kg) (Carberry, 2008; Pimenta and Pinho, 2011). Additionally, the increasing amount of carbon fiber composites produced raises concern on waste disposal and consumption of non-renewable resources, with the associated negative environmental impact. In this context, the introduction of recycled carbon fibers (RCF) in conductive cementitious materials could potentially convert an expensive product and waste disposal into a profitable reusable material with high retention of mechanical properties (Pimenta and Pinho, 2011) and a 30 to 40% cost savings versus virgin carbon fibers.

So far, research published on the use of RCF in conductive cementitious materials is limited to the characterization of the mechanical and electrical properties of the resulting composite paper presents the first broad experimental study that explores the heating capacity of conductive concrete with recycled carbon fibers for de-icing and self-heating applications at laboratory and industrial scale. Prisms of 40×40×160 mm were fabricated to characterize the electrical properties of two different conductive concretes. Slabs of 300×600×40 mm with two electrode configurations were submitted to different heating test scenarios varying the duration of the heating cycles and the voltage applied.

Finally, three full-scale benches (700×2000×150 mm) with different electrode disposals were fabricated at Escofet 1886 industrial facilities and tested to assess the current heating capacity of the material in real-scale urban furniture applications.

5.2.- EXPERIMENTAL PROGRAM.

5.2.1.- Materials.

Ultra high performance concrete mixtures contained CEM I 52.5R cement and siliceous aggregates with particle size distribution ranging from 0 to 5 mm. A high purity calcium carbonate filler (d50 < 3 μm) was used to contribute to higher compactness and

workability of the mixture. A superplasticizer based on a polycarboxylate solution (MasterGlenium ACE 425) and a viscosity modulator based on siliceous nano-particles (Meyco ms 685) were employed.

Recycled carbon fibers (Carbiso CT6/CT12) and micronized carbon fibers were used to improve the electrical and thermal conductivity of the concrete matrix. The carbon fiber is produced from a primary recycling process of trimmings, defective pieces or deteriorated carbon fiber reinforced composite materials. The main origin of these residues are companies dedicated to the manufacture of compounds for the aerospace, automotive and similar industries. The carbon fiber is obtained by shredding and subsequent pyrolysis to eliminate the polymeric resins impregnated to the fiber. The micronized carbon fibers present particle sizes of d90-d70 = 0.425 and d20 = 0.300 mm. The properties of the carbonaceous materials used are included in Table 5.1.

Fiber	PROPERTIES	UNIT	VALUES
Recycled Carbon Fiber	Carbon fiber content	%	100
	Density	kg/m^3	1800
	Nominal length	mm	6/12
	Diameter	µm	7
	Tensile strength	MPa	4150
	Young modulus	GPa	252
	Electrical conductivity	S·cm^{-1}	100-1000
Micronized Carbon Fiber	Carbon content	min %	95
	Ash content	max %	6
	Moisture	max %	0.5
	Density	g/ml	0.65-0.85

Table 5.1. Properties of the recycled carbon fibers and micronized carbon fibers.

5.2.2.- Composition and preparation of concretes.

In total, two concrete compositions were designed with different carbonaceous addition contents. Table 5.2 describes the composition of the concretes used. The first mixture consists of an ultra-high-performance concrete (UHPC) with 9 kg of recycled carbon fibres per m3 of concrete (0.407 % vol.) to increase the electrical and thermal conductivity of the material (referred to as RCF).

The plain concrete dosage adopted corresponds to mixes typically used by the company Escofet 1886 in the manufacturing process of urban furniture and architectonic façades. The second mixture additionally incorporates 36 kg of micronized carbon fibres per m3 of concrete (1.65 % vol.) to further increase the electrical and thermal conductivity

of the material (referred to as R+MCF). The proportions of the carbonaceous additions were set from previous tests on conductive concretes (Faneca *et al.*, 2018; Segura *et al.*, 2019).

Material	Units	RCF	R+MCF
Cement	kg/m³	800	800
Sand	kg/m³	1161	1161
Limestone filler	kg/m³	200	200
Water [kg/m3]	kg/m³	110	110
Superplasticizer	% bcw[a]	3.7	3.7
Nano silica	% bcw[a]	7.1	7.1
Recycled carbon fiber	kg/m³	9	9
Micronized carbon fiber	kg/m³	-	36

a: By cement weight

Table 5.2. Composition of the concretes

The mixing process was performed in a planetary mixer at the industrial facilities of the company Escofet 1886 to reproduce the typical fabrication practices adopted in the precast industry. Aggregates, limestone filler and cement were first mixed for 60 s. Then, water was added and mixed for 180 s. Nano-silica and superplasticizer were then incorporated to the mix and homogenized for additional 180 s, each. The carbonaceous additions were added to the mix after incorporating the water and additives, with no previous dispersion of the fibers. Previous research has proved that this procedure provides a good dispersion of the fibers into the cementitious matrix (Faneca *et al.*, 2018). Unfortunately, no data about the combined effects of fibers and the micronized addition is available.

Prismatic specimens with dimensions 40×40×160 mm were fabricated from the mixes indicated in Table 5.2 according to UNE-EN 196–1 (AENOR, 2005) to characterize the electrical properties of the concretes. These specimens incorporate six stainless steel threaded shanks of 6 mm diameter and 30 mm length to act as electrodes. The placing of these electrodes was carried out after compacting the fresh concrete in the molds. Figure 5.1a shows a scheme of the electrodes positioning on the specimens.

Slabs (S) of 300×600×40 mm were fabricated from the mixes indicated in Table 5.2 to characterize the thermal behavior of larger specimens. In this case, two different electrode disposals were incorporated to create the electric flux. Figure 5.1b shows a scheme of the electrodes positioning on the slabs. The first configuration (TDS) consisted in two steel deployé sheets with rhomboidal grid of 30×13 mm placed 20 mm from the transverse edges of the element (section A-A' in Figure 5.1b). The latter configuration replaced the deployé sheets by a wider squared steel grid (TSG) of 40×40 mm. Grids on both configurations were connected to the external part of the element by stainless steel

threaded shanks of 6 mm diameter and 30 mm length. The placing of these electrodes was carried out after compacting the fresh concrete in the molds. All specimens remained in the molds for 24h with liquid curing agents and afterwards were kept under controlled temperature (20° ± 5 °C) and humidity (70 ± 10 %) conditions until testing.

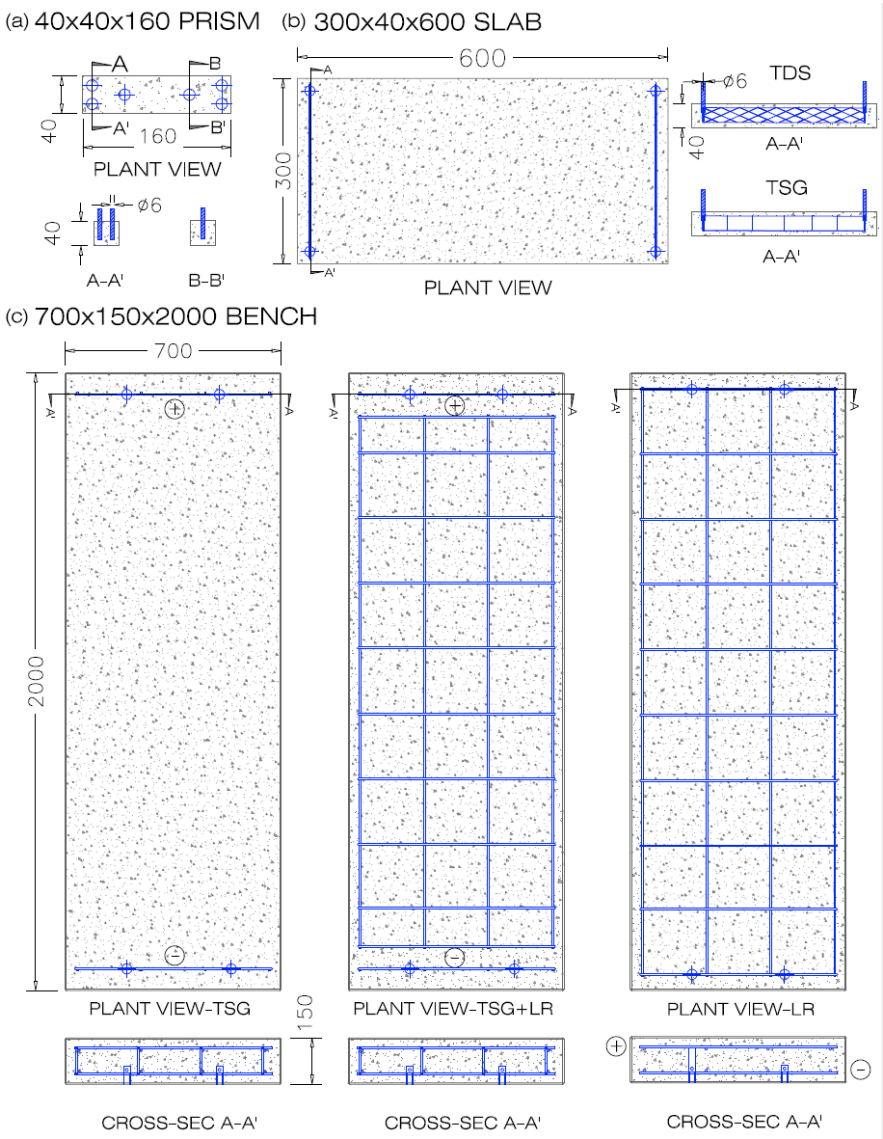

Figure 5.1. Scheme of the electrodes positioning on the specimens. All dimensions in mm

Finally, three benches with dimensions 700×2000×150 mm were fabricated to assess the heating capacity of the material in real-scale conditions, each with a different electrode disposal (Figure 5.1c). The simplest configuration consisted in transversal square grids (TSG) on both edges of the slab. The second bench incorporated upper and lower longitudinal reinforcement (LR) to increase the electrical conductivity of the element, without these being connected to the inlet electrodes (TSG). The third bench replaced the TSG configuration by using directly the upper and lower longitudinal reinforcement as inlet/outlet electrodes. Notice that the latest configuration reduces drastically the distance

between electrodes. In this case, the electric flux generated travels vertically from the lower to the upper longitudinal reinforcement. Figure 5.2 presents the visual aspect of the real-scale benches fabricated.

Figure 5.2. Visual aspect of the full-scale benches fabricated for the thermal characterization.

The nomenclature adopted during the analysis of the results to identify the different specimens, electrode configurations and concrete mix followed the pattern: "Specimen type (B/S/BENCH)"_"electrode configuration (TDS/TSG/TSG+LR/LR)"_"concrete mix (RCF/R+MCF)".

5.3.- CHARACTERIZATION METHODS

5.3.1. Electrical characterization

The characterization of the electrical conductivity was performed on 40×40×160 mm prisms by using an impedance analyst system Agilent HP 4192A together with an instrumentation amplifier as the front-end to allow 4-probe measurements (4w) (Gersing, 1991) with an effective voltage of 1 V AC to avoid polarization effects in the electrodes (Wen and D D L Chung, 2006; Wen and Chung, 2007). Figure 5.3 shows the experimental set up and the 4w configuration adopted to perform the electrical characterization.

Measurements were obtained with the frequency scanning from 10 Hz to 1 MHz, providing electrical impedance (Z, in Ω) and phase (, in °). The electrical impedance is described by Eq. (5.1) and is composed of a real part (electrical resistance, R) and an imaginary part (reactance, X). R and X are obtained from Eq. (5.2) and Eq. (5.3), respectively.

$$Z = R + jX \quad \text{Eq. (5.1)}$$

$$R = Z\cos\left({}^{\phi\pi}/_{180}\right) \quad \text{Eq. (5.2)}$$

$$X = -Z\sin\left({}^{\emptyset\pi}/_{180}\right) \quad \text{Eq. (5.3)}$$

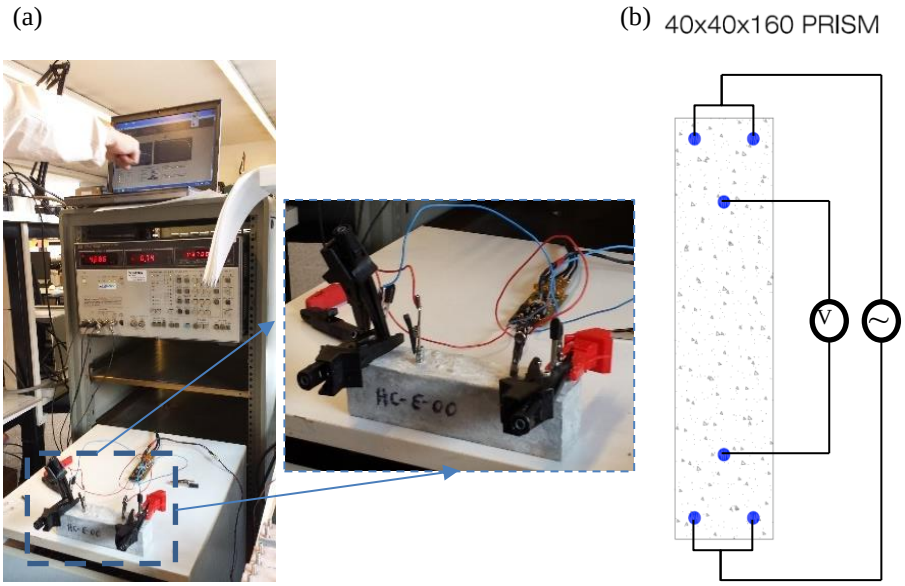

Figure 5.3. (a) Measurement equipment and (b) 4w configuration for the electrical characterization.

Once the electrical resistance is obtained, it is possible to compute the electrical resistivity of the material ρ [Ω·m]. This property assesses the specific electrical resistance of each material that opposes the electrical flow and can be computed as shown in the Eq. (5.4), where S is the cross-section [m²] and L the length [m].

$$\rho = R\,{}^{S}/_{L} \qquad \text{Eq. (5.4)}$$

5.3.2.- Thermal characterization.

The heating behavior of the conductive cement-based materials casted was characterized on two different stages. The first stage evaluated the heating capacity of the 300×600×40 mm slabs by modifying the duration of the heating cycles and the voltage applied. The duration of the heating cycles evaluated were 3 h and 48 h. For the 3 h test, a constant voltage was applied throughout the heating cycle to the specimens via the different electrode configurations incorporated. The 48 h test was comprised by 2 cycles of 8 h heating period followed by a 16 h cooling period. Different voltages were adopted during the tests to evaluate different heating kinetics (11/18/25 V in the 3 h heating and 25/33 V in the 48 h cycles).

The thermal characterization of the different configurations is evaluated in terms of the increase of temperature in the center of the slab, the temperature gradient between the center of the element and the inlet electrode and the electrical resistance of the material throughout the test. The electrical resistance is estimated based on the effective voltage (Veff) and current (Ieff) monitored during the tests. Since the voltage and current are in

phase, the electrical resistance (R) can be computed by the Ohm's law as indicated in Eq. (5.5).

$$R = V_{eff}/I_{eff} \quad \text{Eq. (5.5)}$$

Such characterization covers important aspects required in concrete mixtures for self-heating applications, which are the achievement of certain heating rates, the uniformity of the temperature distribution within the element and the capacity of the material to sustain different voltages during long periods without affecting its heating properties. Additionally, the power consumption computed by Eq. (5.6) is reported in each test.

$$P_{eff} = V_{eff} I_{eff} \quad \text{Eq. (5.6)}$$

The second stage evaluated the heating capacity of the three full-scale benches fabricated. In this case, the duration of the heating cycles was set at 3 h and the voltages applied varied from 2 to 21 V. The different voltages applied were not adopted to perform comparative analyses between the different electrodes configurations incorporated in the benches. Instead, these values correspond to the maximum voltage (and thus, maximum heating capacity) sustained by the material prior to degradation of the conductive and thermal properties. In other words, the full –scale trials were designed to show the full potential of the material in real-scale applications. Table 5.3 summarizes the distribution of the heating tests performed and the voltages evaluated over the different specimens evaluated. All tests were performed at the frequency of 50 Hz.

Specimens	3h heating	8h heating/16h cooling
S_TDS_RCF	11/18/25 V	25 V
S_TSG_RCF	11/18/25 V	25 V
S_TDS_R+MCF	11/18/25 V	-
S_TSG_R+MCF	11/18/25 V	-
BENCH_TSG_RCF	21 V	-
BENCH_TSG+LR_RCF	11 V	-
BENCH_LR_RCF	2 V	-

Table 5.3. Tests performed for the thermal characterization

Figure 5.4a presents the experimental set up adopted during these tests. Temperature variations are registered by type K thermocouples embedded in the material. Figure 5.4b shows the exact location of the thermocouples placed in the slabs and benches. For the 300×600×40 mm slabs, these were located in the middle section 1 cm away from the inlet electrode and at the center of all specimens. On the other hand, full-scale benches incorporated 12 thermocouples arranged all over the slab. A virtual square grid is depicted in dotted red lines on the plant view of Figure 5.4b to facilitate the identification of the

sensors and the analysis of the results. A can be seen, those near the longitudinal edges (rows A and C) were placed at the middle section of the bench while those located in the central region (row B) were arranged closer to the upper external surface to characterize the temperature perceived by the user.

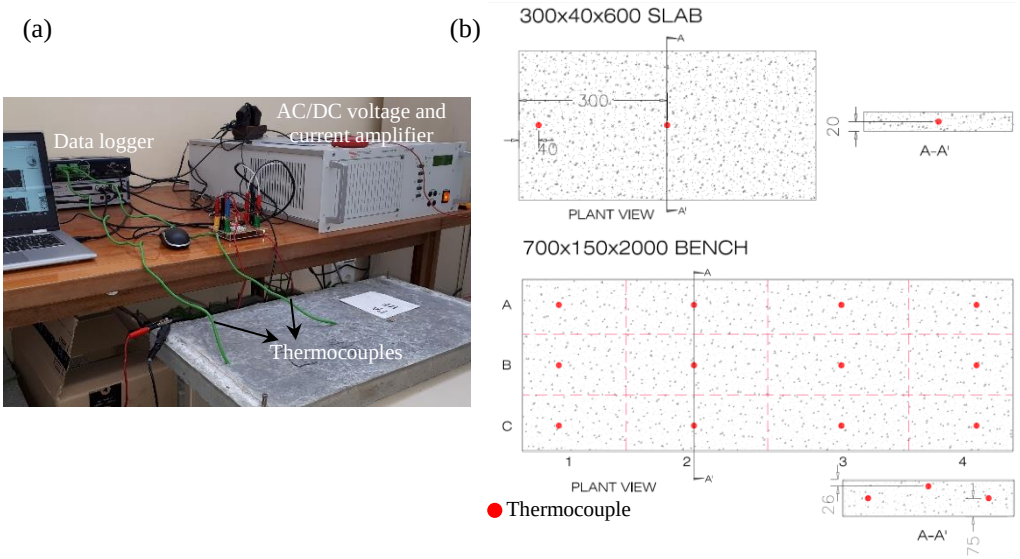

Figure 5.4. (a) Experimental set up for the thermal characterization tests and (b) Thermocouples placement in slabs and benches.

5.4.- RESULTS AND DISCUSSION.

5.4.1.- Electrical characterization of the carbonaceous materials.

Figure 5.5 shows the variation of the electrical resistivity within the range of frequencies evaluated for both concrete mixtures used in this study (RCF and R+MCF). Results for the specimens with recycled and micronized carbon fibers are depicted in the main vertical axis while samples with only recycled carbon fibers are represented in the secondary axis. The error bars included correspond to +1/-1 standard deviation associated with the 3 specimens tested for each material. An additional dotted blue line is added at 50 Hz to locate the standard frequency of electrical mains.

RCF specimens present a constant electrical resistivity of 0.055 Ωm, regardless of the frequency applied. On the other hand, R+MCF samples obtained electrical resistivities ranging from 0.27-0.44 Ωm. The reduction of resistivity with the increase of frequency is commonly associated with insulator materials. This behavior might be caused by polarization effects. Some authors have suggested that polarization effects are not eliminated by the use of AC but are rather manifested in the form of introduction of a capacitance in parallel with the electrical resistance. As the frequency of the applied current is increased, the effect of the capacitance is reduced (Faneca *et al.*, 2018).

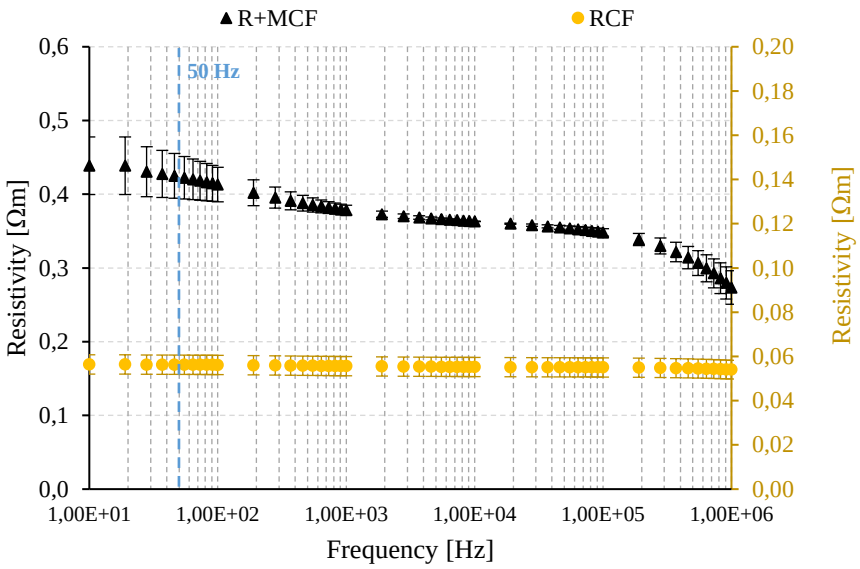

Figure 5.5. Electrical resistivity variation with the frequency.

At the frequency of 50 Hz, which is the one applied during the heating tests, R+MCF material obtained a resistivity of 0.42 Ωm. This value is 7.6 times higher than the one obtained for RCF material, indicating that the addition of micronized carbon fibers causes a very significant increase of resistivity. This trend was not initially expected, as micronized carbon fiber is a highly conductive material. However, the results obtained seem consistent both statistically and with the outcomes of the heating tests performed in 300×600×40 mm slabs (presented in section 5.4.2). Therefore, these should not be attributed to possible malfunctions of the measurement equipment or singular fabrication flaws. Instead, results suggest that the addition of MCF hinders the homogeneous distribution of carbonaceous products within the concrete matrix and disrupts the electrical continuity of the material.

5.4.2.- Thermal characterization in slabs.

5.4.2.1. 3h heating cycle in slabs.

The first test series involved the application of three different effective voltages (11V, 18V and 25 V) during 3 h on rectangular concrete slabs with both types of electrode disposals (TSG and TDS) and carbonaceous additions (RCF and R+MCF). Figure 5.6 presents the heating curves obtained for all specimens tested based on the electrode configuration adopted. Figure 6a depicts the specimens with TDS electrode configuration while Figure 6b presents the samples with TSG configuration. The temperature variations presented correspond to the values registered at the center of the specimen, as this region is more representative of the real heating potential of the material.

Figure 5.6 includes average power consumption values registered in each test. These values are maintained constant throughout the heating test duration, with a

maximum +1 standard deviation of 0.9 W. Room temperature during the tests ranged between 19 - 21 ºC.

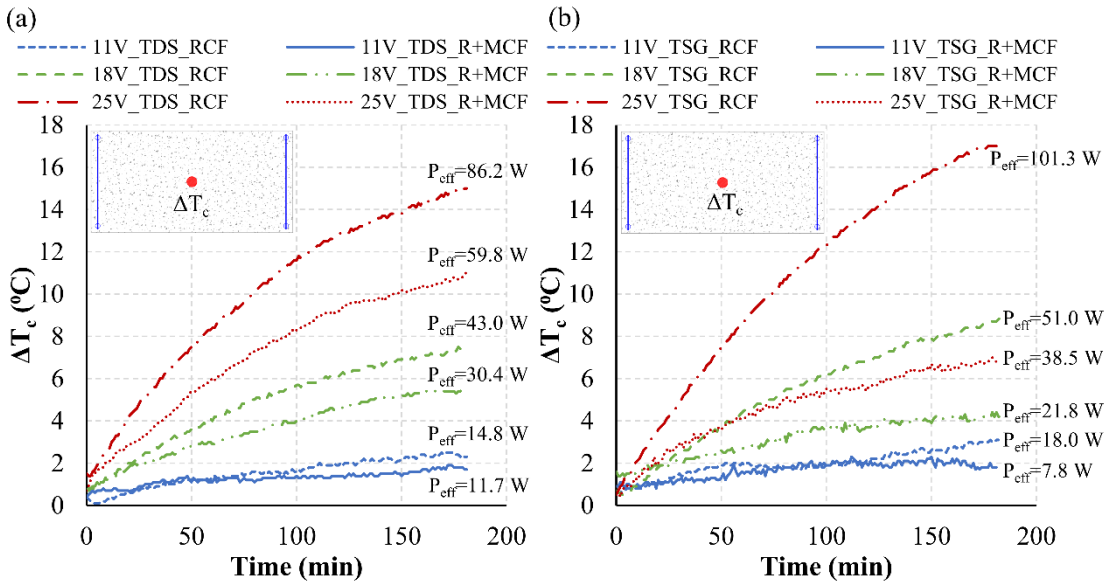

Figure 5.6. Heating curves based on material (RCF and R+MCF) for electrode configuration (a) TDS and (b) TSG.

The positive values registered at the beginning of the test indicates that the inner region of the concrete element was at a higher initial temperature than the ambient. The heating curves describe a linear increase of temperature over time followed by a second stage characterized by a decrease on the heating rate. The duration of the first stage decreases with the intensity of the voltage applied while the heating rate reduction during the second stage is more evident for high voltages.

As expected, results show increasing heating rates with the voltage applied. Temperature variations registered at the end of the test range from 7 – 17 °C, 4 - 8.5 °C and 2 - 3 °C for 25, 18V and 11 V, respectively. These values reflect that the heating performance (increment of temperature per volt applied) is not constant for the different potentials adopted in this study. For the high voltage configuration, the heating performance ranges between 0.28-0.68 °C/V while for the low voltage configuration, the heating performance decreases to 0.17-0.28 °C/V.

The arrangement of the results adopted allows a direct comparison between the heating capacity associated with the two carbonaceous additions introduced in the concrete mix. On average, temperatures reached at the end of the test by the material with recycled carbon fibers and graphite flakes are 25 and 50 % lower than the ones achieved by the material with only carbon fibers for TDS and TSG electrode configurations, respectively. These results suggest that the additional incorporation of graphite flakes into the mix

significantly worsen the performance of the material for heating applications, especially if the TSG electrode configuration is adopted.

Figure 5.7 rearranges the same set of results to allow a clear assessment of the influence of the electrode disposal (TDS or TSG) on the heating capacity of RCF (Figure 5.7a) and R+MCF slabs (Figure 5.7b). Figure 5.7a shows similar heating curves for both electrode configurations in specimens with only reinforced carbon fiber, indicating that the electrode disposal plays a minor role on the heating performance of material RCF. However, this trend is not maintained in R+MCF (Figure 5.7b). In this case, specimens with TDS electrode configuration display higher heating curves than specimens with TSG disposal for all voltages evaluated. These results suggest that in low conductive materials, the increment of steel surface allows a more efficient transfer of the electric charges between the electrode and the conductive concrete.

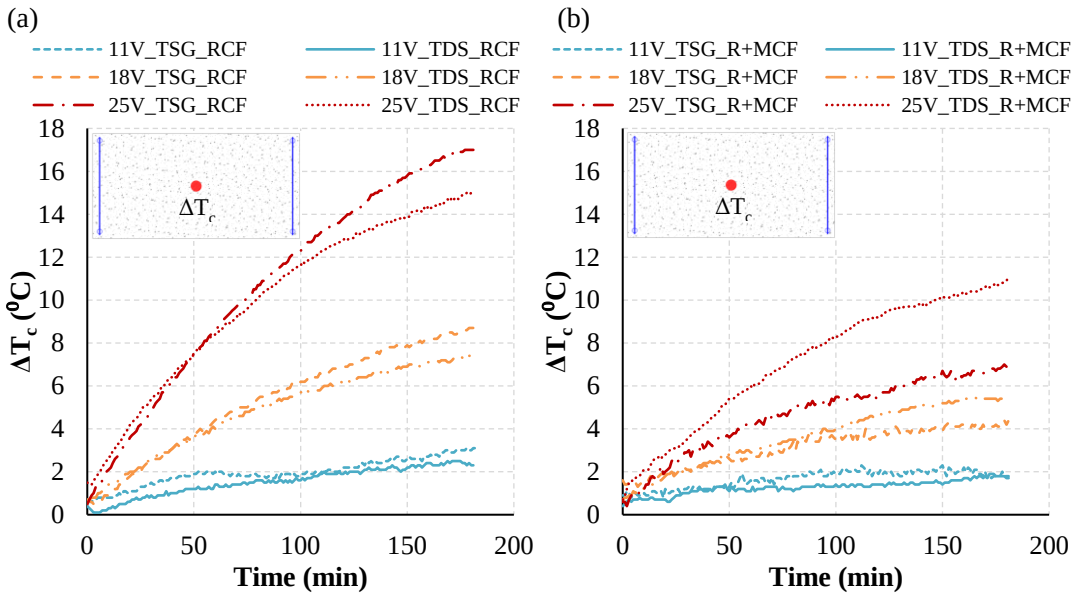

Figure 5.7. Heating curves based on electrode configuration (TDS and TSG) for (a) RCF and (b) R+MCF.

Even though temperature gradients are inherent to the heating mechanism induced by the Joule effect, if not limited, these might compromise the serviceability of the structure and generate high internal stresses that might affect the structural performance of the element. Therefore, the development of self-heating concrete mixes not only comprises the assessment of the heating rates but also the evaluation of the temperature distribution within the element.

Figure 5.8a and Figure 5.8b depict the influence of the voltage and the carbonaceous addition on the temperature drop registered between the center of the slab (ΔTc) and near the inlet electrode (ΔTi) for TDS and TSG configuration, respectively. Independently of the electrode disposal, temperature gradients are characterized by a rapid increase followed by a second stage where the temperature lost tend to a constant value, especially for medium

and high voltages. As expected, results show increasing temperature drops with the voltage applied, suggesting that temperature gradients increase proportionally with the heating rate.

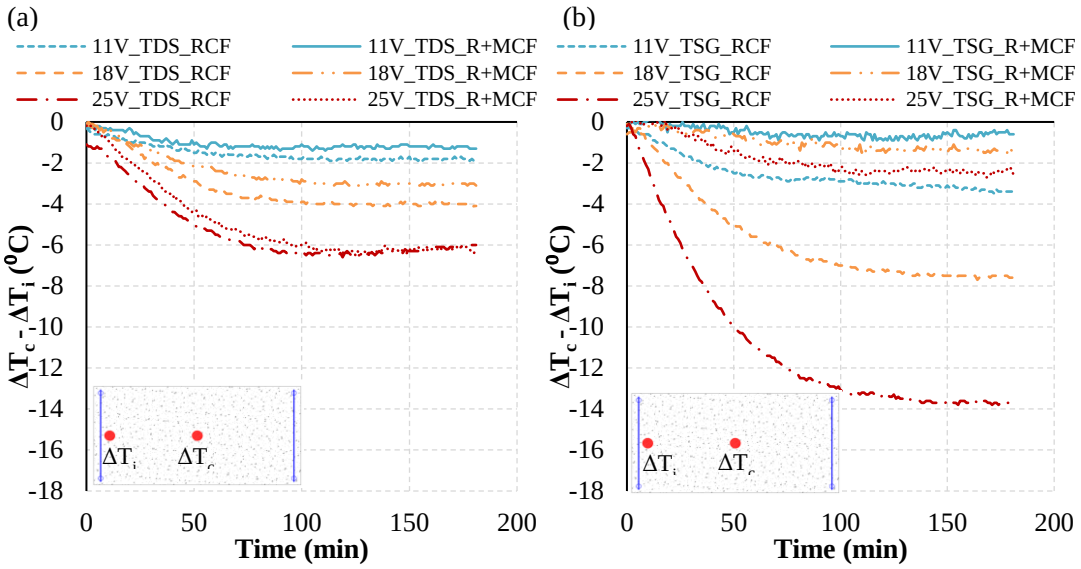

Figure 5.8. Temperature drops registered between the inlet electrode and the center of the slab in (a) TDS and (b) TSG electrode configurations.

Temperature drops registered at the end of the test range from 1–6 °C and 1-14 °C for TDS and TSG configuration, respectively. These results suggest that the TDS electrode disposal limits the magnitude of heat peaks nearby the electrode location, allowing a more efficient heat transfer to the conductive concrete. Figure 8a shows a minor influence of the type of carbonaceous addition on the temperature gradients registered throughout the test. Therefore, the temperature drops registered in specimens with TDS electrode disposal is mainly attributed to the intensity of the voltage applied.

On the other hand, Figure 5.8b depicts much larger temperature drops in RCF specimens than in R+MCF slabs. These results seems to be related to the small heat transmission surface of the electrode configuration TSG, when compared to the TDS. The small contact area of the TSG configuration demands a highly conductive cementitious material to distribute efficiently the electrical charges throughout the specimen. Otherwise, high local temperature peaks are generated nearby the electrode location and the temperature drop increase significantly, especially for high voltage configurations.

Finally, Figure 5.9 presents the evolution of electrical resistance displayed by the specimens tested. The shaded domains represented corresponds to the envelope covered by the electrical resistance curves measured in each specimen for all voltages (11V, 18V and 25 V). Results show constant values throughout the test duration, regardless of the voltage applied.

In other words, the variations of voltage and intensity were proportional within the range considered in the tests. This suggests that the material is able to sustain all testing conditions without deteriorating its conductive properties. Values obtained range from 6 to 15.7 Ω, for TSG_RCF and TSG_R+MCF material configuration, respectively. As expected, electrical resistance values are inversely proportional to the heating capacity of the material at the center of the slab.

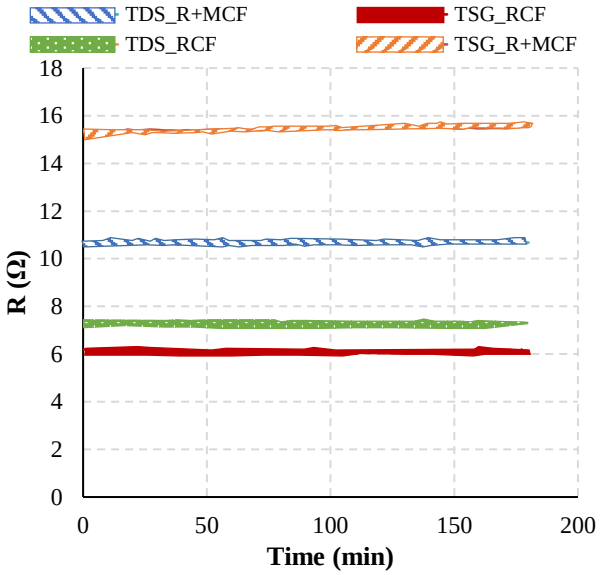

Figure 5.9. Electrical resistance evolution.

5.4.2.2. 2 cycles of 8h heating/16h cooling in slabs.

The second test series involves the application of the high voltage configuration (25 V) on concrete slabs with recycled carbon fiber addition (RCF) and both types of electrode disposals (TSG and TDS) during 2 continuous cycles of 8 h heating/16 h cooling. This testing configuration allows the study of the performance of the different specimens under repetitive long heating cycles with high heating rates, which might be representative of the real field conditions. Room temperature during the tests ranged between 24 - 28 °C.

Figure 5.10a shows the temperature evolution registered at the center of the specimen with respect to room temperature over the test duration. The first heating cycle presents the same trends as described for 3 h tests in both electrode configurations, with a rapid temperature increase followed by a plateau. Notice that specimens TSG_RCF do not follow a natural heating profile near the first plateau region. Instead, these experience a sudden halt, indicating a possible deterioration of the material. The increments of temperature registered reached 18 °C at the end of the 8 h heating period, which is a similar value than the one obtained during the 3 h tests at the same voltage. During the disconnected period, the material experiences a rapid decrease of temperature followed by a plateau at 1 - 2 °C, over room temperature.

The second heating sequence, 24 h after test start, shows different behaviors for TDS and TSG electrode configurations. Concrete slabs with TDS electrodes display the same heating and cooling rates than the ones described for the first cycle, suggesting no degradation of the conductive and self-heating properties of the material after 8 h of high voltage application. However, slabs with TSG electrode configuration are not able to induce any significant heating during the whole cycle. This behavior indicates that the conductive properties of the material might be completely deteriorated, possibly since the plateau region of the first heating cycle, as commented previously.

The average power consumption measurements registered during the heating cycles also reflects this deterioration of the conductive properties of the specimens with TSG electrode disposal (Figure 10a). While during the first cycle both specimens were able to transfer similar average rates of electrical energy per unit time, during the second cycle a dramatic loss of power consumption is registered for the TSG specimen.

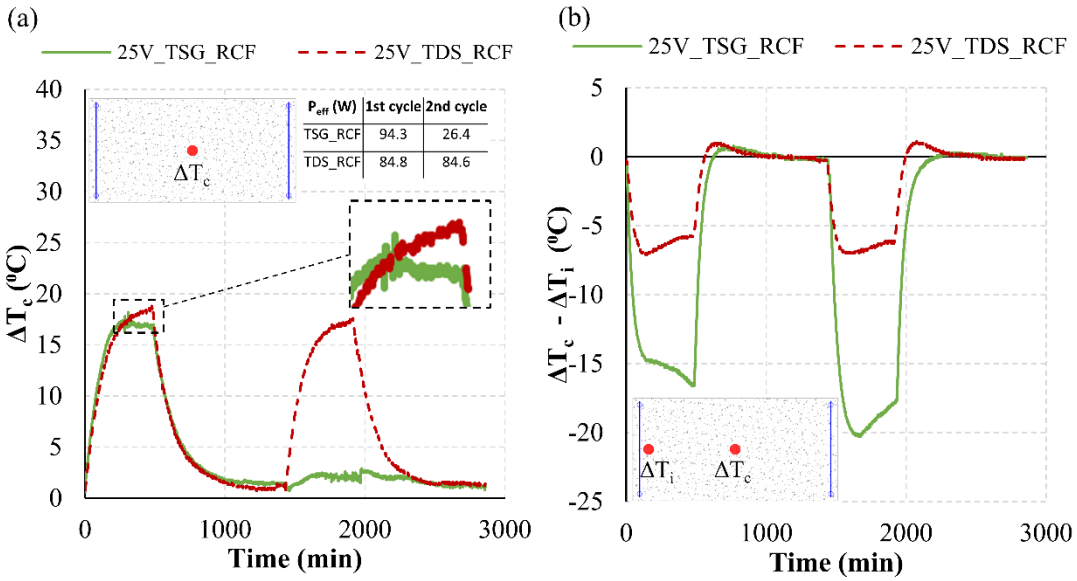

Figure 5.10. (a) Temperature evolution at the center of the slab and (b) Temperature drop

Figure 5.10b depicts the temperature drop registered between the center of the slab (ΔTc) and near the inlet electrode (ΔTi) for TDS and TSG configuration. In general, temperature gradients increase rapidly during the first hours of the heating stages, start to decrease slightly during the plateau stage of the heating cycles and decrease rapidly during the cooling phases. Maximum temperature gradients registered for TDS and TSG disposal during the first cycle are 7 and 17 °C, respectively. Notice that even though both electrode configurations reached similar heating rates (Figure 10a), the temperature drops for TSG disposal are 2.4 times higher than for TDS configuration. These results are consistent with the outcomes presented in section 5.4.2.1 and confirm the better performance of the TDS disposal when it comes to minimize temperature gradients within the specimen.

Under a steady energy supply and material properties, once the material reaches its highest heating potential, temperature gradients tend to decrease over time until constant temperature distribution across the specimen. TDS_RCF samples reflect this normal behavior with the decrease of temperature gradients during the plateau region of the heating cycles. However, the slight increase of temperature variation depicted by the TSG_RCF specimen during this period can only be explained by a degradation of the conductive properties of the material, as the energy supplied remained constant.

The degradation of the conductive properties in the specimens TSG_RCF is confirmed during the second heating stage. Figure 5.10a shows that this mixture does not register any relevant increase of temperature at the center of the slab during this period. On the other hand, the temperature drop depicted in Figure 5.10b indicates that the thermocouple located nearby the inlet electrode did register an increase of temperature during the second heating stage. In other words, the concrete near the inlet electrode was heated, but the conductive properties of the material were not sufficient to heat the center of the slab, indicating severe degradation of the matrix.

Finally, Figure 5.11 shows the electrical resistance during the first heating cycle for TSG_RCF and TDS_RCF specimens. Specimens with TDS electrode configuration describe a constant resistance over the two heating cycles, indicating that the specimens were able to sustain the maximum temperature consistently over long periods without any degradation.

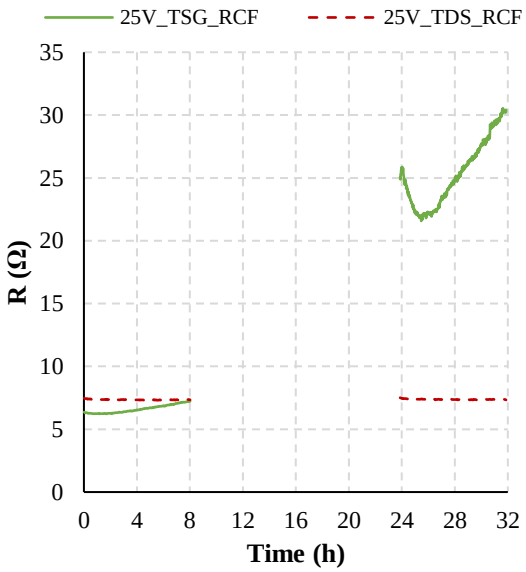

Figure 5.11. Electrical resistance R evolution during the heating cycles.

On the other hand, samples with TSG electrode disposal depict an increase of electrical resistance from the second hour of the heating cycle. This suggests an increasing reduction of the material conductive properties over time, which coincides with the unnatural heating profile described during the plateau region of the first heating cycle and the following incapacity of generating heat at the center of the specimen.

5.5.- Thermal characterization in real-scale benches.

Figure 5.12 - Figure 5.15 present the results associated with the thermal characterization of real-scale benches with TSG, TSG+LR and LR electrode configurations, respectively. All tests were performed at room temperature between 26 - 29 °C. The full temperature profile for each of the 12 thermocouples arranged is only displayed for the first bench configuration (BENCH_TSG_RCF) to show the typical temperature evolution profiles registered (Figure 5.12).

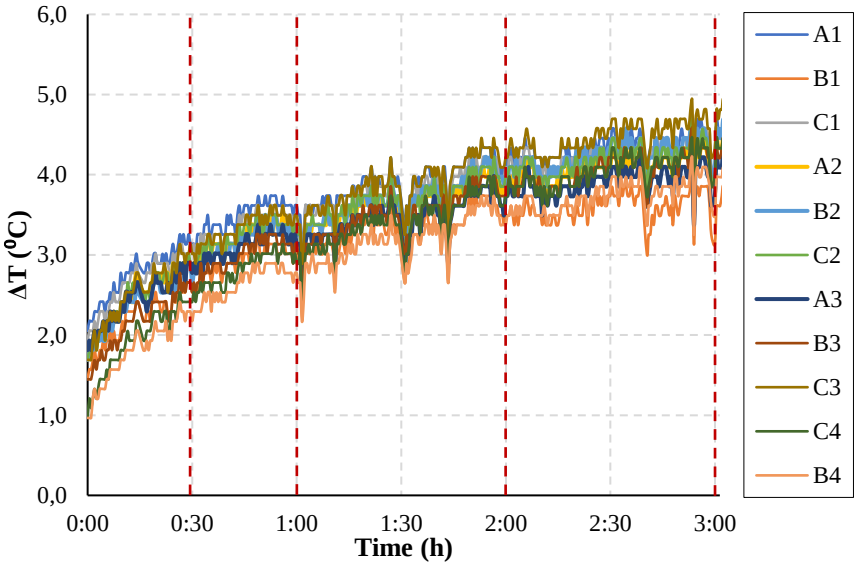

Figure 5.12. Complete temperature evolution on BENCH_TSG_RCF with 21 V.

As can be seen, the large amount of thermocouples incorporated hinder the interpretation of the graphs. Therefore, results are presented instead in Figure 5.13-Figure 5.15 as heating snapshot maps after 30 min/1 h/2 h/3 h of test onset. Figure 5.12 includes vertical dotted red lines at the times captured in the heat maps for the first bench configuration. The temperature depicted is the difference between the temperature registered by the sensor and the room temperature. Each thermocouple incorporated is representative of the heating capacity of the rectangular region defined by the virtual grid included in each figure, as described in Figure 5.4b. The range of the color limits adopted in all figures is maintained to allow color-based comparison between the different benches evaluated.

The bench with the TSG electrode configuration and no steel reinforcement reaches increments of temperature between 2.1-3.1 °C after 30 min at 21 V (Figure 5.13). The thermocouple located at A4 grid was not working thus no temperature is available there. The largest temperature value is obtained near the inlet electrode (1A) while the lowest temperature is registered at the thermocouples situated near the outlet electrode (4B, 4C). The temperature drops between these locations is limited to less than 1 °C, which is a very low temperature variation considering the distance between electrodes (almost 2 m).

During the 1 h – 2h heating period, temperature variations increase more slowly, reaching temperatures between 3.4-4.2 °C. After 2 h of heating, the bench seems to have arrived to its maximum heating potential at this voltage, as temperature are maintained. The average power consumption registered during this test was 25.9 W, with a +1 standard deviation of only 0.08 W.

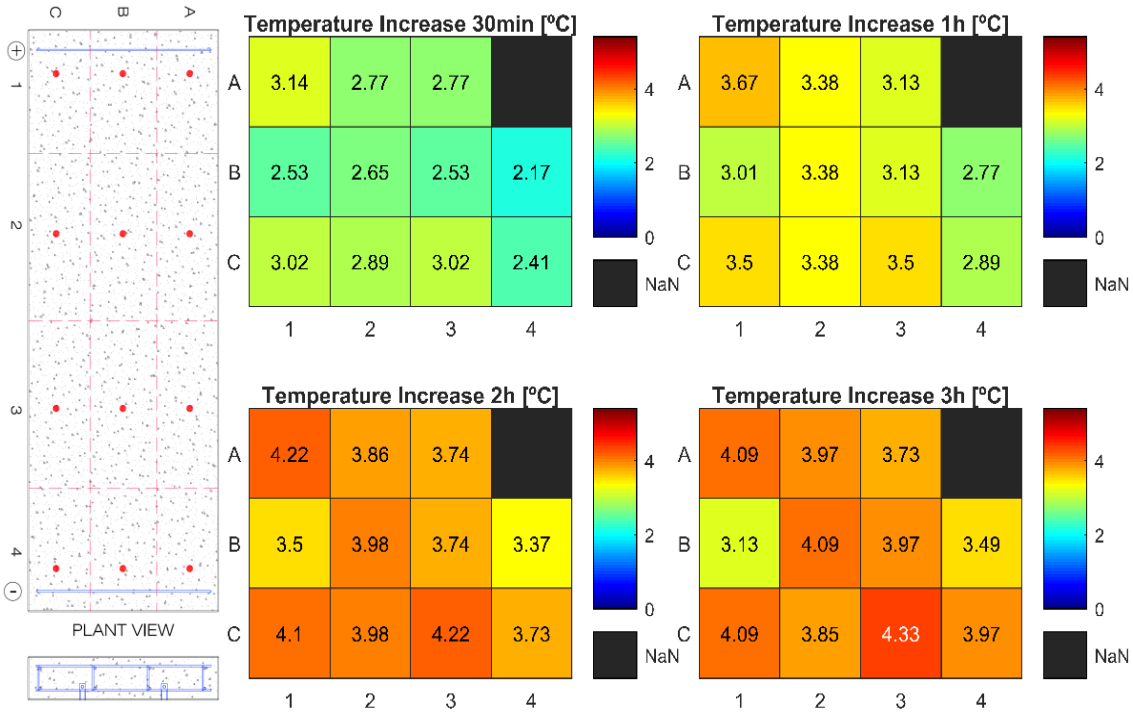

Figure 5.13. Heating maps at 30min/1h/2h/3h on BENCH_TSG_RCF with 21 V.

The bench with an additional longitudinal reinforcement (TSG+LR, Figure 5.14) reaches temperature increments of 3.1-4.5 °C after only 30 min of 11 V application. Then, temperature profiles increase slightly until the end of the test, where the increase in temperature ranges from 3.5-5.4 ºC.

The temperature drops registered between the hottest and coolest locations increase from 1.3 (at 30 min) to 1.9 °C (at 3 h), which are still a low temperature gradient given the dimensions of the element. The average power consumption registered during this test was 26.1 W, with a +1 standard deviation of only 0.08 W.

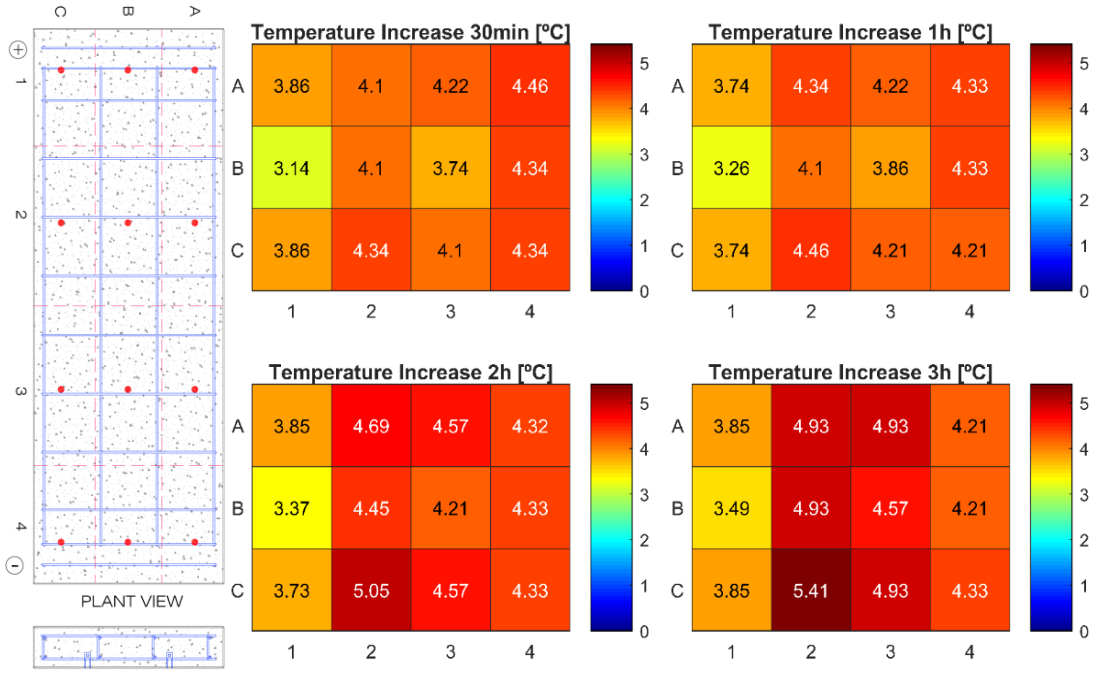

Figure 5.14. Heating maps at 30min/1h/2h/3h on BENCH_TSG+LR_RCF with 11 V.

Finally, the bench that uses the longitudinal reinforcement itself as inlet and outlet electrodes shows increases in temperature from 1.9-2.9 °C after 30 min at 2 V (Figure 5.15).

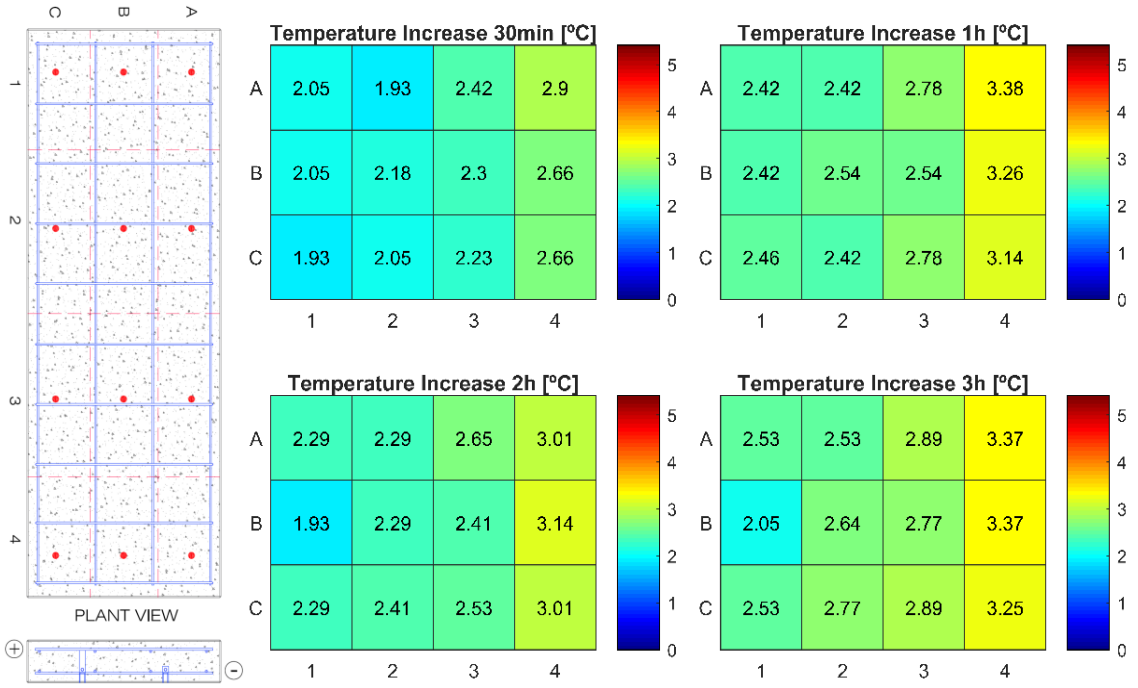

Figure 5.15. Heating maps at 30min/1h/2h/3h on BENCH_LR_RCF with 2 V.

Temperature continue to increase slightly until 2.4-3.4 °C after 1 h of voltage application. At this point, the temperature reached is maintained until the end of the heating

period. Even though the temperature increase showed by this electrode configuration is lower than the temperatures reached in previous benches, the heating performance of this bench is significantly superior if the voltage applied is considered. The temperature increase per volt applied (°C/V) of this configuration is 7.5 and 3 times larger than the BENCH_TSG_RCF and BENCH_TSG+LR_RCF, respectively. In terms of electrical consumption, this configuration registered an average power consumption during the test of only 7.7 W, with a +1 standard deviation of 0.06 W.

Similarly, to all other real-scale benches evaluated, temperature drops registered in BENCH_LR_RCF between the hottest and coolest locations are limited to values around 1 ºC throughout the test duration. Unlike some of the values obtained in the laboratory-scale slabs presented in section 5.4.2.1, the temperature drops registered in benches neither compromise the comfort nor the structural performance due to thermal-induced stresses. These results indicate that with the current set of technology, temperature drops can be maintained at acceptable ranges if the increase of temperature is limited to 3-4 °C, over room temperature. Therefore, the technology developed seems to be potentially applicable at de-icing applications in urban furniture in climates where the lowest temperatures remain within the range of -3 or -4 °C. However, heating tests should be validated at room temperatures of such ranges.

5.6.- CONCLUSIONS

This paper presents a broad experimental study that explores the current capacity of conductive concrete for de-icing and self-heating applications in urban furniture, from small-scale laboratory specimens to full real-scale benches. The following specific findings may be derived from this study.

- RCF material (concrete with recycled carbon fibers) is about 7.5 times more conductive than the R+MCF (concrete with recycled and micronized carbon fibers). This indicates that the addition of micronized carbon fibers lower significantly the conductive properties of the composite.
- Temperature variations reached at the end of the 3h heating test range from 7 - 17, 4 - 8.5 and 2 - 3 °C for 25V, 18V and 11 V, respectively. R+MCF slabs attain 25-50 % lower temperatures than RCF slabs. These results suggest that the additional incorporation of graphite flakes into the mix also worsen the heating performance of the material.
- Results on the 3h and 24 heating tests indicate that the TDS (transversal deployé sheets) electrode disposal limits the magnitude of heat peaks nearby the electrode location, allowing a more efficient heat transfer to the conductive concrete and reducing the temperature gradients within the elements and the possibility to deteriorate the conductive properties of the material.

- Real-scale tests show that benches are able to heat uniformly 2-4 °C, over room temperature after 30 minutes of voltage application. After 3 h, increments in temperature reach 3-5 °C. Such performance places the current technology developed as potentially applicable at de-icing applications in climates where the lowest temperatures remain within the range of -3 or -5 °C. Slightly lower temperature values might be obtained at the external surface of the benches, as the thermocouples were embedded 2.6 cm. Further tests should be performed at room temperatures of this range to confirm the results obtained.

Capítulo 6: CONCLUSIONES Y PERSPECTIVAS FUTURAS

6.1.- INTRODUCCIÓN.

Tras la exposición previa de los trabajos desarrollados y los resultados obtenidos en la elaboración de la presente tesis doctoral, es necesario hacer una reflexión final que reúna de forma sintética las aportaciones realizadas. Ello es más evidente en una tesis por artículos, que corresponde a planteamientos más desagregados

El objetivo del presente capítulo es, por un lado, presentar tanto las conclusiones generales con una visión más amplia de la totalidad del trabajo realizado, como las conclusiones específicas asociadas a los aspectos más relevantes estudiados durante el proceso experimental realizado, clasificados según origen y tipología. Por otro lado, se plantean unas perspectivas futuras, relativas a posibles líneas de investigación derivadas de los trabajos aquí incluidos.

Dado que la tesis doctoral se ha desarrollado por compendio de artículos, si bien se mantiene una estructura similar por capítulos, se hace un análisis general que trata de dar cohesión a todo el documento; en definitiva, a agregar los artículos que se han presentado, por separado, en los capítulos 3, 4 y 5.

6.2.- CONCLUSIONES GENERALES

Esta tesis recoge el estudio de un extenso planteamiento experimental en cuanto a variables, materiales y pruebas realizadas. Cada una de las posibilidades exploradas, es susceptiva de un mayor análisis en profundidad, inabarcable en el marco de los recursos disponibles en la realización de esta tesis, si bien cabe señalar que el objetivo global propuesto al inicio del trabajo (apartado 1.2), se ha cubierto de forma muy satisfactoria.

Hay que añadir, que el carácter aplicativo del estudio, ha focalizado recursos en obtener resultados, no sólo científicamente contrastados, sino industrialmente aplicables, o que como mínimo demostraran una viabilidad de producto futura que animará a nuevas inversiones privadas en el desarrollo de esta vía de investigación o asociadas a ella.

Destacar que, durante la realización del estudio, la distribución y presentación comercial de las fibras de carbono recicladas ha variado debido a la introducción de nuevas tipologías y procedencias, factor que ha complicado el estudio, pero que ha mejorado los resultados obtenidos, dado que se ha mejorado la dispersión de estas con su evolución.

Las conclusiones generales del trabajo quedan fijadas en los diferentes ámbitos estudiados:

- Hay una contribución diferente a la conductividad del material, en función del esqueleto granular empleado. Con agregados de menor tamaño y mayor proporción de pasta cementicia en las dosificaciones UHPC, respecto a las dosificaciones HC, se ha podido captar una menor resistividad de la matriz, mejor capacidad de adicionar cantidades mayores de fibra, una distribución más uniforme de estas y además se ha podido observar un fenómeno de percolación por la pasta cementicia, descrito en el apartado 3.4.2.

- Las tipologías de fibras empleadas más largas y desagregadas (CFRAN, C10/30) o más cortas y agregadas (CT12, CFTrim), con diferencias notables de geometría, longitud o agrupamiento, influyen en las características eléctricas del material, modificándolas. Principalmente la tipología de fibra, afecta a la dispersión de estas, lo cual influye en la conductividad.

- Mediante la caracterización eléctrica se ha comprobado como los resultados obtenidos con la fibra reciclada son equiparables con la utilización de fibra de carbono de primer uso. También se ha podido validar la consistencia de los resultados de los equipos y sistemas de medición empleados y su correlación con otras propiedades como trabajabilidad, homogeneidad de las mezclas y propiedades mecánicas.

- Ha quedado definida la existencia de un umbral de capacitancia Ct, valor de frecuencia que delimita diferentes tipos de conductividad presentes en el material,

que se gobierna o bien por la matriz de hormigón o bien por las fibras. Nuevamente la distribución de las fibras influye en este aspecto, al condicionar el espesor de recubrimiento de matriz que presentan las fibras, factor que influye en Ct. Este umbral de capacitancia podrás ser utilizado en el diseño periférico de componentes en función del tipo de conductividad que interese evaluar en el uso final de estos materiales.

- El comportamiento piezoeléctrico del hormigón se amplifica con la adición de fibras de carbono recicladas de acuerdo el aumento de la conductividad asociado. De igual forma, factores como la dispersión de la fibra y la forma de esta, que afectaban a la conductividad, se han podido detectar en esta característica.

- La respuesta piezoeléctrica se modifica, incrementándose, cuando se consigue sobrepasar la conductividad iónica de la matriz i se activa la conductividad electrónica de las fibras de carbono, por encima del umbral de percolación.

- Se ha conseguido reproducir la capacidad de autocalentamiento descrita en laboratorio a modelos a escala real, consiguiendo incrementos de temperatura de hasta 4°C, compatibles para aplicaciones de deshielo en el exterior. Paralelamente se han confirmado deterioros de capacidades conductivas del material a determinadas temperaturas i tiempos de uso que limitarían los usos finales del material

- El sistema de conexión a la corriente eléctrica, se demuestra esencial en la aplicación final, influyendo en la distribución de temperatura en los elementos y la posible prevención de degradación de las propiedades conductivas.

6.3.- CONCLUSIONES ESPECÍFICAS

Las conclusiones específicas que se incorporan, responden a las líneas temáticas trabajadas y se desarrollan algo más que en los capítulos, al estar desconectadas de los mismos. Cada una de estas líneas son:

6.3.1.- Matriz de hormigón, componentes, diseño y trabajabilidad

Si bien la matriz de hormigón actúa como una fase aislante o no conductora; el esqueleto granular, tipología de agregados y comportamiento en estado fresco si han afectado posteriormente al comportamiento eléctrico del material compuesto final de diversas formas.

Ya en las primeras experimentaciones, el uso de un hormigón convencional (HE) con un tamaño de árido de hasta 12 mm presentó dificultades de trabajabilidad en estado fresco, al aumentar la cantidad de fibras de carbono adicionadas. La capacidad de admitir fibra en

la matriz está gobernada por el tamaño de los áridos, y a mayor tamaño de estos, menor es la cantidad de fibra adicionada aceptable por la matriz, a igualdad de fluidez del hormigón en estado fresco. Mejores resultados de trabajabilidad se obtuvieron con la utilización del hormigón de altas prestaciones (UHPC), en el que el menor tamaño de árido empleado permitía alojar mayor cantidad de fibras, con menor pérdida de fluidez de la mezcla. Factor por el que se siguió utilizando de forma general esta matriz en el resto de ensayos realizados.

La incorporación de fibras a la matriz y la trabajabilidad de la mezcla son dos características relacionadas y de efectos contrapuestos en el objetivo de dotar de conductividad del hormigón. Así se ha comprobado, como se esperaba, qué a mayor cantidad de fibra, la respuesta conductora del compuesto mejora, tal como se muestra en la figura 6.1, pero no de una forma lineal y constante. La pérdida de trabajabilidad con el aumento de la cantidad de fibras, trabaja en contra de la conductividad, debido al empeoramiento de las características de la matriz, asociado a mayores cantidades de aire ocluido.

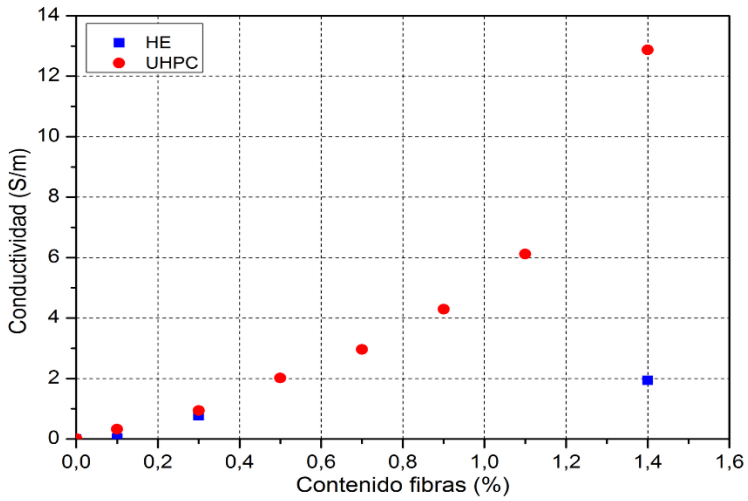

Figura. 6.1: Aumento de la conductividad asociado al contenido de fibras en una matriz de hormigón convencional (HE) y de otras prestaciones (UHPC).

Este efecto también se refleja en las capacidades mecánicas del material, que deberían aumentar con la incorporación de las fibras (en especial los resultados a flexión), pero quedan de la misma forma limitados por la pérdida de propiedades de la matriz.

De estos resultados se extrae la necesidad de establecer un correcto balance entre contenido de fibras trabajabilidad y conductividad, que en este estudio se ha situado en contenidos de fibra alrededor de 0,6% - 0-8% en volumen para la dosificación de UHPC i tipos de fibras empleadas en concreto.

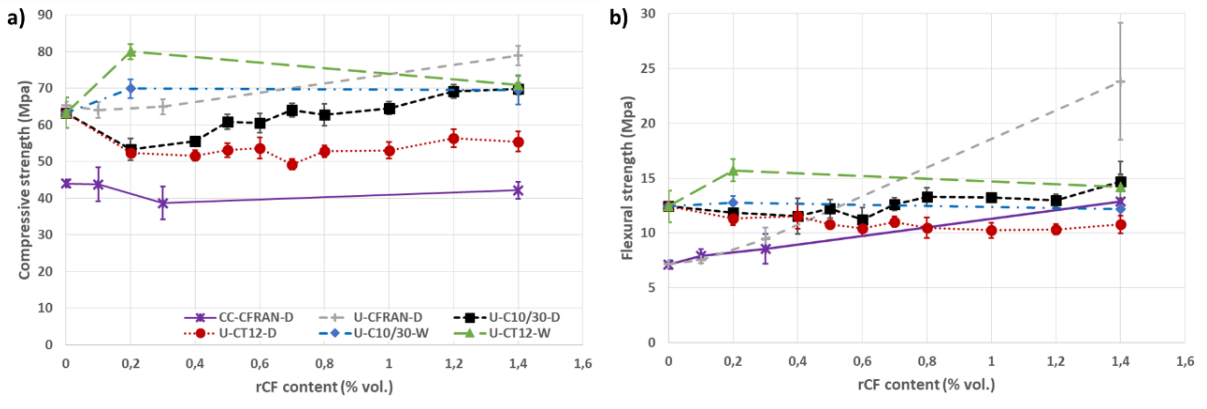

Figura 6.2: Evolución de las propiedades mecánicas con el incremento de fibras (de diferentes tipos) adicionado, a) resultados a compresión, b) resultados a flexión.

6.3.2.- Tipología y contenido de fibras de carbono recicladas.

Tal como se ha mostrado, en el apartado 3.3.2, se han utilizado, para los ensayos, dos tipologías de fibras de carbono recicladas diferenciadas, así como dos diferentes métodos de adición en la mezcla (en húmedo o en seco). De forma análoga al tamaño de los agregados, el número de fibras y su longitud tienen influencia no solo en la caracterización eléctrica, sino también en la trabajabilidad y comportamiento mecánico.

Las fibras de carbono desfibriladas, y de mayor longitud (CFRAN), presentaron de inicio mayores dificultades en el proceso de mezcla, desestimándolas de inicio para la matriz de hormigón convencional (HE), y posteriormente tras los resultados de los ensayos de caracterización eléctrica, fueron desestimadas en los ensayos de calentamiento y prueba piloto. Paralelamente la forma de suministro de esta tipología de fibras ha derivado hacia su presentación en longitud corta y en forma de hebra laminar o "encolada" (CT12-CFran), con una mejor manipulación y logística al disminuir su volumen a un 25% aproximadamente del total. Ver figura 6.3.

La longitud y numero de fibras, asociado al volumen y tipo de fibra adicionado, también ha mostrado su influencia. La característica del factor de fibra, combinado con el diseño de la mezcla, determina la fracción en volumen de fibra incorporable a la mezcla. Excesiva longitud de fibra y/o elevado número de fibras empeoran la trabajabilidad de la mezcla y la dispersión de las fibras, limitando el volumen máximo de fibra adicionable a la mezcla.

Focalizando en la fluidez de la mezcla y dispersión de las fibras, los mejores resultados corresponden a las fibras cortas "encoladas" añadidas en la mezcla húmeda. Las fibras de excesiva longitud generaron bucles o lazos en la mezcla, dificultando su dispersión en contraposición a la fibra corta y amplificando el deterioro de las propiedades de la matriz con el aumento de la fracción en volumen adicionada.

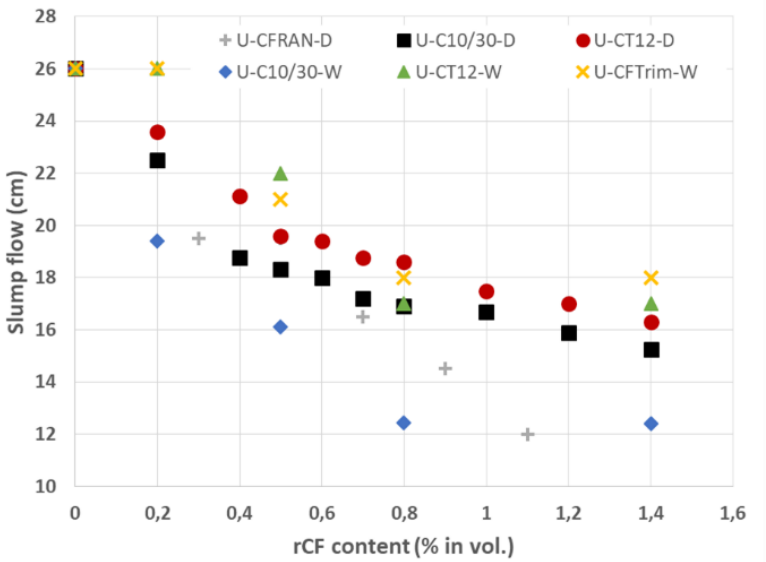

Figura 6.3. Efecto en la fluidez de los diferentes tipos de mezcla en función del contenido de fibra

6.3.3.- Propiedades eléctricas

En la caracterización eléctrica mediante los diagramas de Bode, en primer lugar, se evidenció la diferencia de comportamiento eléctrico entre los dos tipos de matriz (sin adición de fibras), debido a la diferencia de esqueleto granular y tamaño de árido.

La mayor proporción de fase cementosa y menor tamaño de árido (1mm contra 15mm) en la muestra patrón de UHPC, referenció valores inferiores de impedancia, explicados por un fenómeno de percolación en la pasta cementicia. Mientras que, en el hormigón convencional sin fibras adicionadas, la impedancia consigue disminuir al aumentar la frecuencia de la corriente eléctrica aplicada, por disminución de la capacitancia paralela asociada, a elevadas frecuencias.

Mediante la comparación de los diagramas de Bode, también se referenciaron las diferencias existentes en las muestras por el tipo de fibra y el sistema de mezclado, características que gobernaban directamente la homogeneidad de las mezclas y por tanto la dispersión de las fibras en el hormigón.

El sistema de mezclado en seco y la utilización de fibras de larga longitud dio como resultado valores de impedancia superiores, menor influencia del aumento de la adición de fibras en la reducción de la impedancia y resultados discordantes por elevada dispersión de valores. Hay por lo tanto una relación directa entre trabajabilidad, homogeneidad de la mezcla y la conductividad del material, contrapuesta a la cantidad de fibra adicionada. De esta forma, cantidades de fibra adicionadas en torno al 0,6% fueron las que mejor resultado obtuvieron, asociadas a la fibra y sistema de mezclado que permitieron mayor homogeneidad. Valores de adición de fibra inferiores o superiores, obtuvieron peor resultado, por insuficiente fibra en la mezcla o mala distribución de estas respectivamente.

La resistividad de las muestras, como valor característico del material, se calculó a partir de la impedancia a valores de frecuencia de 50 Hz y 100 KHz. El primer valor de frecuencia, es representativo por ser el estándar de la CA suministrada, mientras que el segundo valor de frecuencia está escogido por sobrepasar el umbral de capacitancia Ct. Los valores observados de resistividad son análogos a valores observados en anteriores experiencias utilizando fibra de carbono virgen.

El patrón eléctrico de las muestras, de forma general visualiza una reducción de la impedancia con el aumento de la frecuencia de la corriente eléctrica en los diagramas de Bode, hasta llegar a un valor de estabilización o umbral de capacitancia C_t (figura 6.4). A este valor de frecuencia se supera la conductividad iónica de la matriz, por lo que varía su valor con el tipo de matriz empleada y el espeso de esta que recubre las fibras de carbono.

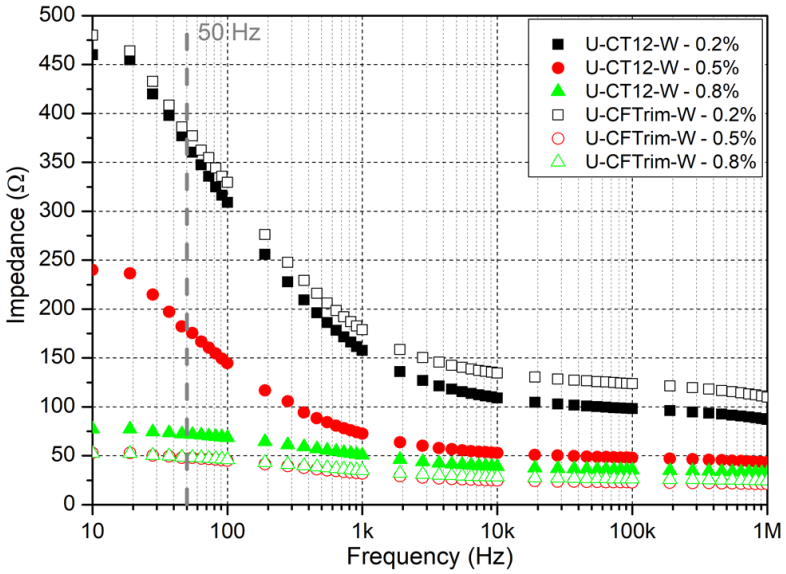

Figura 6.4: Diagrama de Bode de 2 tipologías de fibras que muestra el descenso de la impedancia con el aumento de frecuencia de la corriente eléctrica. El umbral de capacitancia C_t se estima alrededor de 100 kHz y corresponde con la estabilización del valor de la impedancia.

Con los diagramas de Nyquist, es posible analizar y determinar mejor la presencia de este valor característico C_t particular a cada matriz, dosificación y fibra empleada, estableciendo que tipo de conductividad se está produciendo en la muestra (iónica o electrónica), en función de si se está produciendo por la interfase de la matriz o por la fibra de carbono.

El umbral de percolación y el umbral de capacitancia, se muestran como dos valores característicos útiles para la determinación de la cantidad de fibra a utilizar en la mezcla, determinación del tipo de conductividad y frecuencias de trabajo en aplicaciones futuras.

6.3.4.- Respuesta piezoeléctrica

Este tipo de respuesta física del material se evalúa al considerarse básica como funcionalidad sensitiva del hormigón. La posibilidad de captar variaciones de señal eléctrica ante la presencia de tensiones o más concretamente deformaciones, abre la puerta a infinidad de aplicaciones, desde soluciones más ingenieriles y de seguridad como sería la monitorización de deformaciones en infraestructuras civiles, a aplicaciones en conceptos de ciudad inteligente, como podría ser su uso en pavimentos inteligentes capaces de determinar la presencia de individuos a su paso.

En los ensayos realizados, y descritos en el capítulo 4, se ha podido comprobar como la adición de fibra de carbono reciclada, habilita la respuesta piezoeléctrica del hormigón, de acuerdo con el incremento de su conductividad.

La variación de voltaje ($V_{pico\text{-}pico}$) detectada, y el valor absoluto medio, son sensibles a la conductividad del material y por lo tanto a todos los factores que la gobiernan y valores característicos detectados en el capítulo 3.

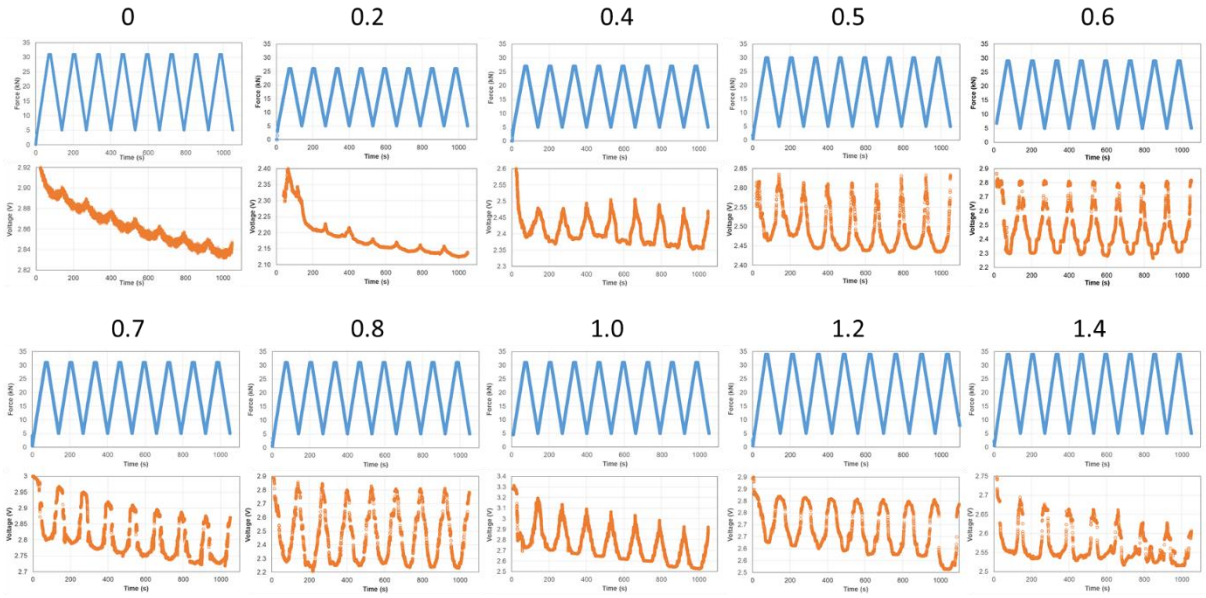

Figura 6.5: Curvas de carga-voltaje para las muestras de hormigón preparadas con fibra de carbono reciclada C10/30 durante las pruebas de compresión. Los números por encima de las curvas indican el % de contenido de fibra en los especímenes de hormigón.

La cantidad de fibra adicionada refleja un aumento de $V_{pico\text{-}pico}$ y evita la caída de tensión media durante el ensayo, asociada a efectos de polarización en la matriz de hormigón. Pero solo hasta los valores de contenido de fibra que permitían una mejor distribución. Una deficiente dispersión de la fibra disminuye la variación del voltaje, aunque se incremente su porcentaje presente. Este efecto resulta en una disminución de la sensibilidad del material.

De igual forma valores característicos como el umbral de percolación y el umbral de capacitancia se reflejan en el comportamiento piezoeléctrico del material, relacionándose con el tipo de conductividad que se produce en el hormigón.

La variación de tensión en los ensayos o la sensibilidad, aumenta con el contenido de fibra hasta llegar al umbral de percolación, alrededor de contenidos de fibras del 0,6%, valor similar por el cual la dispersión de las fibras comienza a ser deficiente.

Con el análisis de la relación señal/ruido (SNR) medida, y relacionándola con el umbral de capacitancia, se ha podido comprobar como los valores de SNR son diferentes por encima o por debajo de este umbral de frecuencia.

En frecuencias por debajo de umbral de capacitancia, la conductividad está gobernada por la matriz de hormigón (conductividad iónica) y por tanto del espesor de la capa que recubre las fibras (interfaz matriz-fibra). Por encima, domina la conductividad electrónica asociada a las fibras de carbono, gracias a que mayores frecuencias permiten sobrepasar la capacitancia asociada a la matriz que recubre las fibras.

6.3.5.- Capacidad de autocalentamiento

En el paso de una corriente eléctrica a través de un material se generan colisiones a nivel atómico, el amortiguamiento de la energía cinética disipa en forma de calor, dando lugar al efecto Joule. Hay un equilibrio necesario entre resistencia y conductividad para conseguir este efecto, ya que, para resistencias muy elevadas, no hay suficiente movimiento de cargas eléctricas que generen estas colisiones. Mientras que, en conductividad muy elevada, el movimiento de cargas se produce sin interferencias o colisiones. En un conductor perfecto no habría calentamiento asociado al paso de la corriente eléctrica.

En el capítulo 3 se ha comprobado este efecto en hormigón con adición de fibra de carbono reciclado, con el objetivo de validar su capacidad autocalefactable y sus posibles aplicaciones en pavimentos con capacidad de deshielo, o de calentamiento enfocado a confort en elementos de uso urbano (bancos, pavimento, etc.).

Los test se han realizado a tres escalas de tamaño de forma incremental, introduciendo nuevas variables como los electrodos de conexión, ciclos y tiempos prolongados de ensayo, con el objetivo de reproducir condiciones finales de uso del material. Adicionalmente se añadió una adición (MCF) conductora con el fin de mejorar la conductividad de la matriz y se verificó mediante la disposición de termopares posibles gradientes de temperatura.

En la caracterización eléctrica inicial la diferencia de conductividad entre las dos tipologías ensayadas, fue de entre 7-8 veces entre ellas, a 50Hz de frecuencia (figura 6.6), pero de forma contraria a lo esperado, factor atribuido a un deterioro de la matriz del hormigón al añadir la nueva adición.

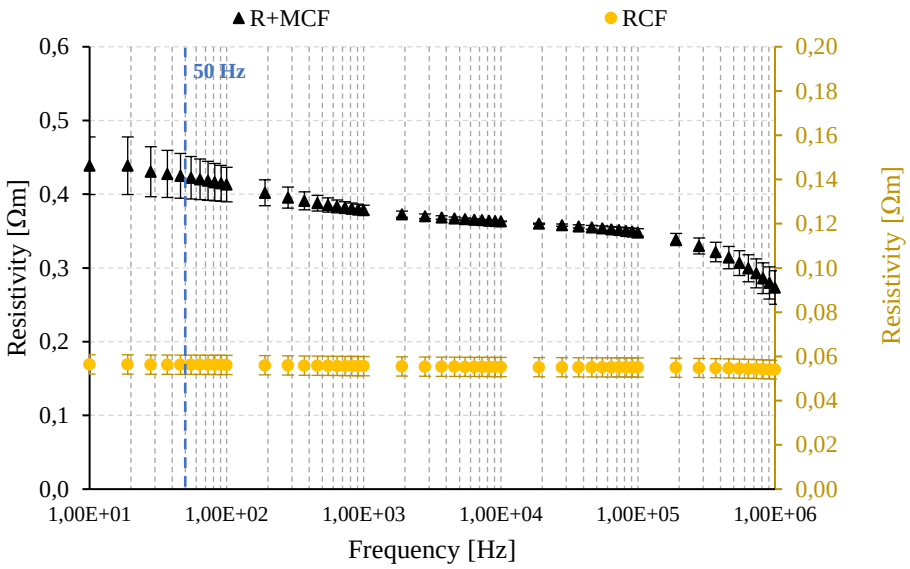

Figura 6.6: Resistividad de los dos hormigones empleados en función de la frecuencia aplicada.

La diferencia entre los electrodos empleados en las placas, estaba centrada en comprobar como una mayor superficie de contacto electrodo/matriz, actuaría en una mejor transmisión de la corriente eléctrica entre ambas fases. Con este fin se dispusieron los termopares en diferentes puntos de forma que fuera posible registrar diferentes gradientes de temperatura.

Por otro lado, los ciclos largos de calentamiento realizados, perseguían conocer posibles deterioros de las características eléctricas el material, producidos por deterioro de alguna de las fases, así como la evolución de la temperatura ante los ciclos de conexión.

Los resultados obtenidos a escala reducida con placas de 600x300x40mm confirmaron diferentes premisas previas:

- A mayor conductividad del material se obtuvieron incrementos de temperaturas más elevados (figura 6.7).
- A mejor transmisión (más superficie de electrodos), distribución más uniforme de temperaturas y menor sobrecalentamiento de electrodos (figura 6.8).
- Aparición de mecanismos de degradación de las propiedades eléctricas a elevadas temperaturas y ciclos largos de tiempo.
- Aparición más rápida de degradación de propiedades eléctricas, en muestras menos conductoras y con peor distribución de la corriente eléctrica en los electrodos.

Resultados similares, pero con mejores resultados a nivel de distribución de calor se obtuvieron en los elementos de la prueba piloto. Con potencias (consumos) relativamente bajos (26W), se aumentó la temperatura de los elementos entre 3 y 5°C,

incrementos que pueden ser válidos, tras más comprobaciones, para deshielo de superficies.

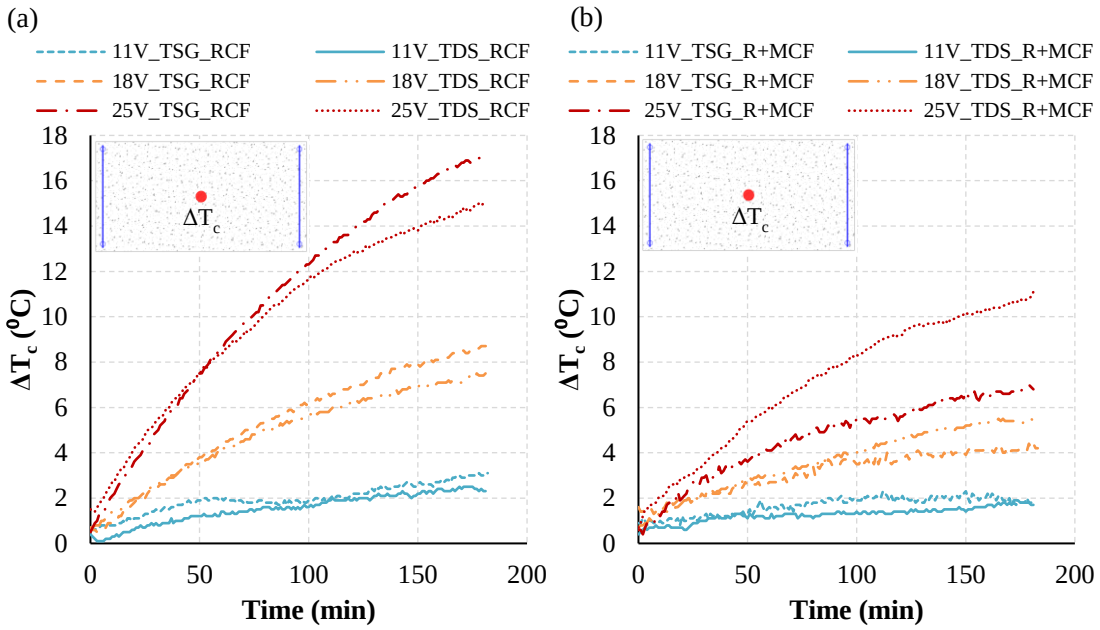

Figura 6.7: Temperatura termopar central en placas de 600x300x40mm, (a) Muestra con fibra de carbono reciclada (RCF) (b) Muestra con fibra de carbono reciclada + adición (R+MCF).

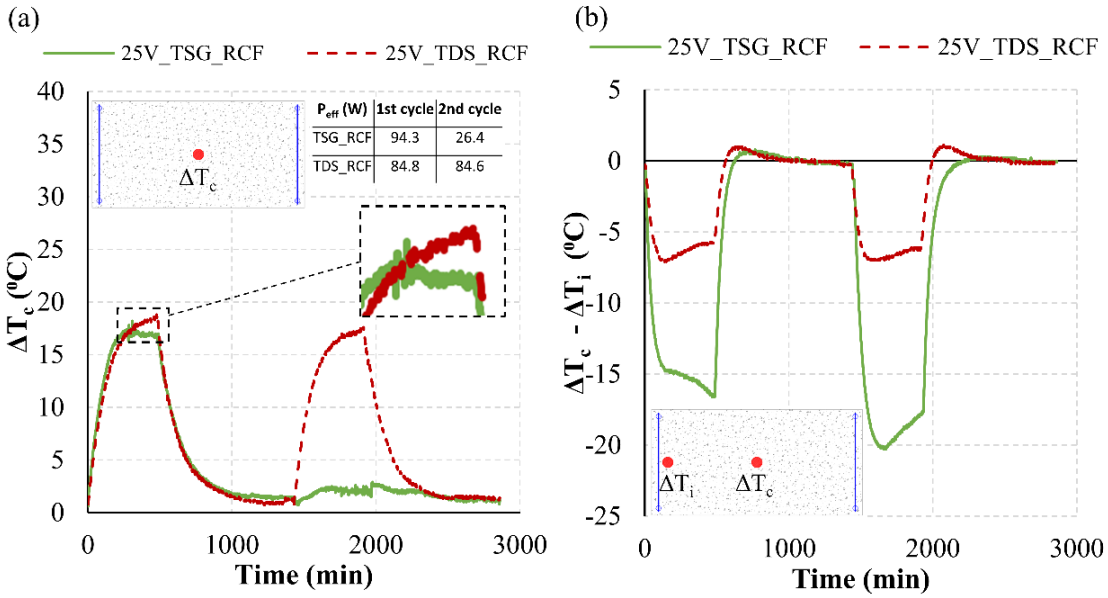

Figura 6.8: Ciclos de calentamiento en placas de 600x300x40mm (a)Evolución temperatura termopar central en placas de 600, (b) Gradiente de temperatura entre centro y electrodos de la placa.

6.4.- PERSPECTIVAS FUTURAS

A la vista de las conclusiones previas alcanzadas en este estudio, los trabajos futuros se pueden focalizar en varios de los aspectos analizados que necesitan de mayor detalle o diferentes posibilidades a considerar, con el fin de obtener un hormigón conductor con fibra de carbono reciclada, suficientemente caracterizado, reproducible y con aplicaciones concretas validadas. Entre estas líneas se encuentran las siguientes:

Matriz cementicia: Validado un esqueleto granular y proporción de pasta cementicia como el empleado en la dosificación tipo UHPC, cabe experimentar con diferentes tipologías de áridos y/o adiciones, diferentes a las de naturaleza silícea empleadas. Así, por ejemplo, fracciones finas de árido (hasta 2-3 mm) provenientes de escoria siderúrgica, añadirían a una posible mejora de la conductividad de la matriz, menores costes económicos y disminución de impacto ambiental, por ser agregados de origen reciclado. En este caso, quizás implicaría modificar algo el esqueleto granular, añadiendo más finos, para evitar la pérdida de trabajabilidad que pueden aportar estas arenas

Fibra de carbono: Durante la realización de este estudio, las tipologías y presentación de las fibras de carbono recicladas, han aumentado y variado, por una evolución en los procesos de reciclado y origen de las fibras. Una adecuación de tamaño y tipología de las fibras adaptado al uso en matrices cementicias sería adecuado al incidir en una mejora de la dispersión de estas, y por tanto con incidencia directa en mejoras de las propiedades conductivas.

Sistemas de transmisión de energía: Dada la influencia observada en las propiedades de las probetas de gran tamaño y prueba piloto, es vital desarrollar electrodos o sistemas que permitan una transmisión de energía más homogénea y en menor intensidad, que evite sobrecalentamientos. Paralelamente la mejora de propiedades conductivas de la matriz beneficiaría la conexión del circuito, electrodo-matriz-fibras, disminuyendo efectos de polarización, sobrecalentamiento y finalmente degradación del material asociados.

Periféricos: Asociados a los sistemas de transmisión de energía y dependiendo de la aplicación final del hormigón conductor, hay diversidad de vías de estudio de mecanismos de suministro y control de energía, captación de señal, seguridad eléctrica y electromagnética, necesarios en todo caso para el funcionamiento de las aplicaciones finales y su posible comercialización.

Modelos numéricos: En paralelo al desarrollo de materiales y procesos, convendría profundizar en modelos numéricos que se pudiesen contrastar con los resultados experimentales y permitiesen en el futuro, estudios previos que reduzcan el número de pruebas para lanzar un producto.

Capítulo 7: BIBLIOGRAFÍA

7.1.- INTRODUCCIÓN

Como cierre del presente documento, en el presente capítulo se recogen las referencias utilizadas en el mismo. Estas referencias son, por un lado, las incluidas en los capítulos 1 y 2, que se incorporan como nuevas a las ya incluidas en los artículos publicados (correspondientes a los capítulos 3,4, y 5).

La estructuración que se ha hecho es agruparlas en el conjunto, por orden alfabético, para favorecer al lector, la búsqueda de las referencias. Por otro lado, si en el documento se cita una fuente de una página web y, no corresponde a una publicación de tipo científico, se ha incluido la referencia en el pie de página, para mantener la trazabilidad metodológica de toda la información utilizada

7.2.- REFERENCIAS CITADAS

ACI Committee 544 (2002) 'State-of-the-Art Report on Fiber Reinforced Concrete Reported by ACI Committee 544', ACI Structural Journal, 96(Reapproved).

AENOR (2000) 'UNE-EN 1015-3:2000 Methods of test for mortar for masonry. Determination of consistence of fresh mortar (by flow table)'.

AENOR (2005) 'UNE-EN 196-1:2005 Methods of testing cement. Part I: Determination of strength.'

Akonda, M. H., Lawrence, C. A. and EL-Dessouky, H. M. (2013) 'Electrically conductive recycled carbon fibre-reinforced thermoplastic composites', Journal of Thermoplastic Composite Materials. SAGE Publications Ltd STM, 28(11), pp. 1550–1563. doi: 10.1177/0892705713513294.

ARUP and UCL (2017) Resilience of Digitally Connected Infrastructure Systems - National Infrastructure Commission. London. Available at: https://www.nic.org.uk /publications/resilience-digitally-connected-infrastructure-systems/ (Accessed: 28 April 2020).

Azhari, F. and Banthia, N. (2012) 'Cement-based sensors with carbon fibers and carbon nanotubes for piezoresistive sensing', Cement and Concrete Composites. Elsevier, 34(7), pp. 866–873. doi: 10.1016/j.cemconcomp.2012.04.007.

Baeza, F. J., Chung, D. D. L., Zornoza, E., Andin, L. G. and Garces, P. (2010) 'Triple Percolation in Concrete Reinforced with Carbon Fiber', ACI Materials Journal, 107(4), pp. 396–402. Available at: http://www.acsu.buffalo.edu /~ddlchung/ documents/ Triple_percolation_pub.pdf

Baeza, F. J., Galao, O., Vegas, I. J., Cano, M. and Garcés, P. (2018) 'Influence of recycled slag aggregates on the conductivity and strain sensing capacity of carbon fiber reinforced cement mortars', Construction and Building Materials. Elsevier, 184, pp. 311–319. doi: 10.1016/J.CONBUILDMAT.2018.06.218.

Baeza, F J, Galao, O., Zornoza, E. and Garc??s, P. (2013) 'Effect of aspect ratio on strain sensing capacity of carbon fiber reinforced cement composites', Materials and Design. Elsevier Ltd, 51, pp. 1085–1094. doi: 10.1016/j.matdes.2013.05.010.

Baeza, Francisco Javier, Galao, O., Zornoza, E. and Garcés, P. (2013) 'Multifunctional cement composites strain and damage sensors applied on reinforced concrete (RC) structural elements', Materials. Multidisciplinary Digital Publishing Institute, 6(3), pp. 841–855. doi: 10.3390/ma6030841.

Baeza, F. J., Zornoza, E., Andión, L. G., Ivorra, S. and Garcés, P. (2011) 'Variables affecting strain sensing function in cementitious composites with carbon fibers', Computers and Concrete. Techno-Press, 8(2), pp. 229–241. doi: 10.12989/cac.2011.8.2.229.

Bai, Y. H., Chen, W., Chen, B. and Tu, R. (2017) 'Research on electrically conductive concrete with double-layered stainless steel fibers for pavement deicing', ACI Materials Journal, 114(6), pp. 935–943. doi: 10.14359/51700993.

Barrias, A., Casas, J. and Villalba, S. (2016) 'A Review of Distributed Optical Fiber Sensors for Civil Engineering Applications', Sensors. Multidisciplinary Digital Publishing Institute (MDPI), 16(5), p. 748. doi: 10.3390/s16050748.

Cañón, A., Garcés, P., Climent, M. A., Carmona, J. and Zornoza, E. (2013) 'Feasibility of electrochemical chloride extraction from structural reinforced concrete using a sprayed conductive graphite powder-cement paste as anode', Corrosion Science, 77, pp. 128–134. doi: 10.1016/j.corsci.2013.07.035.

Carberry, W. (2008) 'Airplane Recycling Efforts Benefit Boeing Operators', AERO Magazine. Available at: https://www.boeing.com/ commercial/aeromagazine/ articles/ qtr_4_08/article_02_1.html (Accessed: 28 April 2020).

Carmona, J., Garcés, P. and Climent, M. A. (2015) 'Efficiency of a conductive cement-based anodic system for the application of cathodic protection, cathodic prevention and electrochemical chloride extraction to control corrosion in reinforced concrete structures', Corrosion Science, 96, pp. 102–111. doi: 10.1016/j.corsci.2015.04.012.

Ceylan, H. (2014) 'Use of smart sensor systems for health monitoring of the transportation infrastructure system', in 3rd International Conference on Transportation Infrastructure. Pisa.

Chen, B., Wu, K. and Yao, W. (2004) 'Conductivity of carbon fiber reinforced cement-based composites', Cement and Concrete Composites, 26(4), pp. 291–297. doi: 10.1016/S0958-9465(02)00138-5.

Chen, P.-W. and Chung, D. D. L. (1993) 'Carbon fiber reinforced concrete for smart structures capable of non-destructive flaw detection', Smart Materials and Structures, 2(1), pp. 22–30. doi: 10.1088/0964-1726/2/1/004.

Chen, P. W. and Chung, D. D. L. (1996) 'Concrete as a new strain/stress sensor', Composites Part B: Engineering. Elsevier, 27(1), pp. 11–23. doi: 10.1016/1359-8368(95)00002-X.

Chiarello, M. and Zinno, R. (2005) 'Electrical conductivity of self-monitoring CFRC', Cement and Concrete Composites, 27(4), pp. 463–469. doi: 10.1016/j.cemconcomp.2004.09.001.

Chung, D D L (2000) 'Cement-matrix composites for smart structures', Smart Materials and Structures, pp. 389–401. doi: 10.1088/0964-1726/9/4/302.

Chung, D. D L (2000) 'Cement reinforced with short carbon fibers: A multifunctional material', Composites Part B: Engineering, 31(6–7), pp. 511–526. doi: 10.1016/S1359-8368(99)00071-2.

Chung, D. D. L. (2004) 'Electrically conductive cement-based materials', Advances in Cement Research. ICE Publishing, 16(4), pp. 167–176. doi: 10.1680/adcr.2004.16.4.167.

Chung, D. D. L. L. (2012) 'Carbon materials for structural self-sensing, electromagnetic shielding and thermal interfacing', Carbon, 50(9), pp. 3342–3353. doi: 10.1016/j.carbon.2012.01.031.

Coppola, L., Buoso, A. and Corazza, F. (2011) 'Electrical Properties of Carbon Nanotubes Cement Composites for Monitoring Stress Conditions in Concrete Structures', Applied Mechanics and Materials. Trans Tech Publications, 82, pp. 118–123. doi: 10.4028/www.scientific.net/AMM.82.118.

D'Alessandro, A., Ubertini, F., Laflamme, S. and Materazzi, A. L. (2016) 'Towards smart concrete for smart cities: Recent results and future application of strain-sensing nanocomposites', Journal of Smart Cities. Whioce Publishing Pte Ltd, 1(1), pp. 3–14. doi: 10.18063/jsc.2015.01.002.

Ding, Y., Chen, Z., Han, Z., Zhang, Y. and Pacheco-Torgal, F. (2013) 'Nano-carbon black and carbon fiber as conductive materials for the diagnosing of the damage of concrete beam', Construction and Building Materials. Elsevier Ltd, 43, pp. 233–241. doi: 10.1016/j.conbuildmat.2013.02.010.

Ding, Y., Han, Z., Zhang, Y. and Aguiar, J. B. (2016) 'Concrete with triphasic conductive materials for self-monitoring of cracking development subjected to flexure', Composite Structures, 138, pp. 184–191. doi: 10.1016/j.compstruct.2015.11.051.

Ding, Y., Huang, Y., Zhang, Y., Jalali, S. and Aguiar, J. B. (2015) 'Self-monitoring of freeze-thaw damage using triphasic electric conductive concrete', Construction and Building Materials, 101, pp. 440–446. doi: 10.1016/j.conbuildmat.2015.10.135.

Dong, S., Han, B., Ou, J., Li, Z., Han, L. and Yu, X. (2016) 'Electrically conductive behaviors and mechanisms of short-cut super-fine stainless wire reinforced reactive powder concrete', Cement and Concrete Composites. Elsevier Ltd, 72, pp. 48–65. doi: 10.1016/j.cemconcomp.2016.05.022.

European Innovation Partnership on Smart Cities and Communities, European Innovation Partnership on Smart Cities and Communities (2013) Strategic Implementation Plan. Available at: http://ec.europa.eu/eip/smartcities/files/sip_final_en.pdf.

Faneca, G., Segura, I., Torrents, J. M. and Aguado, A. (2018) 'Development of conductive cementitious materials using recycled carbon fibres', Cement and Concrete Composites, 92, pp. 135–144. doi: 10.1616/j.cemconcomp.2018.06.009

Ford, S. J., Shane, J. D. and Mason, T. O. (1998) 'Assignment of features in impedance spectra of the cement-paste/steel system', Cement and Concrete Research, 28(12), pp. 1737–1751. doi: 10.1016/S0008-8846(98)00156-2.

Galao, O. (2012) 'Matrices cementicias multifuncionales mediante adición de nanofibras de carbono'. Available at: http://rua.ua.es/jspui/handle/10045/24963.

Galao, O., Baeza, F., Zornoza, E. and Garcés, P. (2017) 'Carbon Nanofiber Cement Sensors to Detect Strain and Damage of Concrete Specimens Under Compression', Nanomaterials. Multidisciplinary Digital Publishing Institute (MDPI), 7(12), p. 413. doi: 10.3390/nano7120413.

Galao, O., Bañón, L., Baeza, F., Carmona, J., Garcés, P., Baeza, J. F., Carmona, J. and Garcés, P. (2016) 'Highly Conductive Carbon Fiber Reinforced Concrete for Icing Prevention and Curing', Materials, 9(4), p. 281. doi: 10.3390/ma9040281.

Gao, J., Wang, Z., Zhang, T. and Zhou, L. (2017) 'Dispersion of carbon fibers in cement-based composites with different mixing methods', Construction and Building Materials. Elsevier Ltd, 134, pp. 220–227. doi: 10.1016/j.conbuildmat.2016.12.047.

García-Macías, E., Alessandro, A. D. and Castro-triguero, R. (2017) 'Micromechanics modeling of the electrical conductivity of carbon nanotube cement-matrix composites',Composite, 108, pp. 451–469. doi: 10.1016/j.compositesb.2016.10.025.

Gersing, E. (1991) 'Measurement of electrical impedance in organs measuring equipment for research and clinical applications', Biomedizinische Technik, 36, pp. 6–11. https://doi.org/10.1515/ bmte.1991.36.1-2.6

Gomis, J., Galao, O., Gomis, V., Zornoza, E. and Garcés, P. (2015) 'Self-heating and deicing conductive cement. Experimental study and modeling', Construction and Building Materials, 75, pp. 442–449. doi: 10.1016/j.conbuildmat.2014.11.042.

Grünewald, S. (2004) Performance-based design of self-compacting fibre reinforced concrete. Delft University Press. Available at: https: //repository.tudelft.nl/ islandora/object/uuid:07a817aa-cba1-4c93-bbed-40a5645cf0f1?collection=research.

Hambach, M., Müller, H., Neumann, T. and Volkmer, D. (2016) 'Carbon fibre reinforced cement-based composites as smart floor heating materials', Composites Part B: Engineering, 90, pp. 465–470. doi: 10.1016/j.compositesb.2016.01.043.

Han, B., Ding, S. and Yu, X. (2015) Intrinsic self-sensing concrete and structures: A review, Measurement: Journal of the International Measurement Confederation. Elsevier Ltd. doi: 10.1016/j.measurement.2014.09.048.

Han, B., Yu, X. and Kwon, E. (2009) 'A self-sensing carbon nanotube/cement composite for traffic monitoring', Nanotechnology, 20(44), p. 445501. doi: 10.1088/0957-4484/20/44/445501.

Han, B., Yu, X. and Ou, J. (2014) Self-Sensing Concrete in Smart Structures, Self-Sensing Concrete in Smart Structures. Elsevier Inc. doi: 10.1016/C2013-0-14456-X.

Han, B., Yu, X., Zhang, K., Kwon, E. and Ou, J. (2011) 'Sensing properties of CNT-filled cement-based stress sensors', Journal of Civil Structural Health Monitoring. Springer-Verlag, 1(1–2), pp. 17–24. doi: 10.1007/s13349-010-0001-5.

Han, B., Zhang, K., Burnham, T., Kwon, E. and Yu, X. (2013) 'Integration and road tests of a self-sensing CNT concrete pavement system for traffic detection', Smart Materials and Structures. IOP Publishing, 22(1), p. 015020. doi: 10.1088/0964-1726/22/1/015020.

Han, B., Zhang, L., Ou, J., Han, B., Zhang, L. and Ou, J. (2017a) 'Electromagnetic Wave Shielding/Absorbing Concrete', in Smart and Multifunctional Concrete Toward Sustainable Infrastructures. Springer Singapore, pp. 313–328. doi: 10.1007/978-981-10-4349-9_18.

Han, B., Zhang, L., Ou, J., Han, B., Zhang, L. and Ou, J. (2017b) 'Electrothermal Concrete', in Smart and Multifunctional Concrete Toward Sustainable Infrastructures. Springer Singapore, pp. 261–271. doi: 10.1007/978-981-10-4349-9_14.

Han, B., Zhang, L., Zhang, C., Wang, Y., Yu, X. and Ou, J. (2016) 'Reinforcement effect and mechanism of carbon fibers to mechanical and electrically conductive properties of cement-based materials', Construction and Building Materials, 125, pp. 479–489. doi: https://doi.org/10.1016/j.conbuildmat.2016.08.063.

Heymsfield, E., Osweiler, A. B., Selvam, R. P. and Kuss, M. (2013) Feasibility of Anti-Icing Airfield Pavements Using Conductive Concrete and Renewable Solar Energy, Federal Aviation Administration. http://www.tc.faa.gov/its/worldpac/techrpt/tc13-8.pdf

Hixson, A. D., Woo, L. Y., Campo, M. A. and Mason, T. O. (2003) 'The origin of nonlinear current-voltage behavior in fiber-reinforced cement composites', Cement and Concrete Research, 33(6), pp. 835–840. doi: 10.1016/S0008-8846(02)01062-1.

ICE (2017) State of the Nation 2017: Digital Transformation | Institution of Civil Engineers. London. Available at: https://www.ice.org.uk/news-and-insight/policy/state-of-the-nation-2017-digital-transformation (Accessed: 28 April 2020).

Jang, S. H., Kawashima, S. and Yin, H. (2016) 'Influence of carbon nanotube clustering on mechanical and electrical properties of cement pastes', Materials. MDPI AG, 9(4). doi: 10.3390/ma9040220.

Jing, X. and Wu, Y. (2011) 'Electrochemical studies on the performance of conductive overlay material in cathodic protection of reinforced concrete', Construction and Building Materials. Elsevier Ltd, 25(5), pp. 2655–2662. doi: 10.1016/j.conbuildmat.2010.12.015.

Job, S. (2010) 'Composite Recycling - summary of recent research and development', Knowledge Transfer Network, 5(September 2010), p. 26. Available at: https://compositesuk.co.uk/system/files/documents/Composite%20Recycling.pdf

Khadilkar, D. (2013) 'Energy-Harvesting Street Tiles Generate Power from Pavement Pounder - Scientific American', Scientific American. Available at: https://www.scientificamerican.com/article/pavement-pounders-at-paris-marathon-generate-power/.

Kim, G. M., Naeem, F., Kim, H. K. and Lee, H. K. (2016) 'Heating and heat-dependent mechanical characteristics of CNT-embedded cementitious composites', Composite Structures. Elsevier Ltd, 136, pp. 162–170. doi: 10.1016/j.compstruct.2015.10.010.

Konsta-Gdoutos, M. S. and Aza, C. A. (2014) 'Self sensing carbon nanotube (CNT) and nanofiber (CNF) cementitious composites for real time damage assessment in smart structures', Cement and Concrete Composites. Elsevier, 53, pp. 162–169. doi: 10.1016/j.cemconcomp.2014.07.003.

Lai, Y., Liu, Y. and Ma, D. (2014) 'Automatically melting snow on airport cement concrete pavement with carbon fiber grille', Cold Regions Science and Technology. Elsevier B.V., 103, pp. 57–62. doi: 10.1016/j.coldregions.2014.03.008.

Lee, J. J., Kim, D. H., Lee, S. T. and Lim, J. K. (2014) 'Fundamental Study of Energy Harvesting Using Thermoelectric Effect on Concrete Structure in Road', Advanced Materials Research. Trans Tech Publications Ltd, 1044–1045, pp. 332–337. doi: 10.4028/www.scientific.net/AMR.1044-1045.332.

Liu, Q., Xu, Q., Yu, Q., Gao, R. and Tong, T. (2016) 'Experimental investigation on mechanical and piezoresistive properties of cementitious materials containing graphene and graphene oxide nanoplatelets', Construction and Building Materials, 127, pp. 565–576. doi: 10.1016/j.conbuildmat.2016.10.024.

Liu, X. and Wu, S. (2011) 'Study on the graphite and carbon fiber modified asphalt concrete', Construction and Building Materials. Elsevier Ltd, 25(4), pp. 1807–1811. doi: 10.1016/j.conbuildmat.2010.11.082.

Loh, K. J. and Gonzalez, J. (2015) 'Cementitious composites engineered with embedded carbon nanotube thin films for enhanced sensing performance', in Journal of Physics: Conference Series. IOP Publishing, p. 12042. doi: 10.1088/1742-6596/628/1/012042.

Lu, L. Ao, Z., He, Y., Ding, Q., Hu, S. (2008) 'Experimental study on conductive asphalt concrete using steel slag as aggregate', in W. Sun, K. van Breugel, C. Miao, G. Y. and H. C. (ed.) International Conference on Microstructure Related Durability of Cementitious Composites. RILEM Publications, pp. 1043–1050. Available at: https://www.rilem.net/publication/publication/65?id_papier=2741.

Manso, S., Mestres, G., Ginebra, M. P., De Belie, N., Segura, I. and Aguado, A. (2014) 'Development of a low pH cementitious material to enlarge bioreceptivity', Construction and Building Materials, 54, pp. 485–495. doi: 10.1016/j.conbuildmat.2014.01.001.

Manso, S., De Muynck, W., Segura, I., Aguado, A., Steppe, K., Boon, N. and De Belie, N. (2014) 'Bioreceptivity evaluation of cementitious materials designed to stimulate biological growth', Science of the Total Environment, 481(1), pp. 232–241. doi: 10.1016/j.scitotenv.2014.02.059.

Mason, T. O., Campo, M. A., Hixson, A. D. and Woo, L. Y. (2002) 'Impedance spectroscopy of fiber-reinforced cement composites', Cement and Concrete Composites, 24(5), pp. 457–465. doi: 10.1016/S0958-9465(01)00077-4.

McCarter, W. J., Starrs, G., Chrisp, T. M. and Banfill, P. F. G. (2009) 'Complex impedance and dielectric dispersion in carbon fiber reinforced cement matrices', Journal of the American Ceramic Society, 92(7), pp. 1617–1620. doi: 10.1111/j.1551-2916.2009.03057.x.

McConnell, V. P. (2010) 'Launching the carbon fibre recycling industry', Reinforced Plastics. Elsevier Ltd, 54(2), pp. 33–37. doi: 10.1016/S0034-3617(10)70063-1.

Micheli, D. et al. (2017) 'Electromagnetic properties of carbon nanotube reinforced concrete composites for frequency selective shielding structures', Construction and Building Materials, 131, pp. 267–277. doi: 10.1016/j.conbuildmat.2016.11.078.

del Moral, B., Galao, Ó., Antón, C., Climent, M. A. and Garcés, P. (2013) 'Viabilidad de utilización de una pasta de cemento con nanofibras de carbono como ánodo en la extracción electroquímica de cloruros en hormigón', Materiales de Construccion, 63(309), pp. 39–48. doi: 10.3989/mc.2012.03111.

De Muynck, W., De Belie, N. and Verstraete, W. (2010) 'Microbial carbonate precipitation in construction materials: A review', Ecological Engineering, 36(2), pp. 118–136. doi: 10.1016/j.ecoleng.2009.02.006.

Nam, I. W. and Lee, H. K. (2015) 'Image Analysis and DC Conductivity Measurement for the Evaluation of Carbon Nanotube Distribution in Cement Matrix', International Journal of Concrete Structures and Materials. Korea Concrete Institute, 9(4), pp. 427–438. doi: 10.1007/s40069-015-0121-8.

Narayanan, R. and Darwish, I. Y. S. (1987) 'Use of Steel Fibers as Shear Reinforcement', Structural Journal, 84(3), pp. 216–227. doi: 10.14359/2654.

Nguyen, H., Carvelli, V., Fujii, T. and Okubo, K. (2016) 'Cement mortar reinforced with reclaimed carbon fibres, CFRP waste or prepreg carbon waste', Construction and Building Materials, 126, pp. 321–331. doi: 10.1016/j.conbuildmat.2016.09.044.

Nguyen, H., Fujii, T., Okubo, K. and Carvellu, V. (2016) 'Cement Mortar Reinforced with Recycled Carbon Fibre and CFRP Waste', in 17th European Conference on Composite Materials,. Munich: European Society for Composite Materials. Available at: https://www.researchgate.net/publication/309733808_Cement_Mortar_Reinforced_with_Recycled_Carbon_Fibre_and_CFRP_Waste.

Park, S., Ahmad, S., Yun, C. B. and Roh, Y. (2006) 'Multiple crack detection of concrete structures using impedance-based structural health monitoring techniques', Experimental Mechanics. Springer, 46(5), pp. 609–618. doi: 10.1007/s11340-006-8734-0.

Pérez, A., Climent, M. A. A., Garcés, P., P??rez, A., Climent, M. A. A., Garc??s, P., Pérez, A., Climent, M. A. A. and Garcés, P. (2010) 'Electrochemical extraction of chlorides from reinforced concrete using a conductive cement paste as the anode', Corrosion Science. Elsevier Ltd, 52(5), pp. 1576–1581. doi: 10.1016/j.corsci.2010.01.016.

Pickering, S. J. (2006) 'Recycling technologies for thermoset composite materials — current status', Composites Part A: Applied Science and Manufacturing, 37, pp. 1206–1215. doi: 10.1016/j.compositesa.2005.05.030.

Pimenta, S. and Pinho, S. T. (2011) 'Recycling carbon fibre reinforced polymers for structural applications: Technology review and market outlook', Waste Management. Elsevier Ltd, 31(2), pp. 378–392. doi: 10.1016/j.wasman.2010.09.019.

Roberts, T. (2006) 'The Carbon Fibre Industry: Global Strategic Market Evaluation 2006-2010', 10.

Roberts, T. (2007) 'Rapid growth forecast for carbon fibre market', Reinforced Plastics. Elsevier Advanced Technology, 51(2), pp. 10–13. doi: 10.1016/S0034-3617(07)70051-6.

Salonitis, K., Pandremenos, J., Paralikas, J. and Chryssolouris, G. (2010) 'Multifunctional materials: Engineering applications and processing challenges', International Journal of Advanced Manufacturing Technology, 49(5–8), pp. 803–826. doi: 10.1007/s00170-009-2428-6.

Sassani, A., Arabzadeh, A., Ceylan, H., Kim, S., Sadati, S. M. S., Gopalakrishnan, K., Taylor, P. C. and Abdualla, H. (2018) 'Carbon fiber-based electrically conductive concrete for salt-free deicing of pavements', Journal of Cleaner Production. Elsevier Ltd, 203, pp. 799–809. doi: 10.1016/j.jclepro.2018.08.315.

Segura, I., Faneca, G., Torrents, J. M. and Aguado, A. (2019) 'Self-sensing concrete made from recycled carbon fibres', Smart Materials and Structures. IOP Publishing, 28(10), p. 105045. doi: 10.1088/1361-665X/AB3D59.

Shi, Z. Q. and Chung, D. D. L. (1999) 'Carbon fiber-reinforced concrete for traffic monitoring and weighing in motion', Cement and Concrete Research, 29(3), pp. 435–439. doi: 10.1016/S0008-8846(98)00204-X.

Singh, D. A., Mishra, M., Chandra, A. and Dhawan, S. (2011) 'Graphene oxide/ferrofluid/cement composites for electromagnetic interference shielding application', Nanotechnology, 22, p. 465701. doi: 10.1088/0957-4484/22/46/465701.

Sun, M., Li, Z., Mao, Q. and Shen, D. (1998) 'Study on the Hole Conduction Phenomenon in Carbon Fiber-Reinforced Concrete', Cement and Concrete Research. Pergamon, 28(4), pp. 549–554. doi: 10.1016/S0008-8846(98)00011-8.

Sun, M., Liu, Q., Li, Z. and Hu, Y. (2000) 'A study of piezoelectric properties of carbon fiber reinforced concrete and plain cement paste during dynamic loading', Cement and Concrete Research. Pergamon, 30(10), pp. 1593–1595. doi: 10.1016/S0008-8846(00)00338-0.

Taya, M., Kim, W. J. and Ono, K. (1998) 'Piezoresistivity of a short fiber/elastomer matrix composite', Mechanics of Materials. Elsevier, 28(1–4), pp. 53–59. doi: 10.1016/S0167-6636(97)00064-1.

The Economist (2015) 'Building works: An historic opportunity to improve infrastructure on the cheap is in danger of being squandered', The Economist. Available at: https://www.economist.com/news/finance-and-economics/21662593-historic-opportunity-improve-infrastructure-cheap-danger.

Torrents, J. M., Mason, T. O. and Garboczi, E. J. (2000) 'Impedance spectra of fiber-reinforced cement-based composites: A modeling approach', Cement and Concrete Research, 30(4), pp. 585–592. doi: 10.1016/S0008-8846(00)00211-8.

Turner, T. A., Pickering, S. J. and Warrior, N. A. (2011) 'Development of recycled carbon fibre moulding compounds - Preparation of waste composites', Composites Part B: Engineering. Elsevier Ltd, 42(3), pp. 517–525. doi: 10.1016/j.compositesb.2010.11.010.

Vaquero, J. M. M., Cugat, V., Segura, I., Calvo-Torrás, M. A., Aguado, A., Calvo, M. A. and Aguado, A. (2016) 'Development and experimental validation of an overlay mortar with biocide activity', Cement and Concrete Composites. Elsevier Ltd, 74, pp. 109–119. doi: 10.1016/j.cemconcomp.2016.09.004.

Wang, C., Li, K.-Z., Li, H.-J., Jiao, G.-S., Lu, J. and Hou, D.-S. (2008) 'Effect of carbon fiber dispersion on the mechanical properties of carbon fiber-reinforced cement-based composites', Materials Science and Engineering: A. Elsevier, 487(1–2), pp. 52–57. doi: 10.1016/j.msea.2007.09.073.

Wang, C., Yang, X., Li, Q., Guo, T. and Jiang, T. (2019) 'Preparation and performance of conductive gussasphalt concrete', Transportmetrica A: Transport Science. Taylor and Francis Ltd., 15(1), pp. 55–70. doi: 10.1080/23249935.2018.1449913.

Wang, X., Wang, Y. and Jin, Z. (2002) 'Electrical conductivity characterization and variation of carbon fiber reinforced cement composite', Journal of Materials Science, 37(2), pp. 223–227. doi: 10.1023/A:1013107623281.

WEF (2013) Shaping the Future of Construction: A Breakthrough in Mindset and Technology | World Economic Forum. Available at: https://www.weforum.org/reports/shaping-the-future-of-construction-a-breakthrough-in-mindset-and-technology (Accessed: 28 April 2020).

Wei, J., Nie, Z., He, G., Hao, L., Zhao, L. and Zhang, Q. (2014) 'Energy harvesting from solar irradiation in cities using the thermoelectric behavior of carbon fiber reinforced cement composites', RSC Advances. Royal Society of Chemistry, 4(89), pp. 48128–48134. doi: 10.1039/c4ra07864k.

Wen, S. and Chung, D. D. L. (2001) 'Electric polarization in carbon fiber-reinforced cement', Cement and Concrete Research, 31(1), pp. 141–147. doi: 10.1016/S0008-8846(00)00382-3.

Wen, S. and Chung, D. D L (2006) 'Model of piezoresistivity in carbon fiber cement', Cement and Concrete Research, 36(10), pp. 1879–1885. doi: 10.1016/j.cemconres.2006.03.029.

Wen, S. and Chung, D D L (2006) 'The role of electronic and ionic conduction in the electrical conductivity of carbon fiber reinforced cement', Carbon, 44(11), pp. 2130–2138. doi: 10.1016/j.carbon.2006.03.013.

Wen, S. and Chung, D. D. L. (2007) 'Double percolation in the electrical conduction in carbon fiber reinforced cement-based materials', Carbon, 45(2), pp. 263–267. doi: 10.1016/j.carbon.2006.09.031.

Westhof, L. (2006) 'Field experience with a conductive cement-based composite as anode for the cathodic protection of reinforced concrete structures', in Grantham, M., Jauberthie, R., and Lanos, C. (eds) Concrete solutions: proceedings of the second International Conference on Concrete Repair. St. Malo, France: BRE Press, p. 798.

Wiktor, V. and Jonkers, H. M. (2015) 'Field performance of bacteria-based repair system: Pilot study in a parking garage', Case Studies in Construction Materials, 2, pp. 11–17. doi: 10.1016/j.cscm.2014.12.004.

Wong, K. H., Pickering, S. J. and Rudd, C. D. (2010) 'Recycled carbon fibre reinforced polymer composite for electromagnetic interference shielding', Composites Part A: Applied Science and Manufacturing. Elsevier Ltd, 41(6), pp. 693–702. doi: 10.1016/j.compositesa.2010.01.012.

Wu, J., Liu, J. and Yang, F. (2015) 'Three-phase composite conductive concrete for pavement deicing', Construction and Building Materials, 75, pp. 129–135. doi: 10.1016/j.conbuildmat.2014.11.004.

Xie, P., Gu, P., Fu, Y. and Beaudoin, J. J. (1995) 'Determination of blast-furnace slag content in hardened concrete by electrical conductivity methods', Cement, Concrete and Aggregate, 17(1), pp. 79–83. Available at: http://nparc.cisti-icist.nrc-cnrc.gc.ca/npsi/ctrl?action=shwart&index=an&req=5206080&lang=fr.

Xu, J. and Yao, W. (2009) 'Current distribution in reinforced concrete cathodic protection system with conductive mortar overlay anode', Construction and Building Materials. Elsevier, 23(6), pp. 2220–2226. doi: 10.1016/j.conbuildmat.2008.12.002.

Xun, Y., Kun, Z., Liu, X. and Wu, S. (2012) Carbon Nanotube Based Self-sensing Concrete for Pavement Structural Health Monitoring, Report_University of Minesota.

Yakhlaf, M., Safiuddin, M. and Soudki, K. A. (2013) 'Properties of freshly mixed carbon fibre reinforced self-consolidating concrete', Construction and Building Materials. Elsevier Ltd, 46, pp. 224–231. doi: 10.1016/j.conbuildmat.2013.04.017.

Yehia, S. A. and Tua, C. Y. (2000) 'Thin conductive concrete overlay for bridge deck deicing and anti-icing', Transportation Research Record. National Research Council, (1698), pp. 45–53. doi: 10.3141/1698-07.

Yoo, D.-Y., You, I. and Lee, S.-J. (2017) 'Electrical Properties of Cement-Based Composites with Carbon Nanotubes, Graphene, and Graphite Nanofibers', Sensors, 17(5), p. 1064. doi: 10.3390/s17051064.

Zhang, J., Xu, L. and Zhao, Q. (2017) 'Investigation of carbon fillers modified electrically conductive concrete as grounding electrodes for transmission towers: Computational model and case study', Construction and Building Materials. Elsevier Ltd, 145, pp. 347–353. doi: 10.1016/j.conbuildmat.2017.03.223.

Zhang, Q., Yu, Y., Chen, W., Chen, T., Zhou, Y. and Li, H. (2016) 'Outdoor experiment of flexible sandwiched graphite-PET sheets based self-snow-thawing pavement', Cold Regions Science and Technology. Elsevier, 122, pp. 10–17. doi: 10.1016/j.coldregions.2015.10.016.

Zhao, H., Wu, Z., Wang, S., Zheng, J. and Che, G. (2011) 'Concrete pavement deicing with carbon fiber heating wires', Cold Regions Science and Technology. Elsevier, 65(3), pp. 413–420. doi: 10.1016/j.coldregions.2010.10.010.

Zhao, R., Tuan, C., Luo, B. and Xu, A. (2019) 'Radiant heating utilizing conductive concrete tiles', Building and Environment. Elsevier Ltd, 148, pp. 82–95. doi: 10.1016/j.buildenv.2018.10.059.

Zonta, D. et al. (2010) 'Wireless sensor networks for permanent health monitoring of historic buildings', Smart Structures and Systems. Techno-Press, 6(5–6), pp. 595–618. doi: 10.12989/sss.2010.6.5_6.595.

Zornoza, E., Catalá, G., Jiménez, F., Andión, L. G. and Garcés, P. (2010) 'Electromagnetic interference shielding with Portland cement paste containing carbon materials and processed fly ash', Materiales de Construccion, 60(300), pp. 21–32. doi: 10.3989/mc.2010.51009.